THE HOLOCENE ERUPTIVE HISTORY OF MAKUSHIN VOLCANO, ALASKA

By

Kirby Wendell Bean

RECOMMENDED:

John C. Eichelberger

Chris J. Nye

Jim E. Begét
Advisory Committee Chair

Paul W. Layer
Head, Department of Geology and Geophysics

APPROVED:

D. Woodall
Dean, College of Science, Engineering, and Mathematics

Joseph R. Kahn
Dean of the Graduate School

December, 1999
Date

THE HOLOCENE ERUPTIVE HISTORY OF MAKUSHIN VOLCANO, ALASKA

A

THESIS

Presented to the Faculty

of the University of Alaska Fairbanks

in Partial Fulfillment of the Requirements

for the Degree of

MASTER OF SCIENCE

By

Kirby Wendell Bean, B.A.

Fairbanks, Alaska

December, 1999

Abstract

A chronostratigraphic framework of Holocene volcanic deposits has been developed for Makushin Volcano. Four major correlative stratigraphic units have been described texturally and geochemically and form a base for reference. Two early Holocene "caldera forming" eruptive events, dated at 8050 yr B.P. and ca. 8790 yr B.P. respectively, generated the vast bulk of pyroclastic debris which fill valleys proximal to the volcano. Total erupted volume for early Holocene unconsolidated deposits approaches 10 km^3. The eruptions produced very mobile pyroclastic flows that traveled as far as Dutch Harbor (25 km away) where they buried an ancient Native American culture in more than 30 cm of hot ash and rock fragments.

Detailed stratigraphic records reveal that Makushin has maintained a high level of activity throughout the Holocene and therefore a high potential for volcanic hazards. Frequencies of moderate magnitude (VEI 2-4) eruptions average 1 every 200 years over the last 5000 ^{14}C yr B.P.

Table of Contents

List of Figures

List of Tables

Acknowledgements

Funding for this thesis project was provided by the Alaska Volcano Observatory, a joint program of the United States Geological Survey, the Geophysical Institute of the University of Alaska Fairbanks, and the Alaska Division of Geological and Geophysical Surveys. I would like to thank Jim Begét, John Eichelberger, and Chris Nye for giving me the rare opportunity to work on Alaskan volcanos, for their steady financial support, and academic guidance. I would especially like to thank my friends Darren, Michelle, and Evan who also happen to be great sounding boards. Many thanks to peers, faculty, and staff who took the time to answer questions and/or lend a hand along the way.

Chapter 1: Introduction

Better understandings of eruptive histories are critical to the ability to forecast and mitigate hazards associated with future volcanic eruptions. Modern tephrochronological techniques involving detailed stratigraphic examinations and extensive dating of past events now allow quantitative assessments of eruptive intensities and magnitudes (Pyle 1989, Fierstein and Nathenson 1992) thereby providing a more complete knowledge of a volcano's eruptive history and its likely future activity. While such techniques have been applied systematically to volcanoes in the Cascades (Gardner *et al.* 1998, Hildreth & Fierstein 1997), Japan, and other populated areas, few similar studies have been made in the Aleutians. The value of detailed historic eruptive information is not limited to hazard mitigation. Expanding our knowledge of Pleistocene and Holocene volcanic activity can provide insight into parameters that affect global climate change. The identification of widespread volcanic ash deposits, which provide unique volcanic time stratigraphic marker beds are extremely useful to geologists, and also to archeologists trying to unravel the details of prehistoric human cultures.

Approximately 800 miles southwest of Anchorage, almost halfway along the Aleutian Volcanic Arc lies the remote volcanic island of Unalaska. Quaternary volcanism is centered in the northeastern portion of Unalaska Island on the island's largest topographical feature, 1830 m, Makushin Volcano (Fig. 1.1). Makushin has been and continues to be the primary source of Holocene volcanic activity on the island. Evidence of past glaciation on the flanks of several monogenetic satellite vents surrounding Makushin indicates these are late Pleistocene in age (Drewes *et al.* 1961, Nye *et al.* 1986, McConnell *et al.* 1997). The exception is a series of morphologically young tuff cones and maars, located along a linear fracture stretching northwest of the summit towards Pt. Kadin, which appear to have formed during the late Holocene (Drewes *et al.* 1961, Nye *et al.* 1986, McConnell *et al.* 1997).

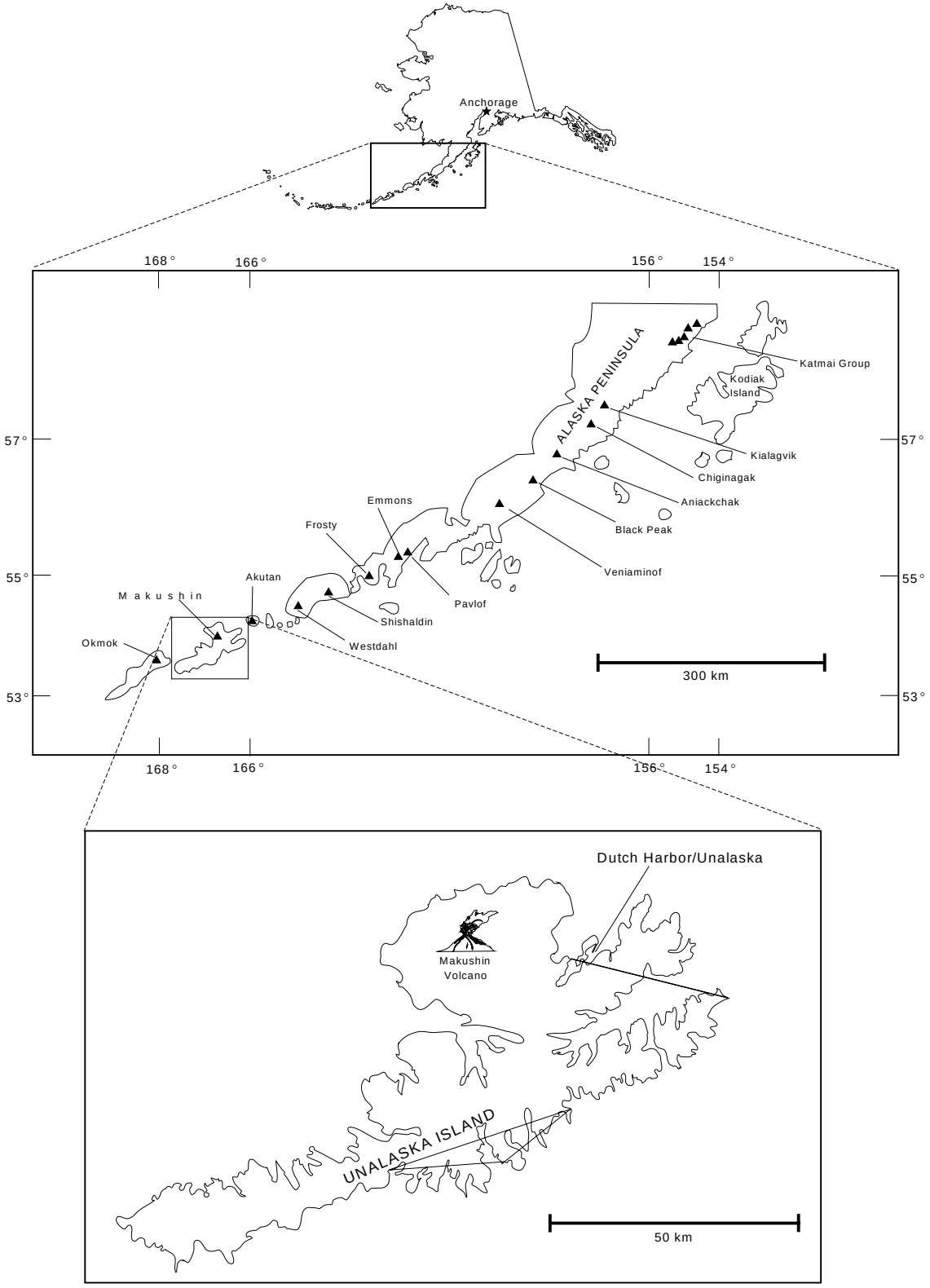

Fig. 1.1 Location of Makushin and other eastern Aleutian volcanoes.

1.1 Proximity of Makushin Volcano to Local Communities

Unlike most Aleutian volcanoes, Makushin is situated close (~25 km) to an Alaskan community. The towns of Dutch Harbor and Unalaska, with a combined year round population of about 4000 residents, comprise the largest community in the Aleutians and the 11th largest in the state of Alaska. With a large, safe harbor with docking facilities for large ships and with multiple fish processing factories, Dutch Harbor is the a base for much of the North Pacific fishing fleet. Of considerable economic importance, Dutch Harbor has consistently ranked as the top U.S. fishing port both in fish volume and in fish value for the last decade. In 1996 the Dutch Harbor fishing and related industry is credited with bringing in more than $100 million, out producing its closest U.S. competitor by more than $20 million dollars (NOAA press release 97-48). Dutch Harbor also contains a sizable airport that handles several Boeing 737 flights a day. The potential impact on human life and activity from volcanic related hazards in Alaska, outside Cook Inlet, is probably nowhere greater than at Dutch Harbor/Unalaska. For these reasons natural hazards to this area should be studied and understood to the maximum degree possible.

1.2 Purpose

The purpose of this study was to develop an eruptive chronology and stratigraphic framework for Holocene tephras and other pyroclastic deposits at Makushin Volcano by mapping volcanic deposits and developing a detailed stratigraphy using radiocarbon geochronology and tephrochonological techniques. Combining detailed eruptive chronology with volume estimates and reconstruction of eruptive mechanism and style during past eruptions, should add greatly to the understanding of the likely behavior of eruptions in the future. In addition to adding to the knowledge base on Aleutian volcanos, it is hoped that this study will provide a solid framework on which future work can be based.

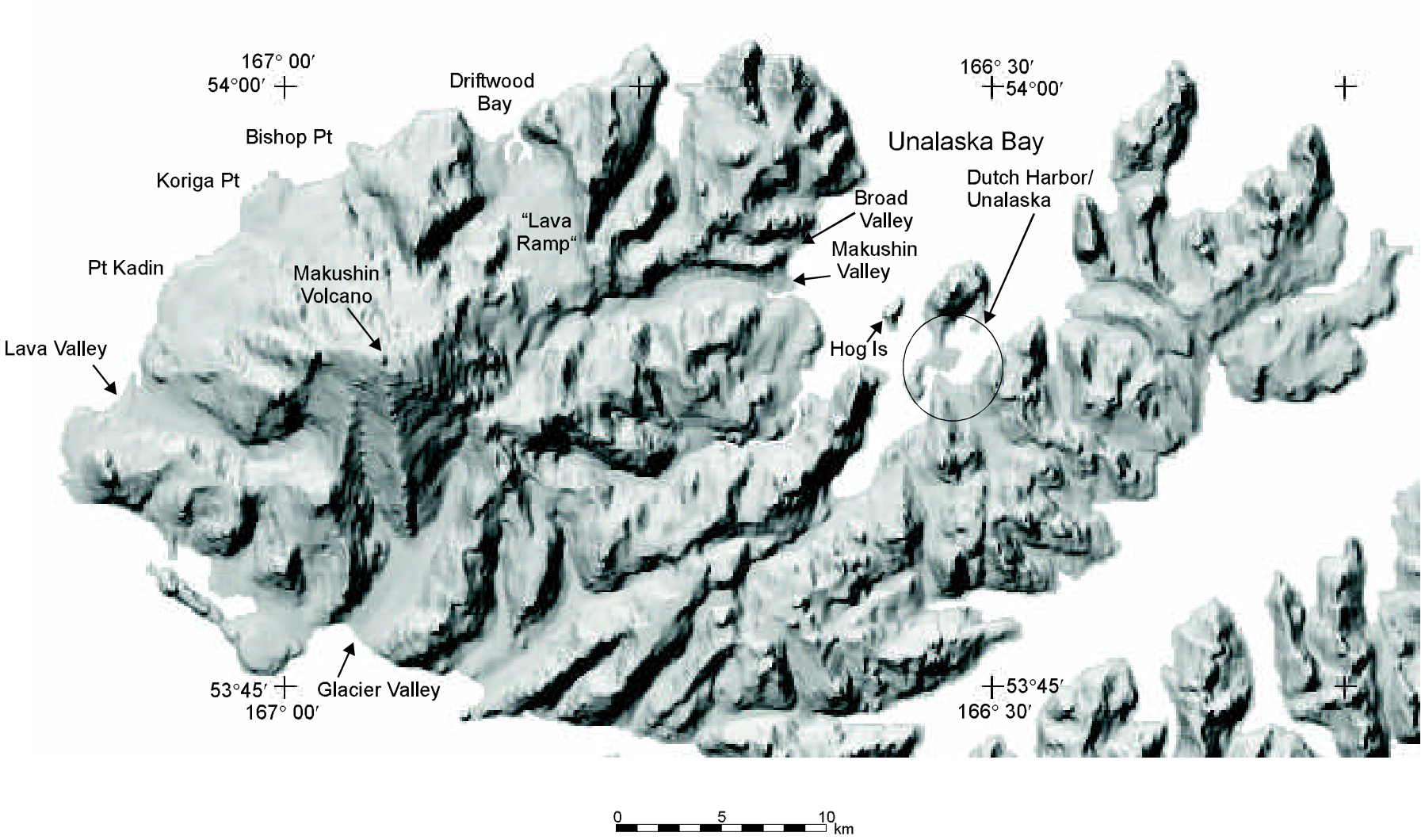

Fig.1.2 Shaded relief map of northern Unalaska Island.

1.3 Background

Drewes *et al.* (1961) produced the first geologic map of Unalaska Island in a report detailing the geology of Unalaska. This map, however, is essentially a bedrock map and unconsolidated volcanic deposits are not mapped, although several simplified soil-ash profiles from around Unalaska bay and reference to "lahars" in Bishop Point valley are mentioned in the report. In his master's thesis, Arce (1983) describes several tephra deposits around Makushin in addition to providing a detailed account of its historic activity. Nye *et al.* (1984) built on the original work of Drewes *et al.* by publishing a detailed map of the Makushin geothermal field, which included the eastern half of Makushin volcano. A lower limiting date, on the proximal valley-filling Holocene caldera forming deposits of 7950 ^{14}C yr B.P. was reported by Reeder (1983) and an upper limiting date of 4280 ^{14}C yr B.P. was reported by Nye *et al.* (1984).) In a report to the Alaska Power Authority, Nye (1986) describes the likely volcanic hazard threats to a proposed power generating plant on the flanks of Makushin. In a review of large-magnitude Holocene Aleutian volcanic activity, Miller and Smith (1987) estimate the bulk volume of caldera-forming products from Makushin to be less than 10 km^3 based on the size of the caldera. Most recently McConnell *et al.* (1997), building on the work of Drewes *et al.* and Nye *et al.*, published a detailed map with complete coverage of volcanic deposits in the entire Makushin Volcanic Field. The work in this study was conducted concurrently with and is directly related to the work of McConnell *et al.*(1997). Some of the whole rock data and age data used in this study were first published in that report.

1.4 Methods

During field mapping, detailed stratigraphic information was recorded in field notes. Field observations were key to the interpretation and correlation of deposits. Stratigraphic relationships, tephra marker beds, and approximately 25 radiocarbon age dates provided relative

and absolute age control. Conventional radiometric age dates on peat were normalized to $d^{13}C_{PDB}$ values of –29.5‰ (see chapter 8 & Appendix V for discussion). Volume estimates were based on standard techniques and on an empirical method developed for this study (see chapter 9). Major tephra deposits between sample sites were correlated using similarity coefficient (SC) comparison (Borchardt *et al.*, 1972) of major element geochemistry of glass shards. Data was obtained using electron microprobe analysis (EMA) using standards and analytical routines as described in Begét *et al.* (1991b). Comparison of tephra whole rock major and trace element data was also possible in some instances. Grain size analyses were useful in characterizing distal flowage deposits.

1.5 Glacial History and Topography of Unalaska Island

Unalaska Island (53°N, 166°W) is an NE/SW trending island approximately 130 km long. It lies about 200 km west of the Alaska Peninsula (Fig. 1.1). The presence of glacial valleys provide a straightforward field method of distinguishing mainly Holocene from older deposits. On Unalaska Island they provide a minimum late Pleistocene age for caldera-forming eruptions and deposition of subsequent valley-filling deposits. Upper limiting dates suggest that late Pleistocene ice caps covering the larger Aleutian islands had retreated by 10 ka B.P. (Black, 1986). However glacial records from southern Alaska suggest that glacial retreat actually began as early as 15 ka. B.P. Climatic warming as early as 14-15 ka B.P. is also supported by pollen records and sea cores (Black, 1986). Today, Unalaska Island, including Makushin volcano, is heavily dissected by glacial valleys. Mountain ranges are typically 600-1000 m in elevation although the summit of Makushin is about 1830 m. A small, phreatically active lava dome sits inside an ice-filled summit caldera, approximately 2x3 km in diameter. Several small but active glaciers flow radially from the summit and, northwest of the volcano, extending to elevations as low as 2000 ft. Age dates from this study indicate that, at least in Makushin Valley, there has not been a major glacial advance in the last ~ 8700 ^{14}C yr B.P.

The Holocene eruptive products comprise thick pyroclastic fans, which fill the proximal portions of glacial valleys surrounding Makushin Volcano. Due to the lush wet climate most areas below snowline are covered with a thick vegetative mat, the source of the common peat layers observed in the field which were so helpful in dating and correlations. Note that most Aleutian-wide studies assume an elevation of 2030 m for Makushin. More recent topographic maps (ca 1989) indicate a maximum elevation of approximately 1830 m.

Chapter 2: Field Methods and Procedures

2.1 Field Work

Fieldwork was conducted during July and August of 1996 and during a brief period in June of 1997. This work was part of a larger initiative by the Alaska Volcano Observatory which included mapping of late Quaternary volcanic deposits as well as the installation of a volcano monitoring seismic network. Helicopter and other logistical support were provided by AVO.

2.2 Sampling Procedure

Approximately 300 tephra and organic samples were collected at 62 sites (Fig. 2.1) around Makushin volcano and Dutch Harbor. A stratigraphic sketch was drawn at each site visited. Detailed descriptions of tephras such as position, thickness, color, lateral continuity, and grain size of each sample was recorded in field notes. Organic horizons were noted as well but the focus was on tephra descriptions. Precise positions of each sample site (Table 2.1) were recorded with the aid of a handheld GPS device.

Tephras deemed significant were collected for geochemical analysis. Tephras with unique characteristics or those likely to be useful as regional marker units were generally considered "significant." Organic material, used to provide limiting ages for deposits, was also collected. Bomb fragments and other juvenile material from lahars, debris avalanches, and pyroclastic flows were also collected for geochemical analysis. Most tephra samples were collected from exposures in stream cuts, gullies, or from coastal bluffs.

Careful sampling procedures were implemented to prevent contamination during the collection process. An exposure face would first be scraped clear to expose a fresh uncontaminated surface. Samples were then carefully collected with a clean trowel, placed in plastic sample bags and carefully labeled. Organic samples were collected in the same manner

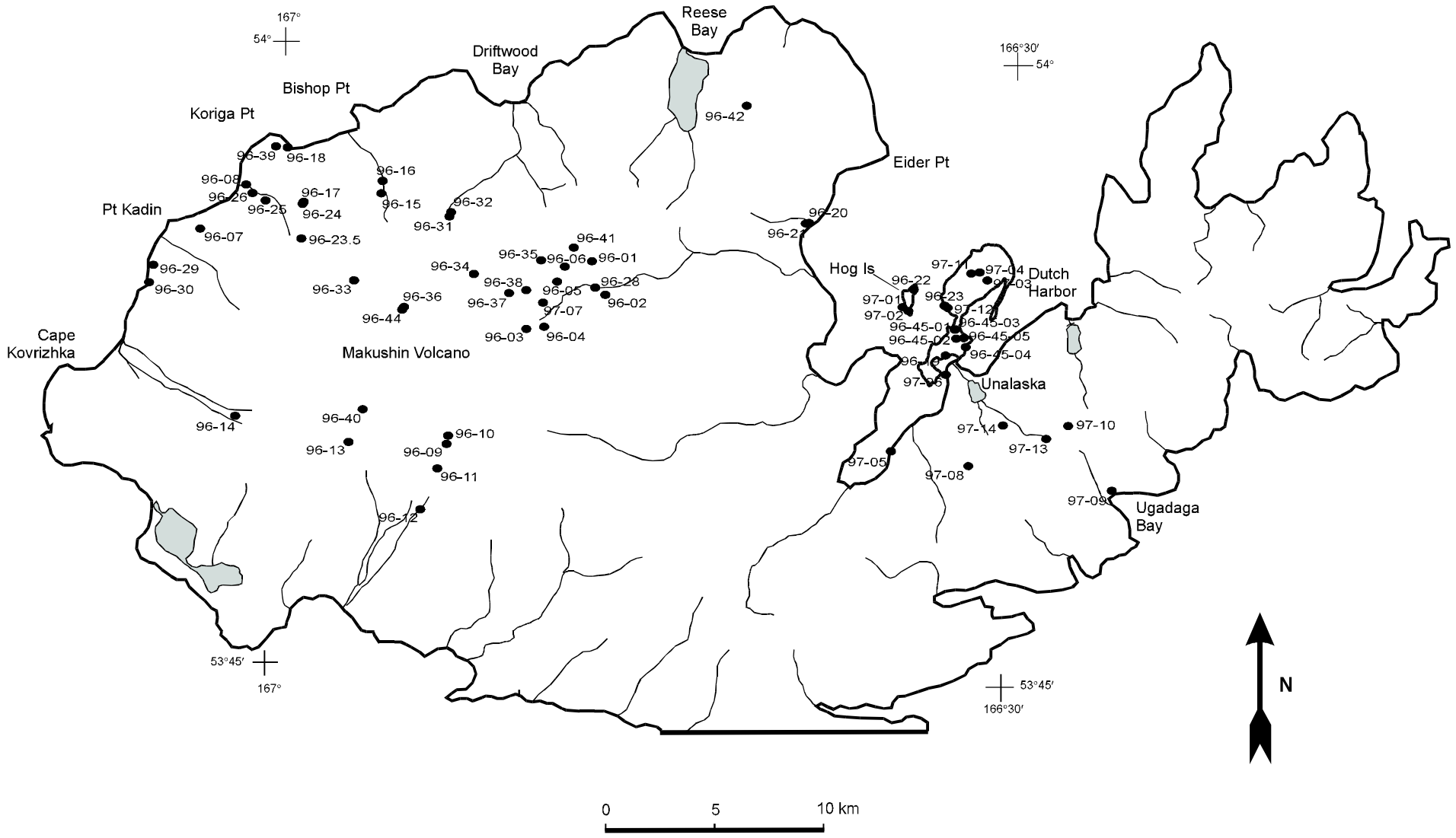

Fig. 2.1 Location of sampling sites from northern Unalaska Island.

and placed in Ziploc® type plastic bags and labeled. As much care as possible was taken not to include live organic matter such as rootlets or organic matter from other organic horizons.

Table 2.1 Precise sampling site locations. Coordinates use North American Datum of 1927.

Site Number	Latitude	Longitude	Site Number	Latitude	Longitude
96MAK01	53°54′57″N	166°47′11″W	96MAK32	53°56′01″N	166°53′01″W
96MAK02	53°54′09″N	166°46′35″W	96MAK33	53°54′18″N	166°56′54″W
96MAK03	53°53′16″N	166°49′47″W	96MAK34	53°54′33″N	166°52′00″W
96MAK04	53°53′20″N	166°49′03″W	96MAK35	53°54′56″N	166°49′16″W
96MAK05	53°54′26″N	166°48′35″W	96MAK36	53°53′42″N	166°54′49″W
96MAK06A	53°54′48″N	166°48′17″W	96MAK37	53°54′07″N	166°50′32″W
96MAK06B	53°54′48″N	166°48′17″W	96MAK38	53°54′12″N	166°49′50″W
96MAK07	53°55′25″N	167°03′16″W	96MAK39	53°57′28″N	167°00′17″W
96MAK08	53°56′31″N	167°01′27″W	96MAK40	53°51′12″N	166°56′22″W
96MAK09	53°50′26″N	166°52′53″W	96MAK41	53°55′16″N	166°47′57″W
96MAK10	53°50′38″N	166°52′50″W	96MAK42	53°58′49″N	166°41′02″W
96MAK11	53°49′50″N	166°53′14″W	96MAK43	53°55′49″N	167°00′31″W
96MAK12	53°48′50″N	166°53′52″W	96MAK44	53°53′38″N	166°54′53″W
96MAK13	53°50′24″N	166°56′54″W	96MAK45-01	53°53′34″N	166°32′15″W
96MAK[14]	53°50′56″N	167°01′34″W	96MAK45-02	53°53′21″N	166°32′10″W
96MAK15	53°56′25″N	166°55′54″W	96MAK45-04	53°53′09″N	166°31′46″W
96MAK16	53°56′43″N	166°55′52″W	96MAK45-05	53°53′22″N	166°31′52″W
96MAK17	53°56′06″N	166°59′07″W	97MAK01	53°53′59″N	166°34′10″W
96MAK18	53°57′27″N	166°59′48″W	97MAK02	53°54′04″N	166°34′24″W
96MAK19	53°52′56″N	166°32′35″W	97MAK03	53°54′46″N	166°30′58″W
96MAK20	53°56′02″N	166°38′20″W	97MAK04	53°54′58″N	166°31′17″W
96MAK21	53°56′01″N	166°38′28″W	97MAK05	53°50′35″N	166°34′42″W
96MAK21B	53°56′01″N	166°38′28″W	97MAK06	53°52′28″N	166°32′33″W
96MAK22	53°54′30″N	166°33′58″W	97MAK07	53°53°55″N	166°49′08″W
96MAK23	53°54′08″N	166°32′41″W	96MAK31	53°55′55″N	166°53′05″W
96MAK23.5	53°53′24″N	166°49′43″W	97MAK08	53°50′17″N	166°31′32″W
96MAK24	53°56′09″N	166°59′04″W	97MAK09	53°49′47″N	166°25′38″W
96MAK25	53°56′09″N	167°00′38″W	97MAK10	53°51′19″N	166°27′23″W
96MAK26	53°56′19″N	167°01′11″W	97MAK11	53°54′56″N	166°31′37″W
96MAK28	53°54′19″N	166°47′01″W	97MAK12	53°54′05″N	166°32′33″W
96MAK29	53°54′30″N	167°05′08″W	97MAK13	53°50′60″N	166°28′23″W
96MAK30	53°54′05″N	167°05′17″W	97MAK14	53°51′17″N	166°30′09″W

Chapter 3: Analytical Methods and Procedures

Tephra and organic samples were collected for geochemical characterization and correlation of deposits. Selected samples were prepared for radiocarbon analyses, electron microprobe analysis (EMA) of glass shards for major elements, whole rock major and trace element analysis, and grainsize analysis. All samples were prepared at facilities of the Department of Geology and Geophysics at the University of Alaska Fairbanks.

3.1 Radiocarbon Sample Preparation

Organic samples were removed from storage bags in the laboratory and air or oven dried at low (20-50 °C) temperatures. All organic samples were inspected for the presence of young rootlets which, if present, were removed by hand picking. The samples were then wrapped in aluminum foil, labeled, and placed in bags for shipment. All organic material was submitted to Beta Analytic Inc. of Miami, Florida for radiometric dating (see chapter 6 for results and discussion). Extended counting time was required for six samples and five other samples were analyzed using the AMS radiocarbon dating technique. Sample preparation was the same for all samples.

3.2 Electron Microprobe Sample Preparation

EMA was preceded by multiple step sample preparation. Tephras were first dried at low (<100 °C) temperatures. Samples were then prepared following the procedures of Pinney (1991). The method involves first rinsing of tephra to remove loose dirt then treating with a Chlorox® type bleach bath to dissolve organics followed by an acid bath in HCl to remove iron staining. Once clean, glass shards were separated from tephras using the heavy liquid Sodium Polytungstate (SPT) as in Pinney (1991) in an effort to further concentrate glass. A few milligrams of glass separate were then set and mounted on a petrographic slide using Hillquist® petrographic epoxy. The epoxy-tephra mixture was cut and ground to a thickness of

approximately 40 microns or until glass shards were exposed. Grain mounts were then polished smooth using successively finer grits starting at 15 µm and ending with a polish of 1 µm. Polishing times varied from 2 to 8 hours per slide with finer grain sizes taking the longest. The slides were carefully cleaned with glass cleaner before the final step of carbon coating. A 250 µm carbon coat was applied to each slide using an Edwards bell-housed coating system. The sample was then ready for electron microprobe analysis.

Mafic tephras underwent an extra step of magnetic separation prior to heavy liquid separation. This helped to separate the glass rich tephra from crystal rich more magnetic tephra. Magnetic separations were performed using a Frantz isodynamic magnetic separator. Each sample was separated into three fractions of magnetic susceptibility; MS=.1, MS>.1 but <1, and MS>1. The low susceptibility fraction tended to be dominated by magnetite and other mafic minerals, the =1 susceptibility fraction was dominated by quartz and feldspars and the remaining fraction was generally enriched in glass.

Heavy liquid separation of mafic tephras (density > 2.42) also required a slightly different approach than Pinney. Instead of preparing a solution of density 2.42 a density gradient was achieved by adding water to a very dense SPT solution and careful mixing at the density boundary. Tephra layers would segregate into different density layers. Each layer was then collected and inspected for the glass content using a petrographic microscope.

3.3 Whole Rock Sample Preparation

Tephra samples submitted for whole rock analysis included both tephra and juvenile blocks and bombs from pyroclastic deposits. Samples were crushed to pea-sized fragments and split into two 40 gram portions. One split was designated for XRF major and trace element analysis and the other split was designated for ICP trace element analysis. Samples were submitted to the

Geoanalytical Laboratory of the Geology Department at Washington State University in Pullman, WA for analysis.

3.4 Grainsize Sample Preparation and Procedure

Grain size analysis was performed on several samples of suspected distal airfall and pyroclastic flow deposits. Sample sizes varied from 15 to 280 grams in total weight. Prior to analysis each 8-inch U.S.A Standard Testing Sieve was weighed to the nearest .1 gram. Sieving was done at mesh increments of ½ phi beginning with –1 phi (2 mm) and ending at 4.5 phi (~.18 mm). A portion of air dried sample was placed in the top sieve in a stack of sieves and shaken for approximately 20 minutes with an automatic sediment shaker. After shaking, each sieve plus tephra was weighed again and the weight of tephra contained within determined to the nearest 0.1 gram. The tephra portion finer than 4.5 phi was caught in a bottom pan and weighed as well so that a total amount of sediment analyzed could be determined. The sieves were scrubbed and cleaned with water and dried before performing the next analysis.

Chapter 4: Description of Volcanic Deposits

Volcanic deposits are mapped and stratigraphy described from eight distinct geographic regions (Fig. 4.1) from around Makushin. Unconsolidated deposits are best preserved in valleys and relatively flat upland areas such as the "Lava Ramp," and are rare in steep upland areas where bedrock lavas are typically exposed. An exception is unglaciated ridges proximal to the volcano where pyroclastic lag deposits exist and a dark sintered to welded scoria flow unit commonly forms a resistant cap.

4.1 Glacier Valley

Unconsolidated volcanigenic deposits are restricted almost entirely to the upper regions of Glacier Valley. The middle and lower portions of Glacier Valley are dominated by alluvial deposits; stream erosion and fluvial aggradation has obscured most evidence of volcanic deposits in the lower valley.

Lahars and debris avalanches are the dominant deposits in Glacier Valley. Their location and distribution is shown in figure 4.2. In addition, these deposits are mantled by up to a meter of various ash and surge deposits.

The lahars in Glacier Valley form low (less than 5 m) flat-topped terraces along the valley sides. The lahars are generally an earthy brown color, are sandy-matrix supported, and have better sorting than the avalanche deposits. Clasts are typically subrounded cobbles to boulders ranging to 0.5 m in diameter. At site 96MAK11 a thin clay-rich lahar deposit overlies debris avalanche deposits. At least two separate lahar deposits are present representing at least one and perhaps more eruptive episodes. These lahars are geographically confined to two separate tributary valleys of Glacier Valley.

A small debris avalanche deposit also occupies the valley sides and interfluvial areas. It ranges in thickness from approximately 40 m at the head of the valley to approximately 10 m

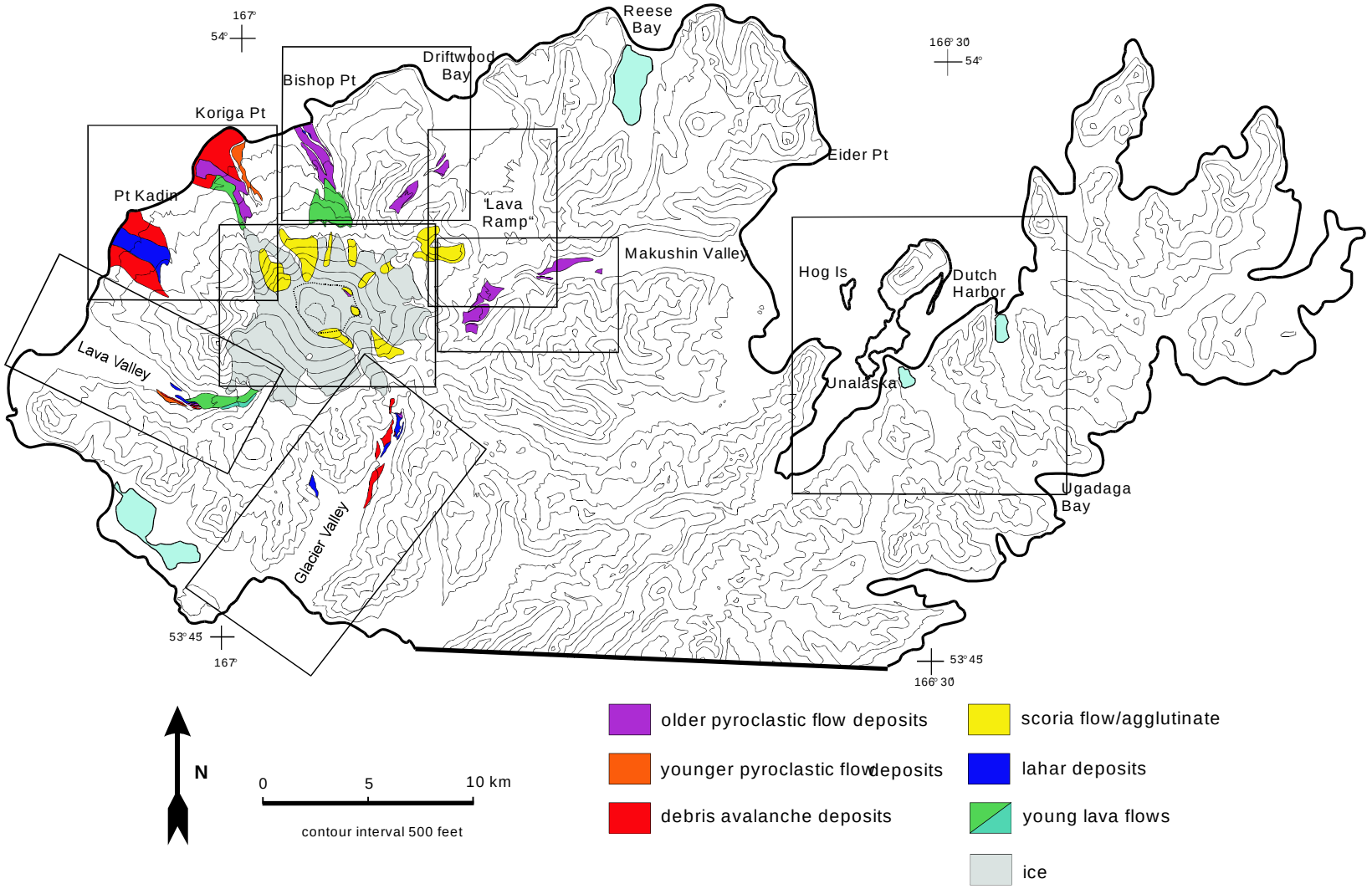

Fig. 4.1 Simplified geologic map of Holocene volcanic deposits, Unalaska Island, Alaska modified from McConnell *et.al* 1997). Rectangles correspond to map coverage of figures in chapter 4.

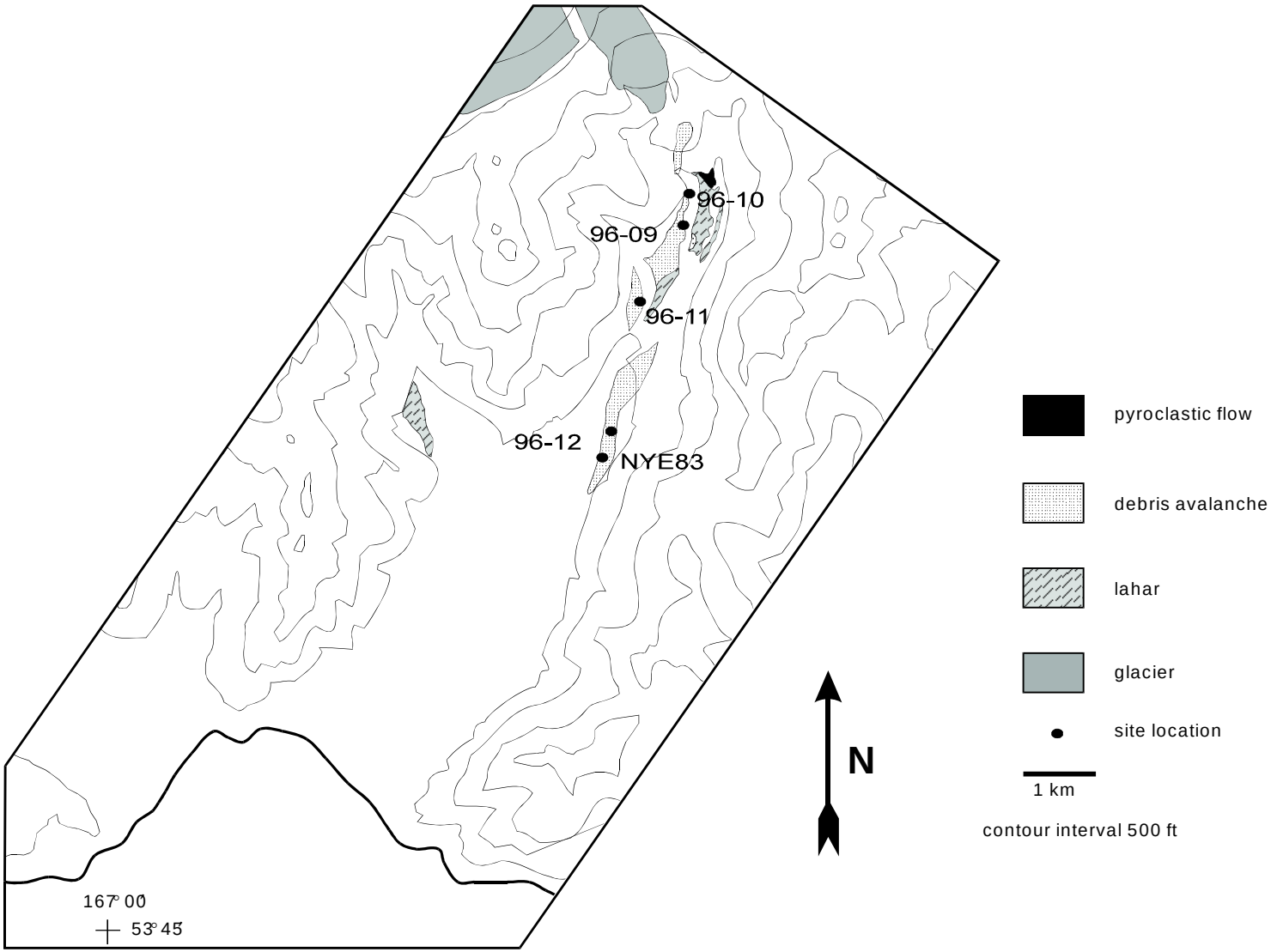

Fig. 4.2 Map of Glacier Valley volcanic deposits.

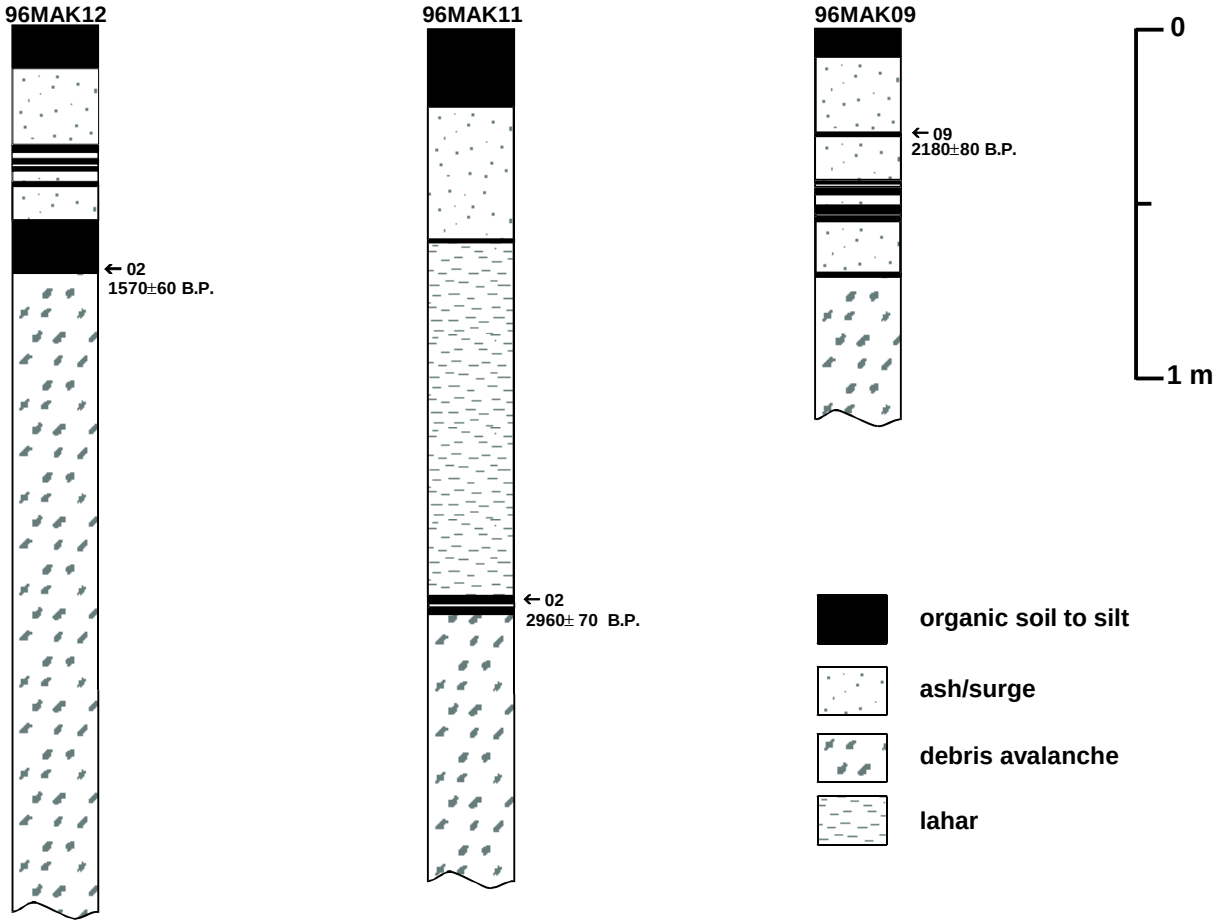

Fig. 4.3 Stratigraphic sections from sites in Glacier Valley.

thick four km down valley where the deposit is truncated by streams. The tops of the these deposits are hummocky. Hummocks with an amplitude of ~4.5 m and a wavelength of ~130 m were measured at site 96MAK09. Down valley near site 96MAK11 hummocks size decreases slightly to ~4 m in height and a length of ~30 m. Comparison of these hummocks with those observed in debris avalanche deposits at Redoubt Volcano (Begét & Nye 1994) and other volcanos suggest that the avalanche was relatively small with little momentum. The deposit itself consists of a distinct, relatively fine-grained orange matrix with large assorted clasts up to 2.5 meters in diameter. Whitish to light orange-brown stringers and clay-rich zones are present and many clasts exhibit sharp fractures most likely caused by impacts during deposition.

Stratigraphic relationships suggest that the lahars are younger in age than the debris avalanche deposits. At one location a lahar overlaps and overlies the debris avalanche deposits. The lahar located in the western tributary shares no contact with the avalanche deposits and therefore its relative age is not known although it is not unreasonable to associate it with the lahar deposits in the more northern tributaries.

Figure 4.3 shows the uppermost stratigraphy of several sites located in Glacier Valley. Tephra accumulations on the debris avalanche deposits here are thinner (generally < 1m) here than on fans in valleys north and east of Makushin, suggesting a younger age. Radiocarbon ages support this interpretation, as most of the mantling tephra deposits are younger than 2250 yr B.P. One date under a lahar at site 96MAK11 suggests that it may have been deposited shortly after 3030 ^{14}C yr B.P. Nye *et al.* (1984) reported an age of 4280±230 ^{14}C yr B.P. for organic material (sample no. Nye83) taken from the uppermost portion of volcanic deposits in Glacier Valley. From sample locations this indicates a minimum age for the debris avalanche deposit.

There are also small remnants of pyroclastic flows present in uppermost Glacier Valley. These deposits are very dark in color with numerous bombs and blocks. The deposits were

inaccessible and close inspection was not possible. They are very similar in color and texture, however, to the sintered scoria ignimbrite found in Makushin Valley and are probably an equivalent deposit.

4.2 Lava Valley

Debris avalanche, lahar, and pyroclastic flow deposits are the primary unconsolidated volcanic deposits in Lava Valley (Fig. 4.4). Two relatively young lava flows are located in the upper reaches of Lava Valley. These extend down to the valley floor where they stratigraphically overlie most of the unconsolidated deposits (Fig. 4.5).

Stratigraphic relationships suggest that the thin wedge of light brown to orange brown massive pyroclastic deposits in the uppermost region of Lava Valley are the oldest unconsolidated volcanic deposits in this area. They are partially overlain by young lavas and lahars overlap at the sides. These deposits are similar in character to pyroclastic flow deposits in Makushin Valley and are most likely of equivalent age. Further down-valley high (20-30 m) terraces along the east side of the valley are comprised of yellow-orange debris avalanche deposits containing a variety of lithologies of lithic clasts. These in turn are overlain by several meters of brown clayey lahar deposits (Fig.4.5). The terraces are capped by approximately 2 m of soils and tephra. Thin brown lahars make up the lower terraces, some of which seem to emanate from the end of the young lava flows suggesting that they are coeval with the lava flows.

Numerous thin tephra deposits mantle pyroclastic flow deposits. Stratigraphic sections from Lava Valley are presented in Fig. 4.5. Section 96MAK14a shows a detailed tephra/soil profile from the uppermost portion of a high terrace. Major depositional episodes are contrasted with periods of soil development in black. The upper four meters record at least 25 separate eruptive events. The high terrace and thick mantle of tephra suggest that these terraces are relatively old and perhaps related to caldera formation. The presence of a pumice deposit (sample 96MAK14-1)

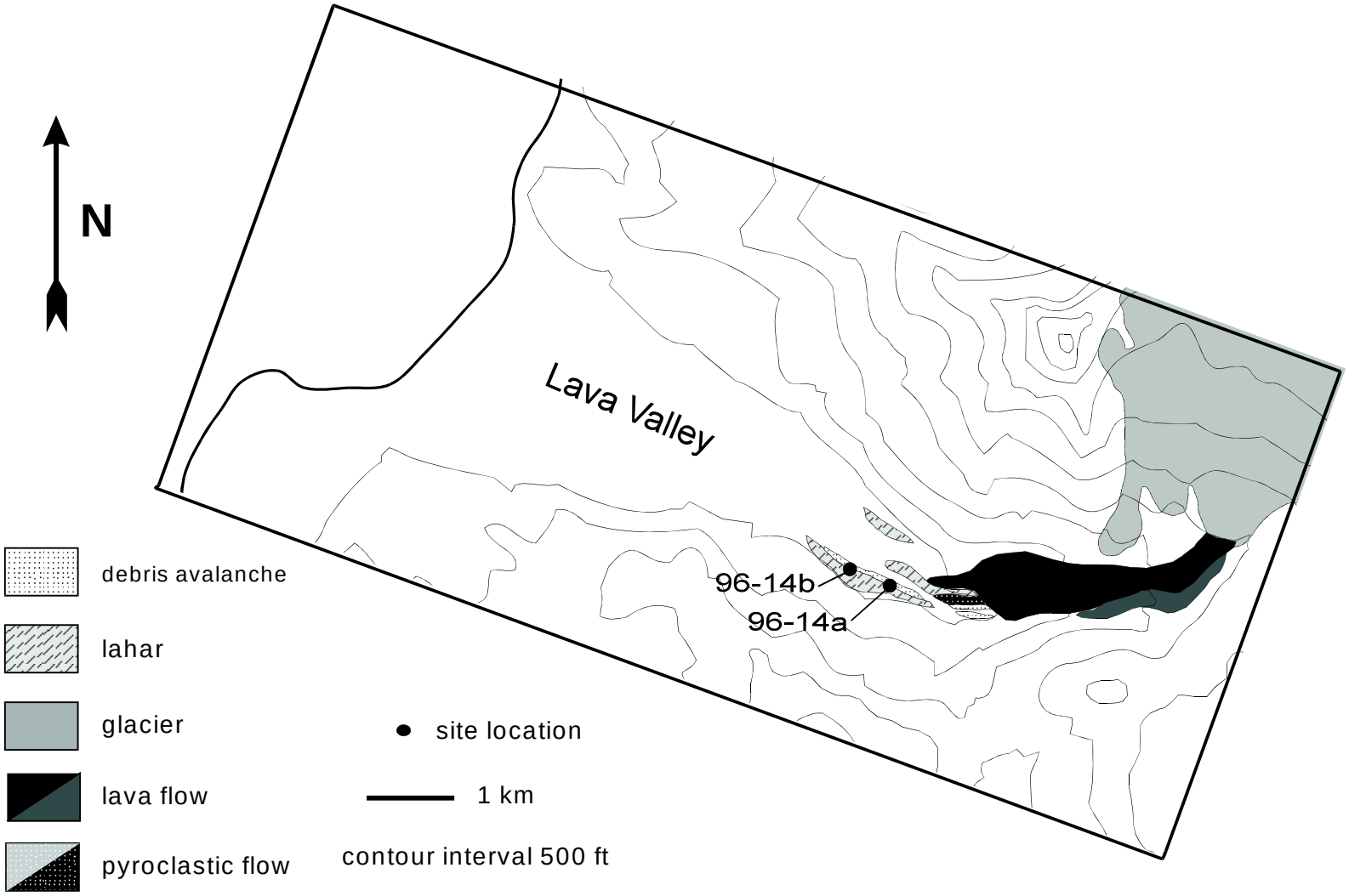

Fig. 4.4 Map of Lava Valley deposits.

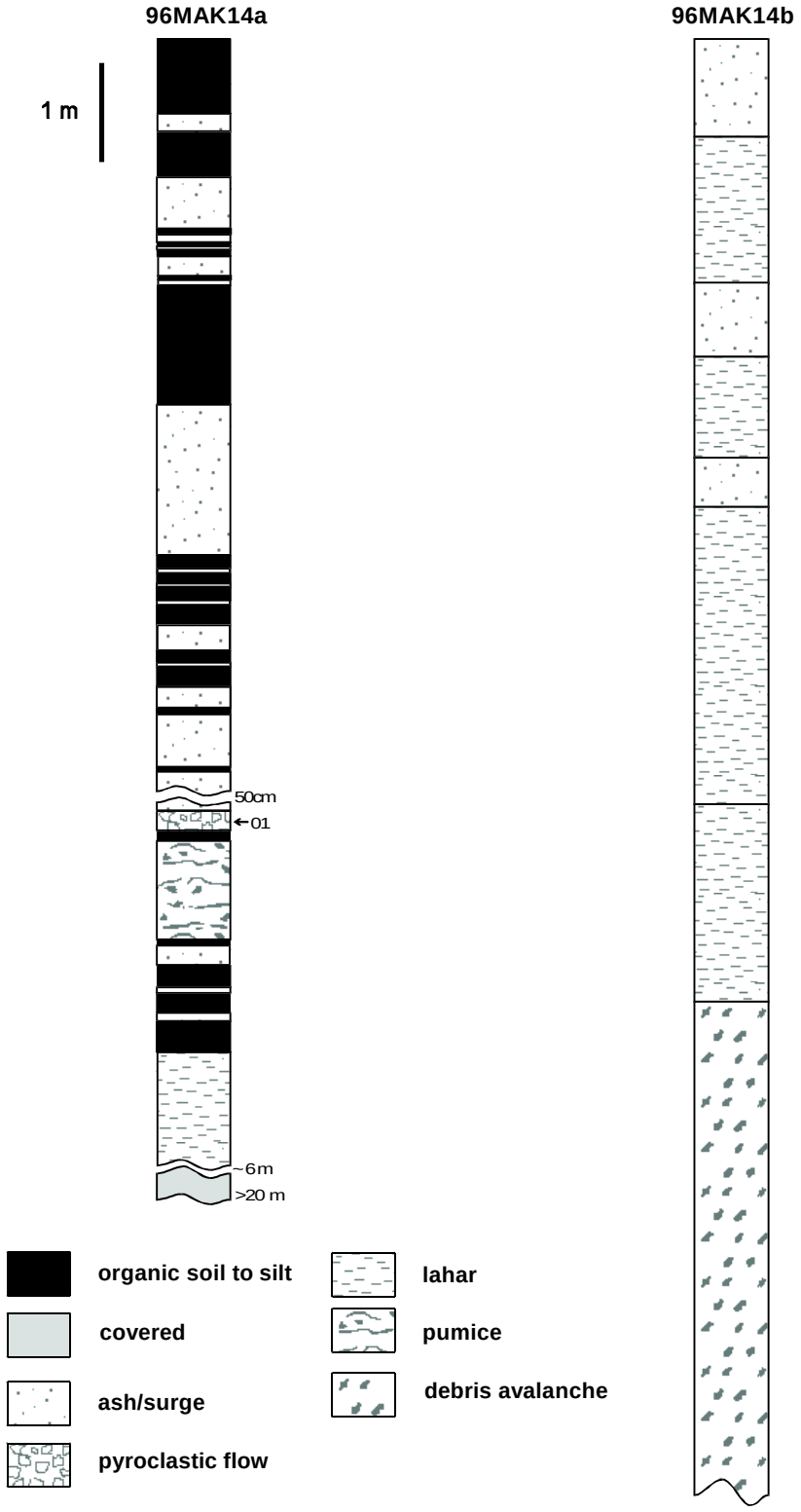

Fig. 4.5 Stratigraphic sections from Lava Valley.

which is chemically similar to thin pumice units found near Pt. Kadin support this interpretation. Approximately 300 m down-valley is stratigraphic section 96MAK14b measured at a more exposed and accessible portion of the same terrace. It shows a more complete composite of the terrace deposits and spans the entire height of the terrace at this location.

4.3 Point Kadin and Koriga Point

Northwest of Makushin, Point Kadin and Koriga Point form two prominent landmarks which jut into the sea. Exposures in stream cuts and beach cliffs reveal that these are mostly comprised of at least one very large Holocene debris avalanche. Erosion by the sea, deposition of younger lahars, pyroclastic flows, and airfall tephra have subsequently obscured much of the original deposit. Figure 4.6 shows the extents of both deposits as well as significant overlying deposits. Lahars partially overlie the avalanche deposits at Point Kadin (Fig. 4.6) while at Koriga Point at least two different pyroclastic flow deposits of different age overlay the debris avalanche. Based on morphology, similar physical characteristics, and stratigraphic comparisons the debris avalanche deposits are interpreted to be of similar age.

Stratigraphic sections of selected sites from the area are displayed in Fig. 4.7. Sections 96MAK29, 39, and 26 show the same general pattern at both Koriga Point and Point Kadin. Several meters of airfall tephra and silts overlie partially exposed debris avalanche deposits, which in turn overlie lava flows. These deposits comprise most of the beach cliff, a thickness of approximately 60 m. At site 96MAK39, an organic soil was discovered lying directly over the avalanche deposits. Radiocarbon dating gave an age of 8550±80 yr. B.P. indicating an early Holocene age for the deposit.

At site 96MAK18, fine grained, cross-stratified surge deposits are intercalated with the coarse debris avalanche deposits (Fig. 4.19). This suggests violent emplacement where lateral blast or

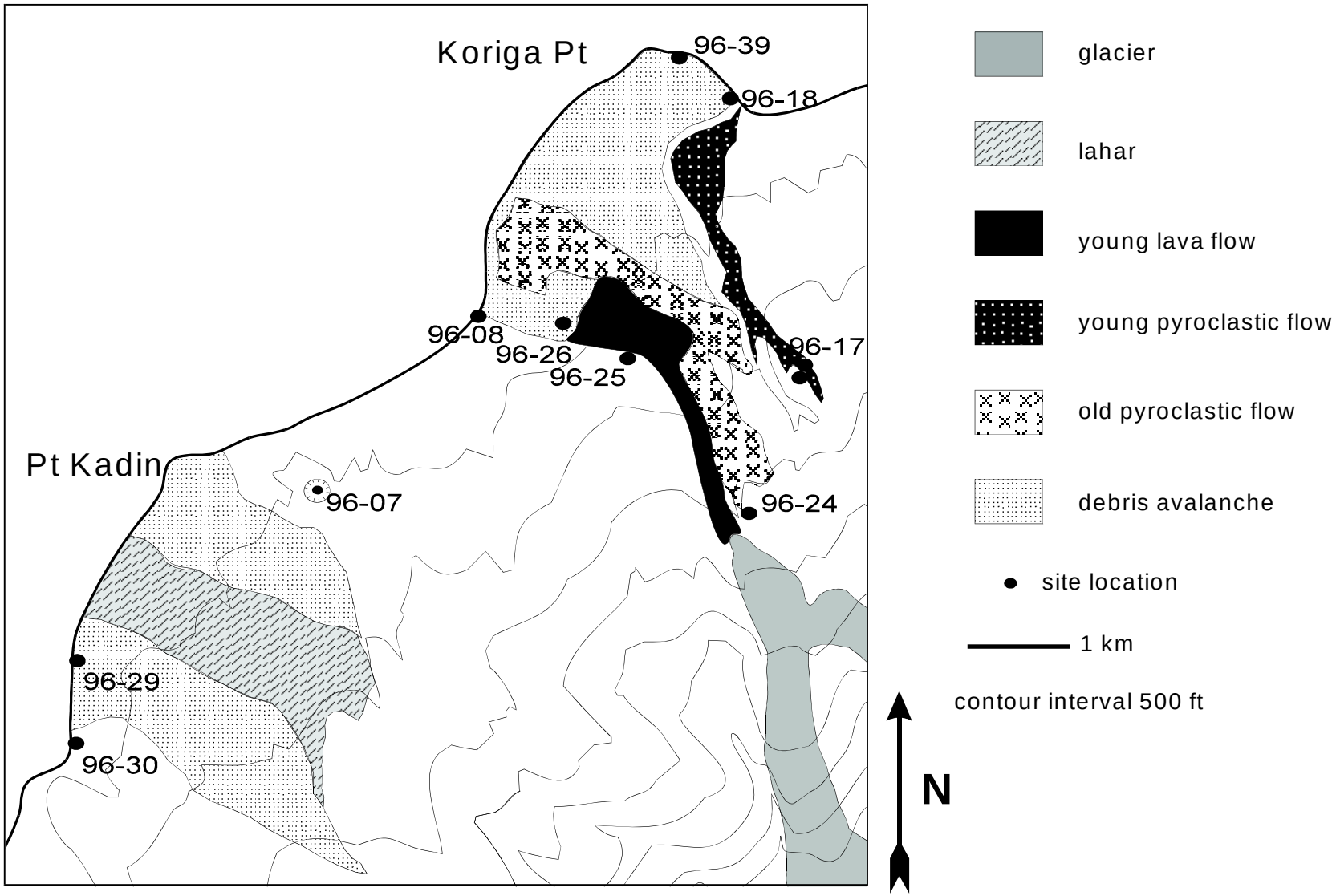

Fig. 4.6 Map of Point Kadin and Koriga Point volcanic deposits.

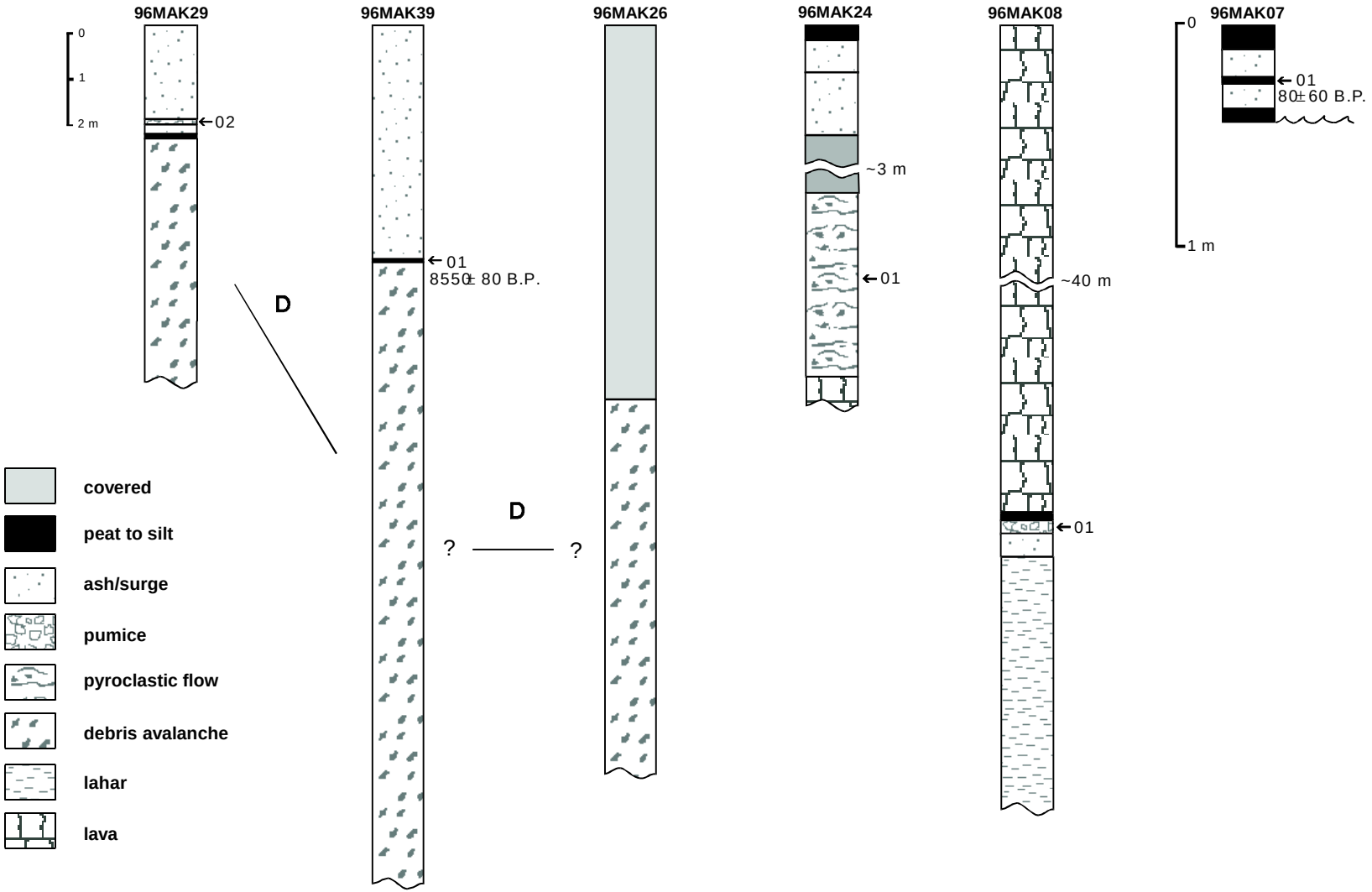

Fig. 4.7 Stratigraphic sections from Point Kadin and Koriga Point. Letters refer to correlation units (see chapter 5).

surges traveled through gravitationally driven avalanche debris. Similar deposits were observed intercalated in the Mount. St. Helens landslide deposits of 1980 (Hoblitt *et al.* 1981).

Section 96MAK08 is a beach cliff exposure adjacent to Koriga Point. Here a thick sequence of Pleistocene lavas form a massive cliff stratigraphically underlain by a distinct white pumice deposit about 30 cm thick. It is relatively fine-grained and very silicic (SiO_2 ~71%) see Appendix I. Although no other similar tephras were discovered during the course of investigations it may eventually prove to be of regional significance due to it's unique geochemistry, high vesicularity, and light color.

One other significant set of features lies between Point Kadin and Koriga Point as noted by Drewes *et al.* (1961), Nye (1986), and McConnell *et al.* (1997). A linear series of at least 10 morphologically young tuff cones and maars stretches from the sea along a fracture zone towards the summit of Makushin Volcano. The explosion craters span a significant amount of time as the most seaward crater has been all but eroded away and forms part of a high beach cliff and the most landward has been partially eroded by glaciation. Some of the craters exhibit overlapping relationships indicating that magma has utilized the fracture system repeatedly to get to the surface. In fact the youngest crater is perhaps as young as a few hundred years. A peat sample dated at 80±60 ^{14}C yr B.P. was taken from the edge of a shallow pond at the bottom of the youngest maar. In addition, only two tephras totaling a thickness of 22 cm were preserved here. Since Makushin is known to have been fairly active during the past few millennium it seems reasonable that such a crater would have collected more than two tephra units if it were of significant age. At the very least, the date provides a maximum age for the most recent significant tephra eruption of Makushin.

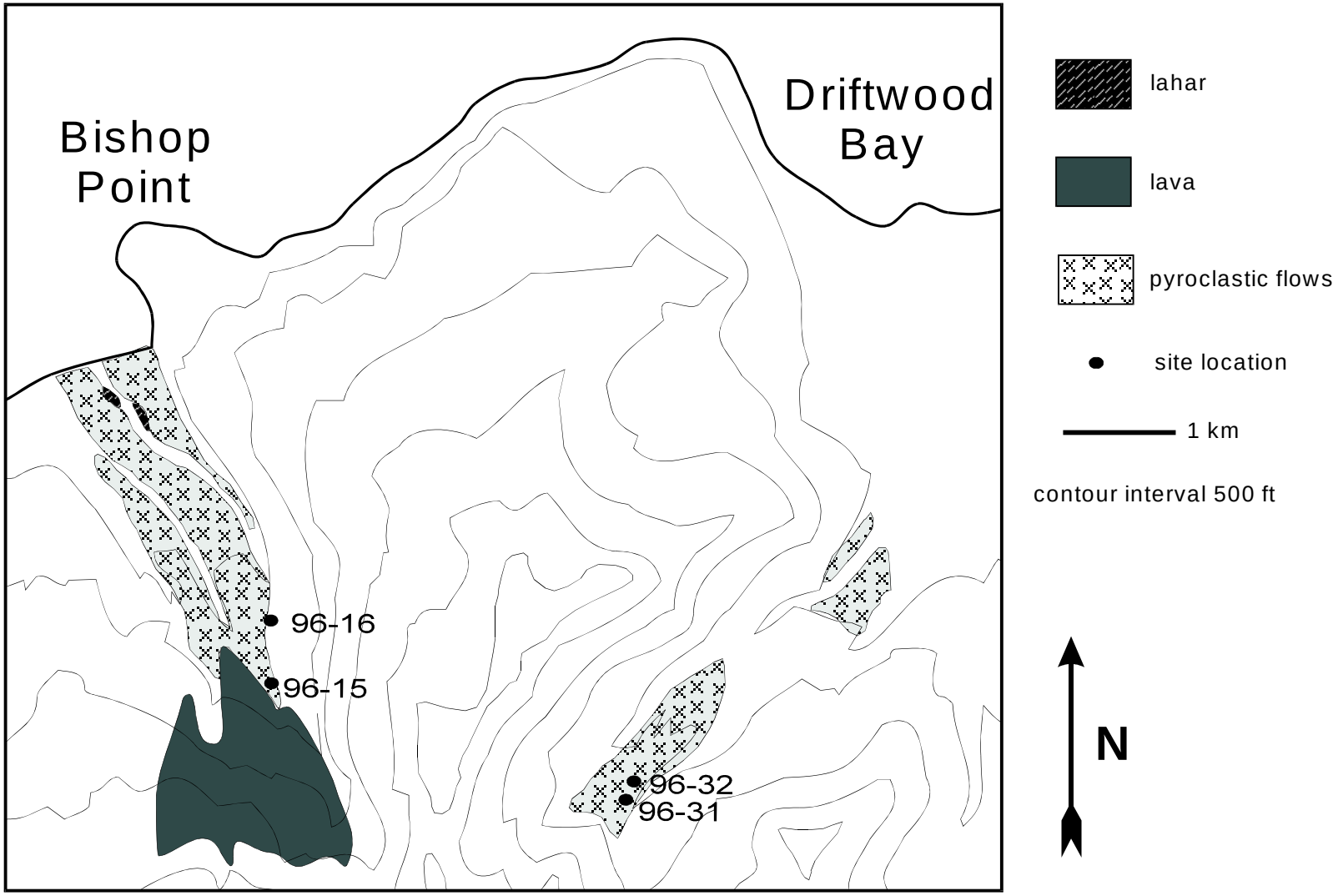

Fig. 4.8 Map of Bishop Point and Driftwood Valley volcanic deposits.

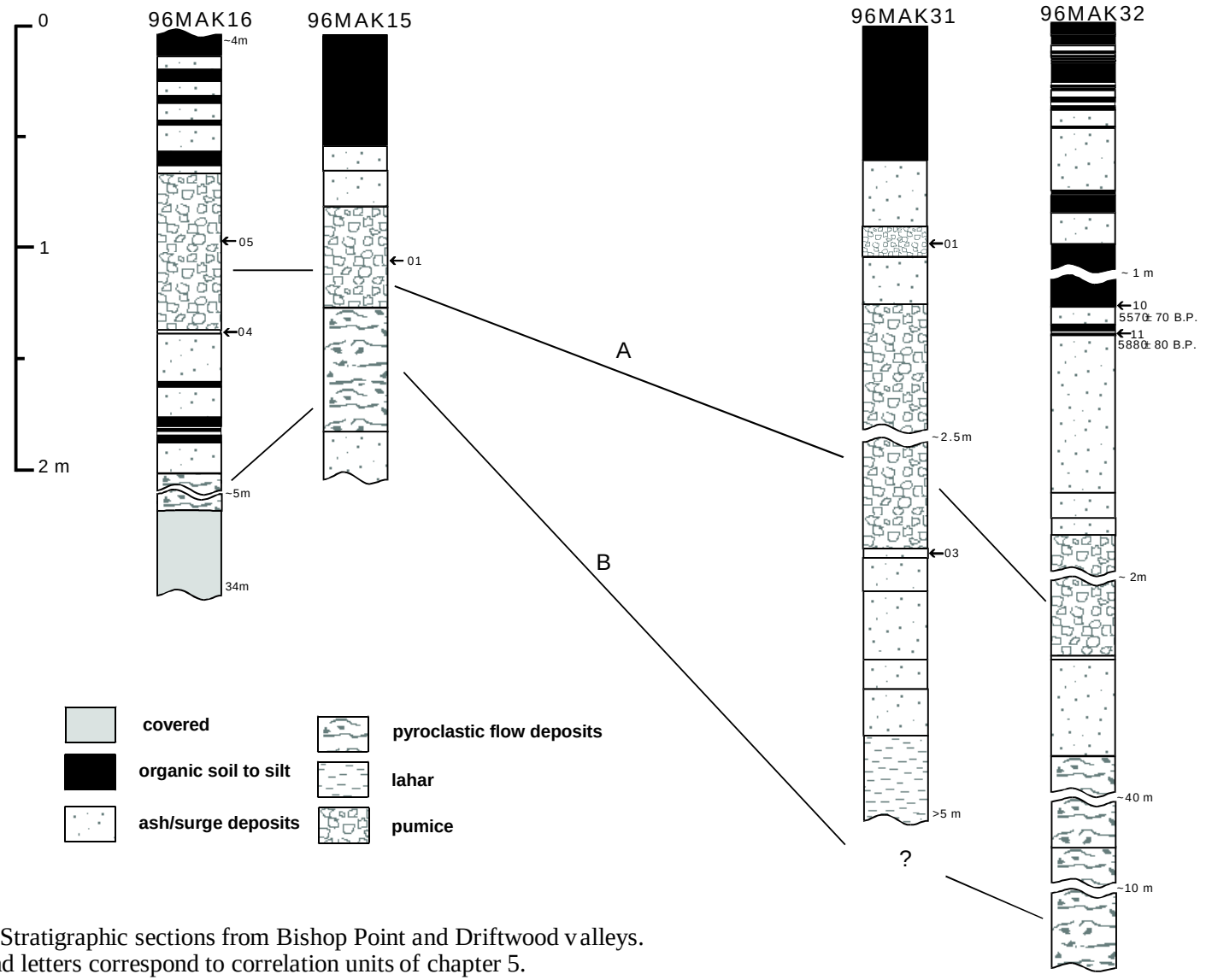

Fig. 4.9 Stratigraphic sections from Bishop Point and Driftwood valleys.
Lines and letters correspond to correlation units of chapter 5.

4.4 Bishop Point Valley and Driftwood Valley

Bishop Point Valley and Driftwood Valley were glaciated and formerly U-shaped but are now almost entirely infilled with unconsolidated volcanic deposits. Pyroclastic flows comprise the vast majority of this infill (Fig. 4.8). Small remnants of lahars are also present as small terraces along incised streams in lower portions of Bishop Point Valley. A significant portion of valley fill from both valleys appears to have eroded away. Bishop Point Valley is truncated by the sea. Driftwood Valley deposits are also eroded by streams coming off of the "Lava Ramp". This makes total volume estimates difficult.

The upper portions of the valley fill appear very similar to valley fill in Makushin Valley. Upper flow units are light brown in color, and massive, with an ashy matrix and occasional dark blocks and bombs. Lower units are lithic- and scoria-rich with a relatively fine grained orange matrix. The lower units are more consolidated (cemented) and form resistant cliffs. Valley fill thickness approaches 100 m in Driftwood Valley and is greater than 60 m in Bishop Point Valley.

Stratigraphic sections from accessible upper portions of both Bishop Point and Driftwood valleys are illustrated in Fig. 4.9. A yellow pumice deposit >2 m thick was found in this area and is hereafter referred to as the "Driftwood Pumice". The thickest occurrences of this pumice deposit occur in these two valleys (Fig. 4.20). The Driftwood Pumice is the most widespread and most distinct marker unit observed in this study and was heavily relied upon as a tephrochronologic dating tool. This unit was identified as far away as Ugadaga Bay more than 30 km to the east.

4.5 Makushin Valley

The upper portions of Makushin Valley contain large, flat-topped, valley-filling pyroclastic fans (Fig. 4.10). Smaller eroded remnants of pyroclastic deposits are preserved further down valley. The deposits themselves are very similar to those in Bishop Point and Driftwood valleys.

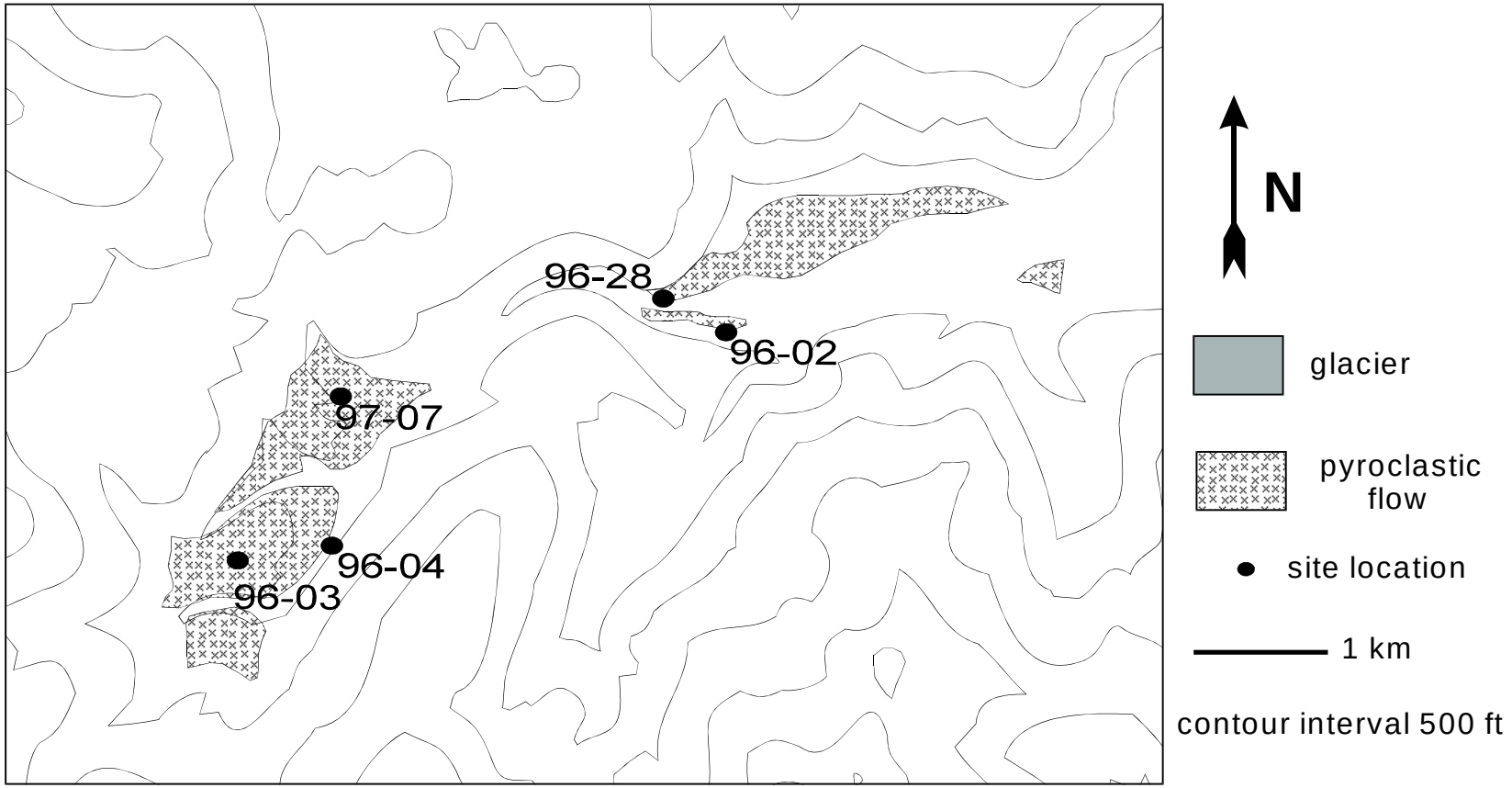

Fig. 4.10 Map of upper Makushin Valley volcanic deposits.

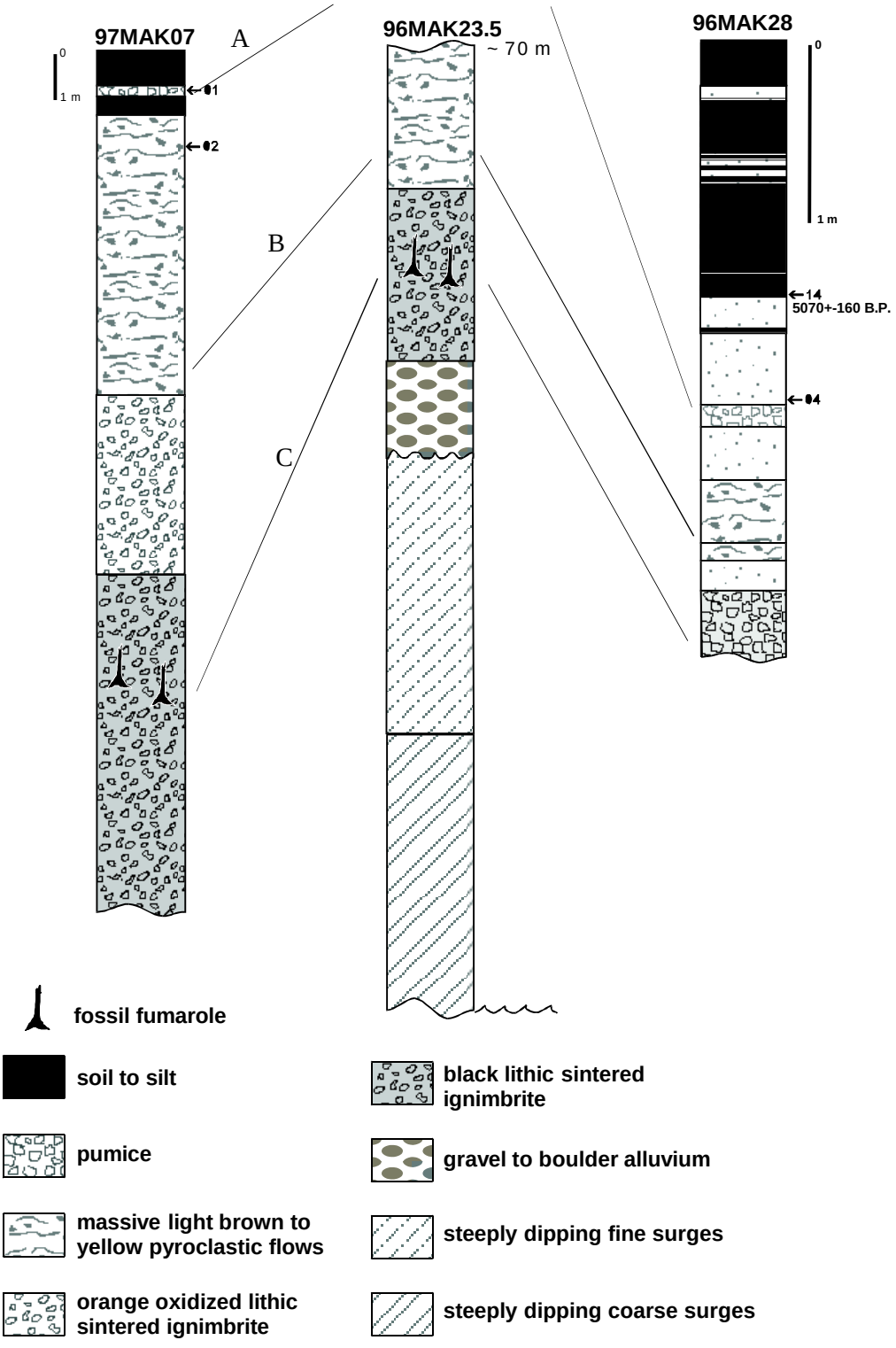

Fig. 4.11 Stratigraphic sections from Makushin Valley. Lines correspond to correlation units of chapter 5.

Pyroclastic fans approach thicknesses totaling nearly 100 meters. Sections illustrated in Fig. 4.11 are representative of the stratigraphy in Makushin Valley. Section 97MAK07 reveals the stratigraphy of the upper portions of the fan while section 96MAK23.5 is from lowest exposed portions of the fan.

The uppermost two or so meters of the fans is comprised of black and orange tephras a few centimeters to tens of centimeters in thickness and intercalated with peat and organic soils. A radiocarbon age from section 96MAK28 (Fig. 4.11) indicates that here the upper two meters is younger than or equal to about 5000 ^{14}C yr B.P.

Arce (1983) recognized five separate lahar flow units comprising the bulk of deposits that fill upper Makushin Valley near Fox Canyon. We interpret the flow units in Makushin Valley to be a series of base surge deposits overlain by scoria flow and block-and-ash flow units. At site 97MAK07, at least five pyroclastic flow units based on sharp contacts, varying textures, fining upward sequences, and color were recognized in the upper portions of the fan.

Section 97MAK07 is the best exposure of the pyroclastic flows. The upper 10 meters of this sediment package consists of a light brown to orange brown poorly consolidated ignimbrite with oxidized yellow to red clasts and black lithics. Bombs greater than 1 meter in diameter are present in this unit. Flow units beneath the previous flow unit are rich in dark lithics and are cemented with a orange fine grained matrix. There is an abrupt change from orange matrix to a black matrix in the consolidated pyroclastic flow at depth of approximately 10 meters. The lithic rich deposit is generally fines depleted and contains common coarse boulder-sized blocks. This may be a type of lag breccia as described in Druitt (1998). Lag breccias are accumulations of material too coarse to be carried by laterally moving density currents. They are commonly associated with caldera collapse.

A distinct dark, sintered to slightly welded cliff-forming scoria-rich ignimbrite flow unit is found beneath the consolidated orange lithic flow units. This unit contains well-developed fossil fumarole pipes as much as 10 cm in diameter. The lowest exposed sections are comprised of several meters of steeply dipping coarse surges which fine upwards. They are separated from overlying pyroclastic flow units by boulder-rich flood deposits approximately 2 m thick, suggesting that the basal surge deposits are not contemporaneous with the pyroclastic flow units.

4.6 Proximal Caldera Deposits

Exposures of relatively unconsolidated Holocene deposits on the flanks of Makushin are largely restricted to ice-free aretes (Fig 4.12). Most of the youngest deposits seen in the valleys and on the Lava Ramp have been eroded away at higher elevations. A black sintered scoria deposit forms a resistant cap approximately two to four meters thick on lava flows and flat surfaces up to 1000-1500 m elevation on the east and northeast flanks of Makushin Volcano (Fig. 4.23). This unit can be traced to the Lava Ramp where it is not sintered and appears as a scoria fall or flow deposit, and to fans in Makushin Valley where it forms a very resistant sintered unit containing fossil fumaroles. Two radiocarbon samples taken from under this unit have been dated at 8730 and 8710 ^{14}C yr B.P. This black sintered deposit is also present in the summit caldera (Fig 4.23) where it is well exposed at several locations along the eastern caldera rim. The scoria unit here unconformably overlies approximately fifty meters of dipping pink to tan coarse to fine surge deposits and breccias that were most likely deposited during the early phase of the same eruption. The dipping surges are stratigraphically correlated with base surges in Makushin Valley.

The unit mapped as pyroclastic lag deposits are remnants of pyroclastic valley filling flow deposits. Generally only the highly resistant lower flow unit, a scoria agglutinate to sintered ignimbrite flow unit is still intact, the less resistant overlying members having weathered away.

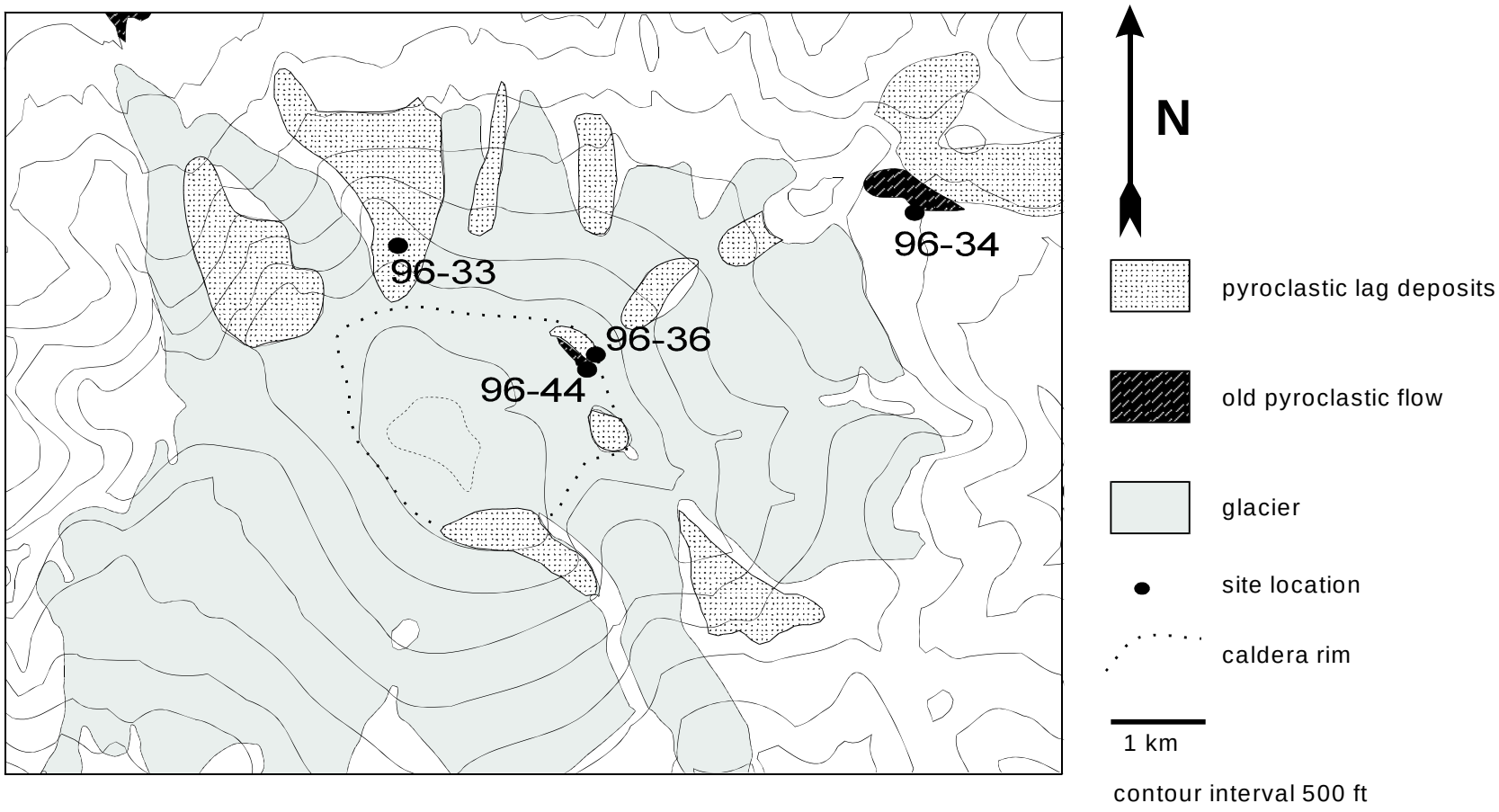

Fig. 4.12 Map of proximal caldera deposits.

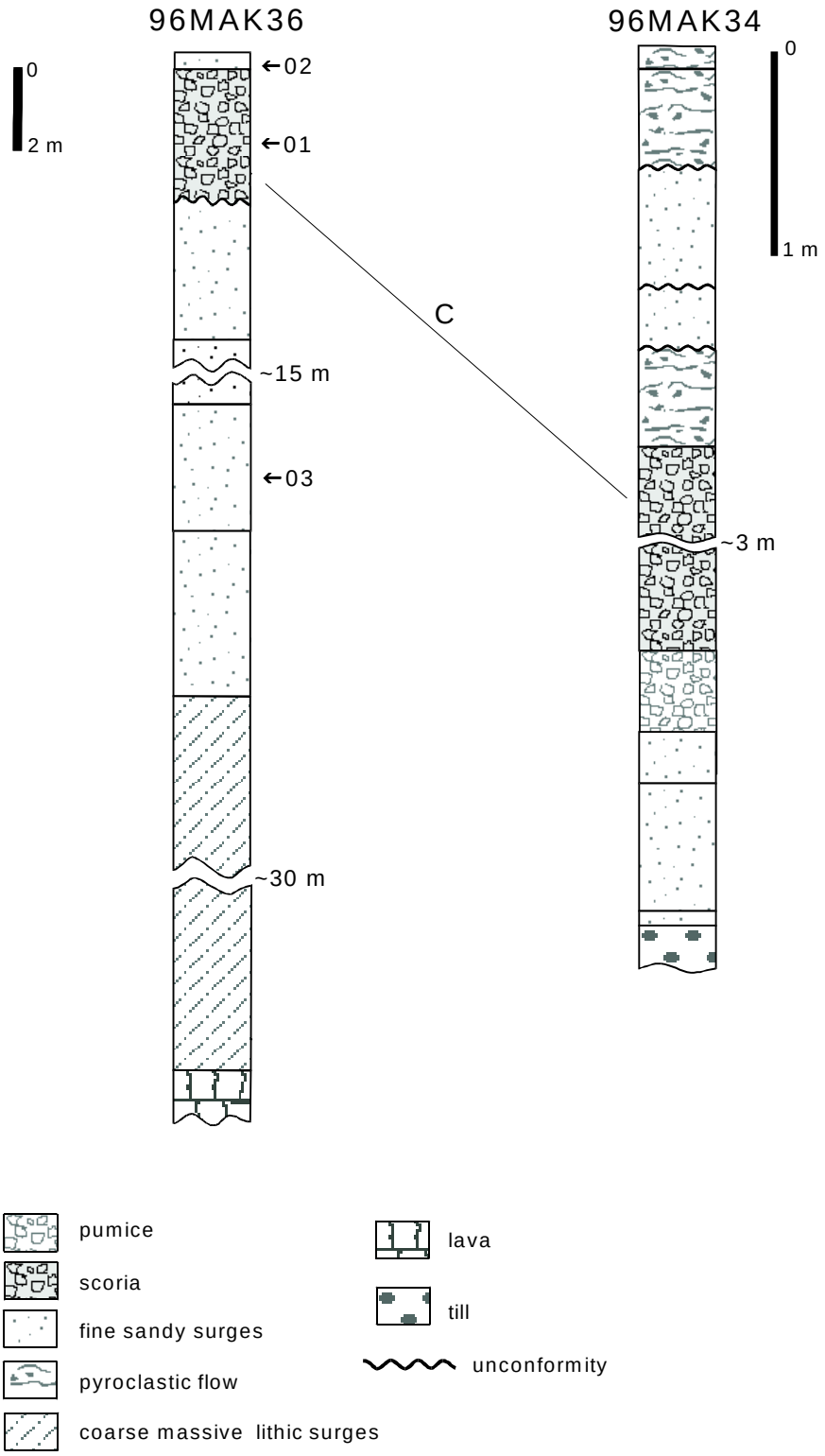

Fig. 4.13 Stratigraphic sections from the caldera rim and flanks. Correlation unit C described in chapter 5.

4.7 "Lava Ramp" Deposits

The feature to the east of Makushin known as the "Lava Ramp" consists of a massive andesite lava flow which fills a small portion of upper Makushin Valley and spills over the divide into the upper portions of Driftwood Valley (Fig. 4.14). Total volume is estimated to be 5 km^3 (Nye *et al.* 1986). $^{40}Ar/^{39}Ar$ age dates of <13 ka and <54 ka as well as the presence of glacial striations indicate that it is late Pleistocene in age (McConnell *et al.*, 1997). The "Lava Ramp" creates a broad flat divide between Makushin and Driftwood valleys. Tephras are generally well preserved here and are often intercalated with peat layers. Gullies, which form a parallel drainage pattern, provide excellent exposures. Site locations on "Lava Ramp" are indicated on Fig. 4.12.

The "Lava Ramp" is ideally situated to preserve tephras. Much of the plateau is too far from the source to preserve the smallest eruptions but close enough to record larger eruptions (VEI 2 and larger). It is located downwind from the dominant wind direction improving the chances for geologic preservation of ash fall deposits. The gently sloping surface features allow the development of many shallow bogs providing much datable organic material. In some areas the Holocene volcanic sediments have been dissected by ephemeral streams providing exposures of near complete Holocene eruption records. The majority of the upper and lower limiting age dates on tephras and the early Holocene eruptions came from these areas.

Stratigraphic sections from "Lava Ramp" reveal a similar depositional sequence to that seen in Makushin and Driftwood valleys (Fig 4.15). The deposits here, however, are thinner and are skewed towards airfall components of eruptions, as most heavy debris from the pyroclastic flows appears to have been channeled into and through valleys. The general stratigraphy is as follows: lava is overlain by a few tens of centimeters of tephras and peat which is overlain by 1 to 2 meters of dark scoria (traceable to lightly welded scoria at the summit) this is overlain by several meters of gray to orange oxidized clay commonly containing accretionary lapilli, sandy layers and

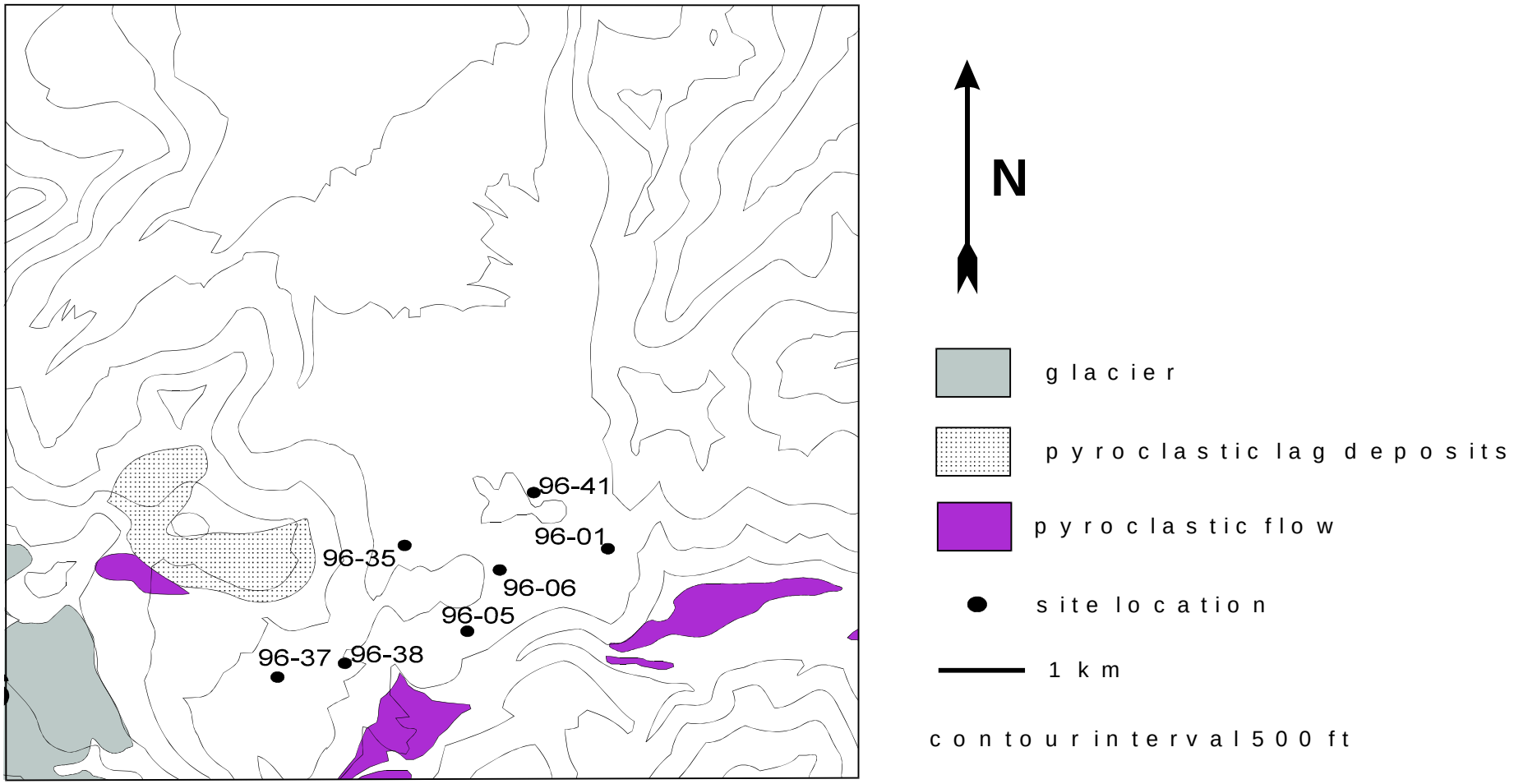

Fig. 4.14 Extents of "Lava Ramp" and sampling locations.

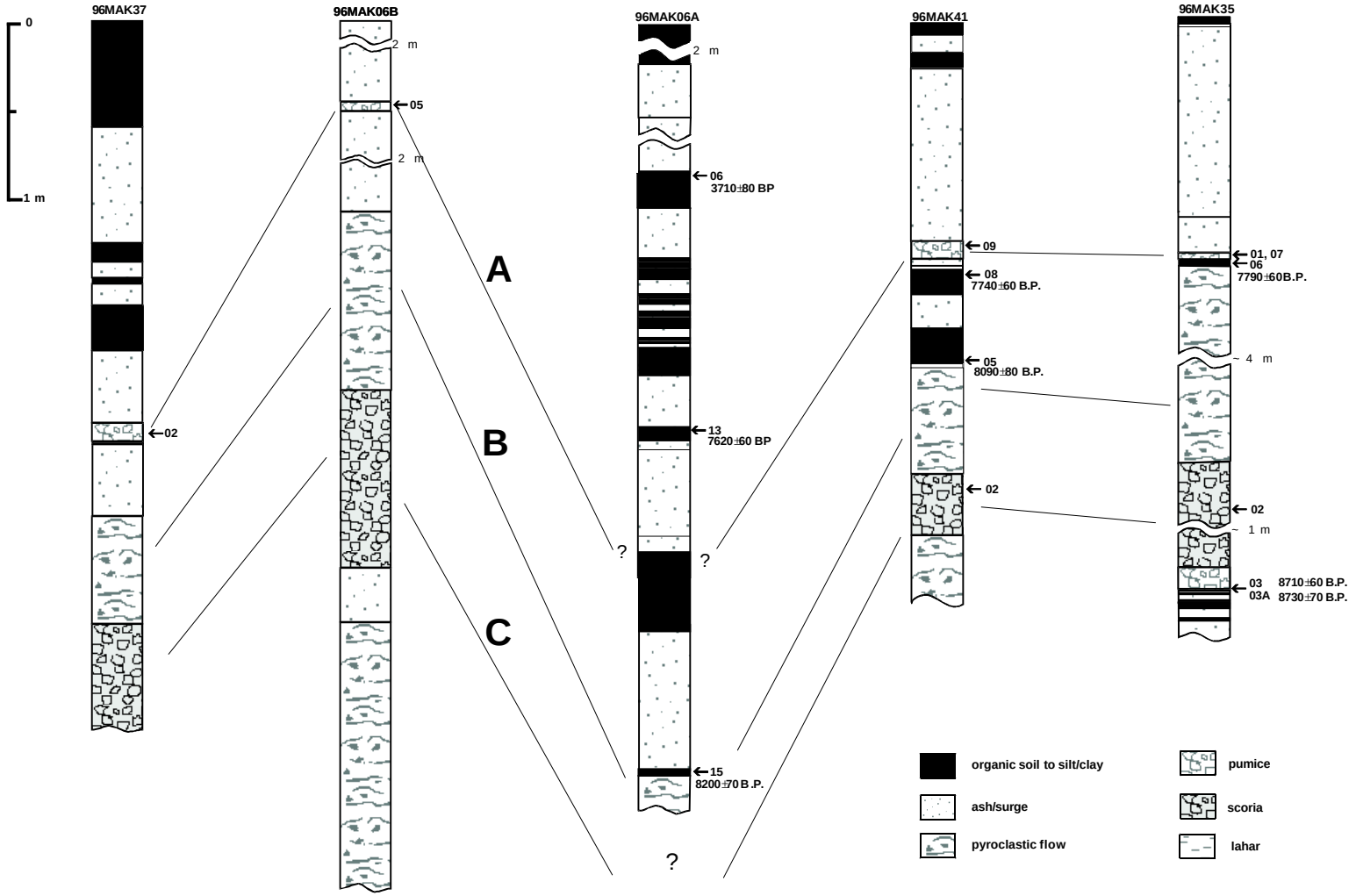

Figure 4.15 Simplified stratigraphic sections from “Lava Ramp” vicinity. See chapter 5 for discussion of correlati on units A,B,C, and D.

occasional scoria bombs. Under a petrographic microscope the clay rich unit contains a large percentage of very fine glass particles some of which appear to have altered to clay. In places this is then overlain by several meters of an orange to yellow massive, sandy, and poorly consolidated pyroclastic flow. This is in turn overlain by several meters of dark tephras and organic layers near the bottom of which is a distinct 10-30 centimeter yellow airfall pumice deposit. Age dates from the Lava Ramp provide upper limiting ages on the pyroclastic flow units (CFE2) and lower limiting age on the airfall component of the earliest Holocene eruption (CFE1) which are correlative with base surges in Makushin Valley.

4.8 Dutch Harbor Deposits

Distal deposits are well exposed in cliffs near Broad Bay, and in road cuts and natural cliffs in and around Dutch Harbor and as far away as Ugadaga Bay (Fig 4.16). The distal stratigraphy can also be correlated with that of Makushin valley and "Lava Ramp." In general, a thin pumice fall unit overlies two pyroclastic flow units separated by a thin soil corresponding to the two large early Holocene eruptions recorded nearer the Volcano.

Section 97MAK01 (Fig. 4.17) at Hog Island is representative of the distal deposits. Bedrock is overlain by soils mixed with thin airfall tephras. A distinct, several cm thick, poorly-sorted orange, coarse sandy flow unit lies above the soils. This flow unit is stratigraphically low in section and thought to represent the earliest large Holocene eruptions. It is informally named the earliest caldera forming event (CFE1) unit. The CFE1 is separated from overlying flow deposits by a thin (~2 cm) organic rich soil which locally contains charcoal fragments. Age dates for this deposit average around 8050 ^{14}C yr B.P. (Table 6.1). The CFE1 is not present at all localities suggesting a more restricted flow and smaller eruptive event, or poorer preservation than later large events.

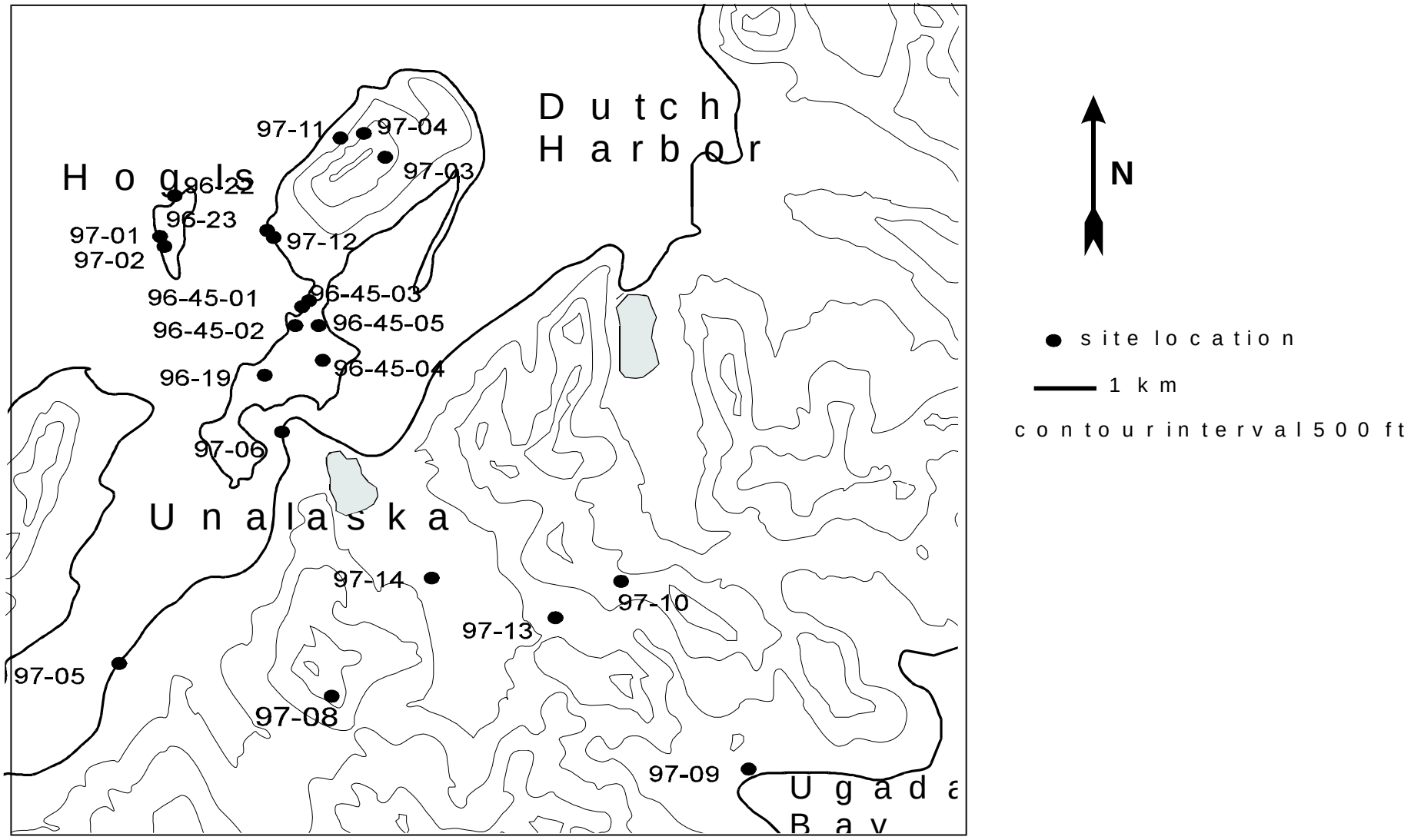

Fig. 4.16 Dutch Harbor sampling locations.

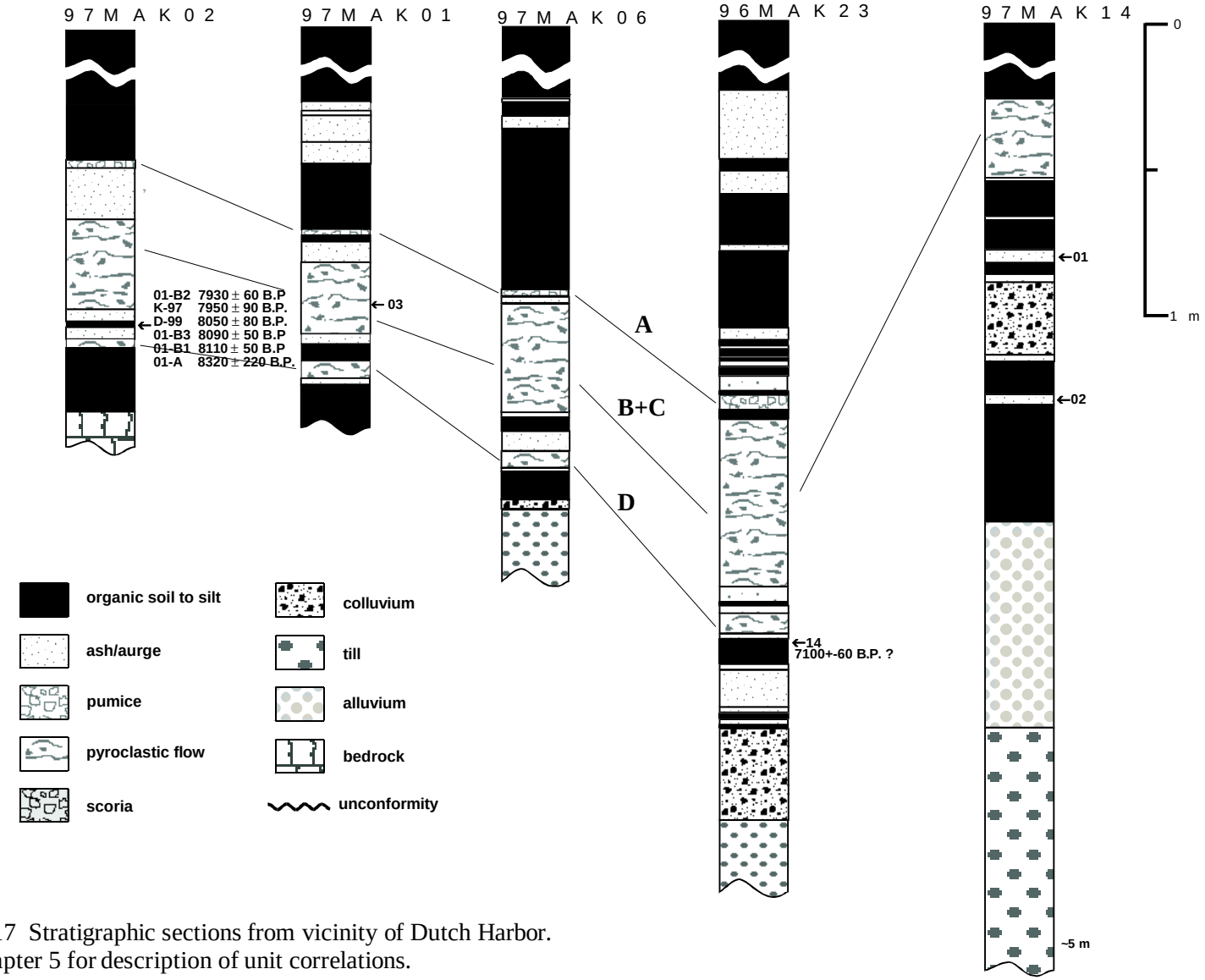

Fig. 4.17 Stratigraphic sections from vicinity of Dutch Harbor.
See chapter 5 for description of unit correlations.

Overlying the lower CFE1 unit is the distinct CFE2 unit. It is orange-red, poorly sorted and massive coarse sand with common pumice, scoria lapilli, and lithics. CFE2 is generally thicker (usually 20-30 cm) than CFE1 but is even thicker in some locations. The base of this unit locally is commonly red and very indurated. At a site near the airport (96MAK23), faint cross-bedding is present and scoria lapilli up to 2.5 cm diameter were found in the deposit (Fig. 4.25). The CFE2 is commonly underlain by several cm of dark gray well-sorted sandy tephras and is less commonly overlain by a thin (~1 cm) of fine orange ash. Several cm of gray ashy silt commonly separate the CFE2 from a thin 2 cm yellow pumice unit containing small glassy lithics. The pumice unit can be found in most distal sites and has been geochemically correlated with proximal deposits of the Driftwood Pumice. The pumice unit is overlain by several tens of cm of black and gray fine grained tephras and sandy to silty organic soils. A thick (.5 m) vegetative mat also containing black to gray tephras generally caps these deposits.

At site 97MAK14, CFE2 deposits were found overlying till from the only known moraine in the Dutch Harbor area. The moraine is exposed behind a local machine shop in Dutch Harbor, and apparently once stretched across what is today Unalaska Lake. The moraine is most likely latest Pleistocene to earliest Holocene in age.

Human artifacts are preserved in the thin soil (dated at ~8050 ^{14}C yr B.P.) underlying the CFE2 volcanic deposits on Hog Island. This horizon represents one of the oldest known human cultures in the Aleutian Islands according to archeologists Dr. Don Dumond professor emeritus at the University of Oregon and Dr. Rick Knecht, director of the Museum of the Aleutians in Dutch Harbor. Human occupation of the Dutch Harbor area ends with this horizon and does not reappear until approximately 4000 years later (Knecht, personal communication 1997). This suggests that the later caldera forming eruption (CFE2) strongly affected and perhaps destroyed local Aleut settlements, and forced any remaining local inhabitants to relocate. Consistent with

our three dates from the same horizon, Knecht (1997 personal communication) and Dumond (1999 personal communication) report age dates of 7950±90 ^{14}C yr B.P. and 8050±80 ^{14}C yr B.P. on soil from the cultural horizon.

The distal deposits are significant in that they provide the most compelling evidence about the violent nature and high mobility of the caldera forming eruptions. Soils here are better developed than in the areas proximal to the volcano and clearly indicate that there was more than one early large eruptive event.

Fig. 4.18 View of upper Lava Valley (A). Lava flows (a) overlie early Holocene pyroclastic flow deposits (b). Young lahars occupy most of the valley bottom (c) while terraces along the southern edge expose debris avalanche deposits (d). The high terraces (B) are composed of multiple deposits where lahars and tephras (e) overlie debris avalanche deposits (f). Note person at far left on terrace for scale.

Fig. 4.19 Debris avalanche deposits at Koriga Point (A). Cross-bedded surge deposits (B) are intercalated with avalanche deposits.

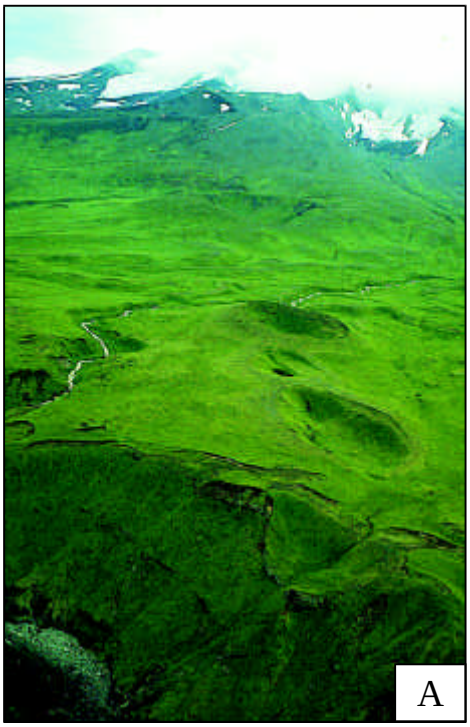

Fig. 4.20 Morphologically young tuff cones and maars along a linear fracture near Pt. Kadin (A), Peat dated in the youngest maar (B) is ~ 80 radiocarbon years old (note Angela Roach for scale).

Fig. 4.21 (A) View of Driftwood Valley deposits. Thick exposures (B) of the "Driftwood Pumice" are exposed in gullies (Deanne Pinney for scale).

Fig. 4.22 Makushin valley-fill (A). Exposure shows poorly consolidated flows (a), sintered ignimbrite (b), fluvial deposits (c), and base surge deposits (d). The steeply dipping base surge deposits (B) are interbedded with finer surge deposits but fine upwards overall. Note Jim Begét for scale in both photographs.

Fig. 4.23 Resistant sintered ignimbrite on flanks of Makushin (A). The ignimbrite can be traced to the caldera rim (B).

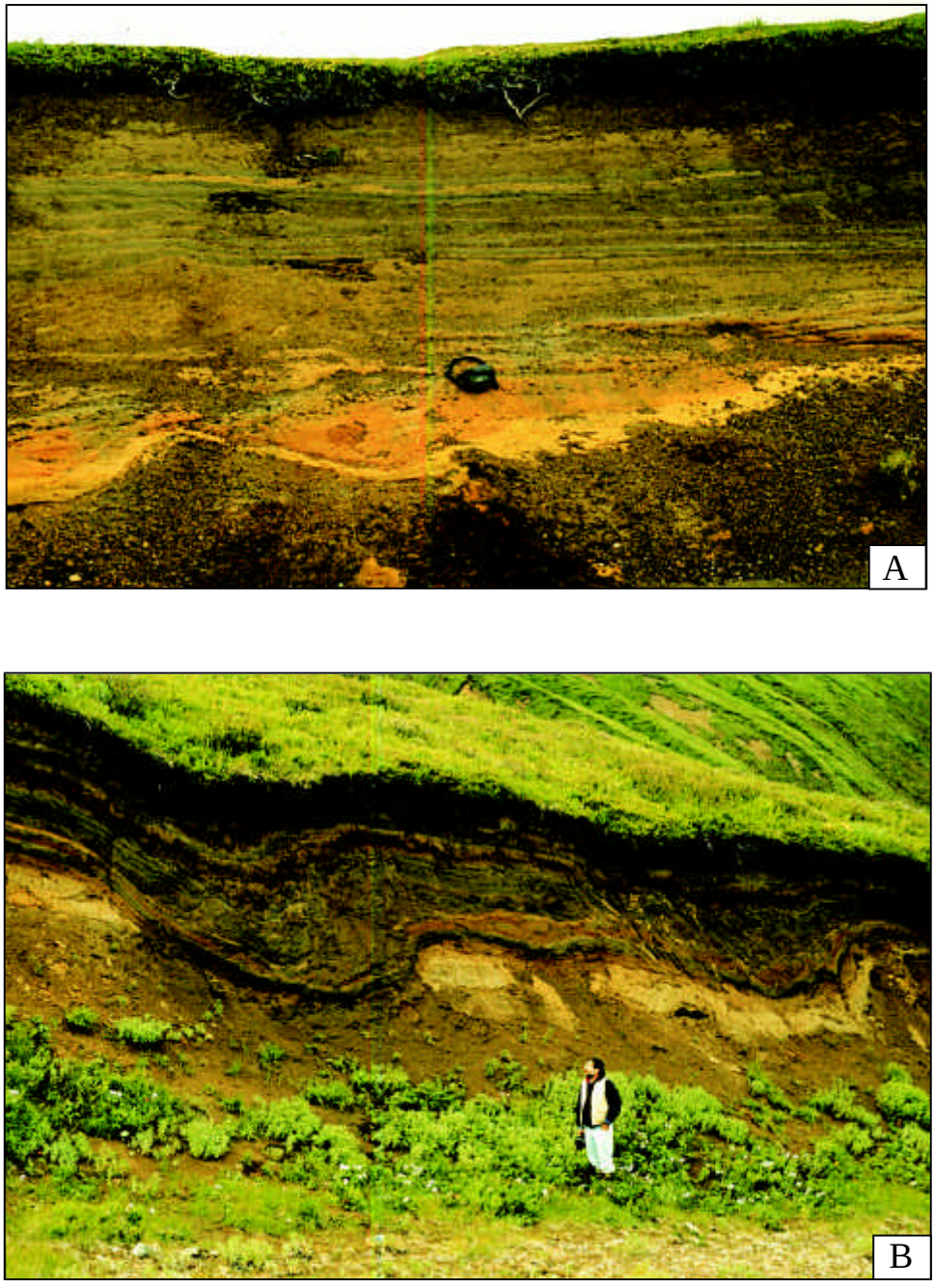

Fig. 4.24 Veneer deposits from the “Lava Ramp” (A). Stratigraphy is similar to valley-fill. Dark scoria is overlain by clayey orange and coarser orange brown flow deposits. These in turn are generally mantled by two to four meters of tephras (B).

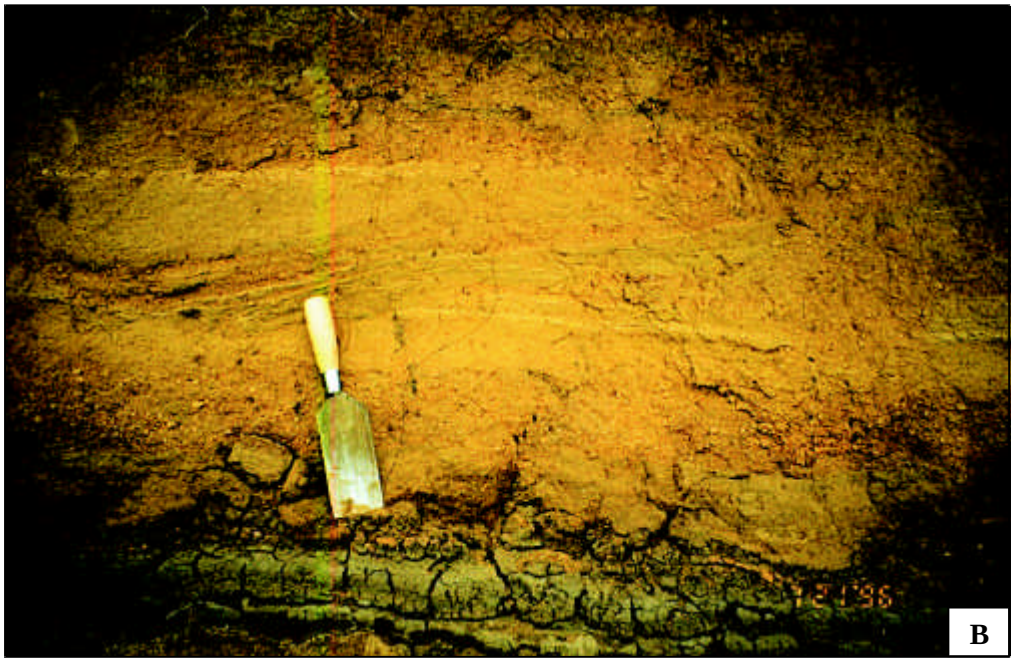

Fig. 4.25 (A) Distal volcanic deposits from large early Holocene eruptions CFE1 and CFE2. (B) Faint cross stratification in CFE2 deposits.

Chapter 5: Stratigraphic Correlations

Correlations of Makushin airfall, surge, and especially flow tephras are hampered by several factors. First, because of the glacial ice cap, there is a very little preservation of or exposed outcrop of Holocene tephras in areas proximal to the vent. Only ridges and aretes and a small portion of the caldera wall are exposed and even there only resistant semi-welded units are preserved. Second, lateral facies changes for deposits such as pyroclastic flows can be extreme over distances as small as a hundred meters. Valley filling pyroclastic deposits, for instance, can be nearly an order of magnitude greater in grainsize and thickness than the veneer deposits of Walker (1983). It is only by tracing these deposit directly from one to the other that we know that they were deposited contemporaneously. Third, facies changes of deposits with distance can be dramatic as well. Pyroclastic flows are known to segregate as they move. In the case of many deposits, especially young ones, this is not particularly a problem as individual deposits can be traced for great distances and changes observed. In the case of Makushin, however, there is a considerable spatial gap between the semi-proximal deposits and distal deposits. The entire lower portion of Makushin Valley is aggrading due to the abundant sediment carried in glacial streams. This has resulted in either the erosion or burial of all older volcanic deposits. In addition, the sea prevents the terrestrial preservation of distal deposits except to the east where only the most extreme distal deposits are preserved in Dutch Harbor. Even here, though, approximately five kilometers of bay and ten kilometers of alluvial filled valley separates semi-proximal deposits from distal deposits.

Stratigraphic correlations are therefore based on a combination of distinct traceable units, stratigraphic position, and age dates. Four volcanic units were most useful in constructing a stratigraphic framework for Makushin Holocene deposits. These units are designated units A, B, C, and D (Fig 5.1) and are described as follows.

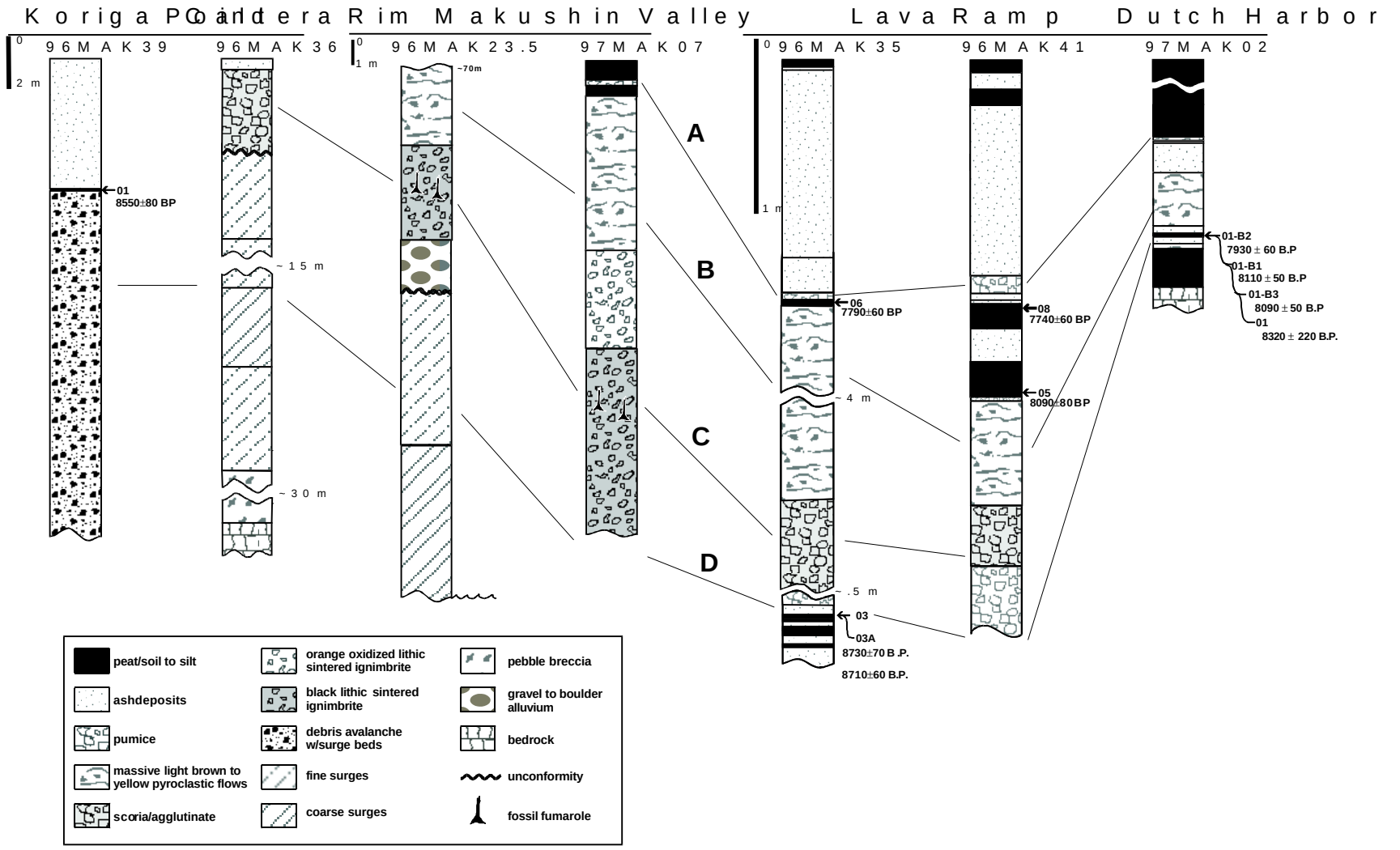

Fig. 5.1 Stratigraphic correlations of units A, B, C, and D from selected sites around Makushin Volcano.

5.1 Correlation A—(Driftwood Pumice)

Correlation A consists of the ubiquitous "Driftwood Pumice" unit. It is found in thicknesses of over a meter in Driftwood and Waterfall Valleys but is generally 15-20 cm thick in the Lava Ramp area and thins to approximately 2 cm thick in the Dutch Harbor area (Fig 5.2). It is easily recognized as a yellow, blocky pumice containing up to ~10% black glassy lithics. Proximally this unit may be underlain by a thin, fine, yellow ash (YA). Dates from under this deposit indicate that it is younger than ~7740 ^{14}C yr B.P. An age date of 5070 ^{14}C yr B.P. places an upper limit on its age although its stratigraphic position suggests that it is much closer in age to the lower limiting ages. Thick soils and tephras under this deposit however preclude the possibility that it was deposited shortly following the Holocene caldera forming eruptions. This deposit is distinct in the field and has a unique geochemistry; analyses are reported in Appendices 1 and 2.

5.2 Correlation B

Correlation B is a series of pyroclastic flow units defined as much by the distinct underlying scoria unit as by its own distinct qualities. Because this unit consists of pyroclastic flow units its characteristics vary dramatically from the valley fills to the lava ramp. In Makushin Valley for instance it is several meters of massive, loosely-consolidated orange silty ash deposit containing large black blocks and bombs. On "Lava Ramp" the deposit appears as at least two units locally, and ranges from 1 to more than 5 meters in thickness depending on the locality. The first lower unit here is a gray to orange/white clayey unit with common accretionary lapilli and occasional black bombs and scoria. This in turn is overlain by a coarser yellow-orange, sandy pyroclastic flow unit. Radiocarbon ages from organic samples (96MAK41-05, 96MAK6A-15) found near the "Lava Ramp" indicate that the deposits are ca 8140 ^{14}C yr B.P.

Distally this unit coalesces with unit C and is not distinct. In the Dutch Harbor it is an orangish-red to red with a sandy to silty, poorly sorted matrix containing pumice, scoria, and

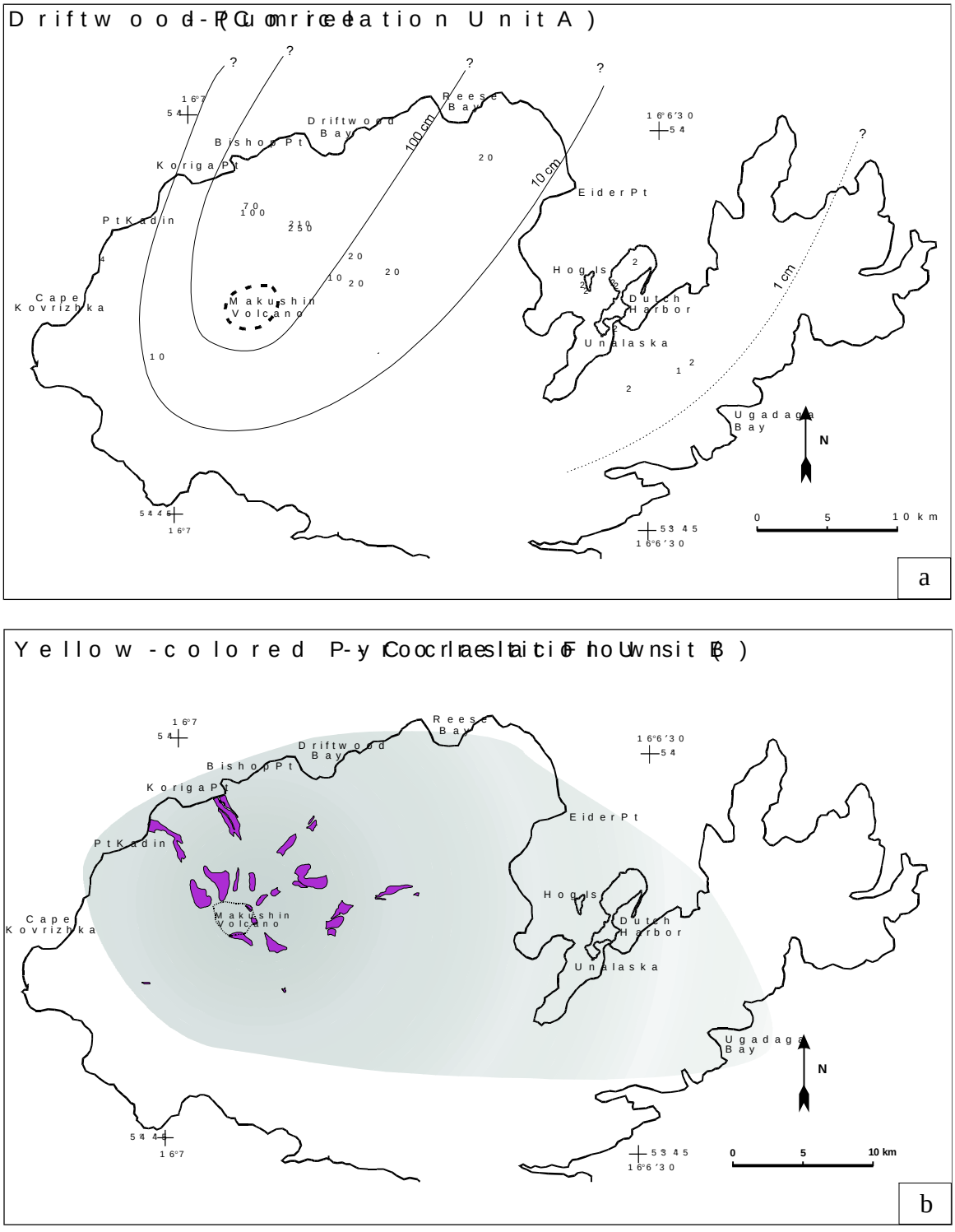

Fig. 5.2 Distribution maps of regionally correlated pyroclastic units. (a) Isopach map of Driftwood Pumice, Unit A (b) Distribution of yellow pyroclastic flows, Unit B. Shaded area represents approximate distribution of pyroclastic veneer and coignimbrite airfall components. Darkest shade where thickest.

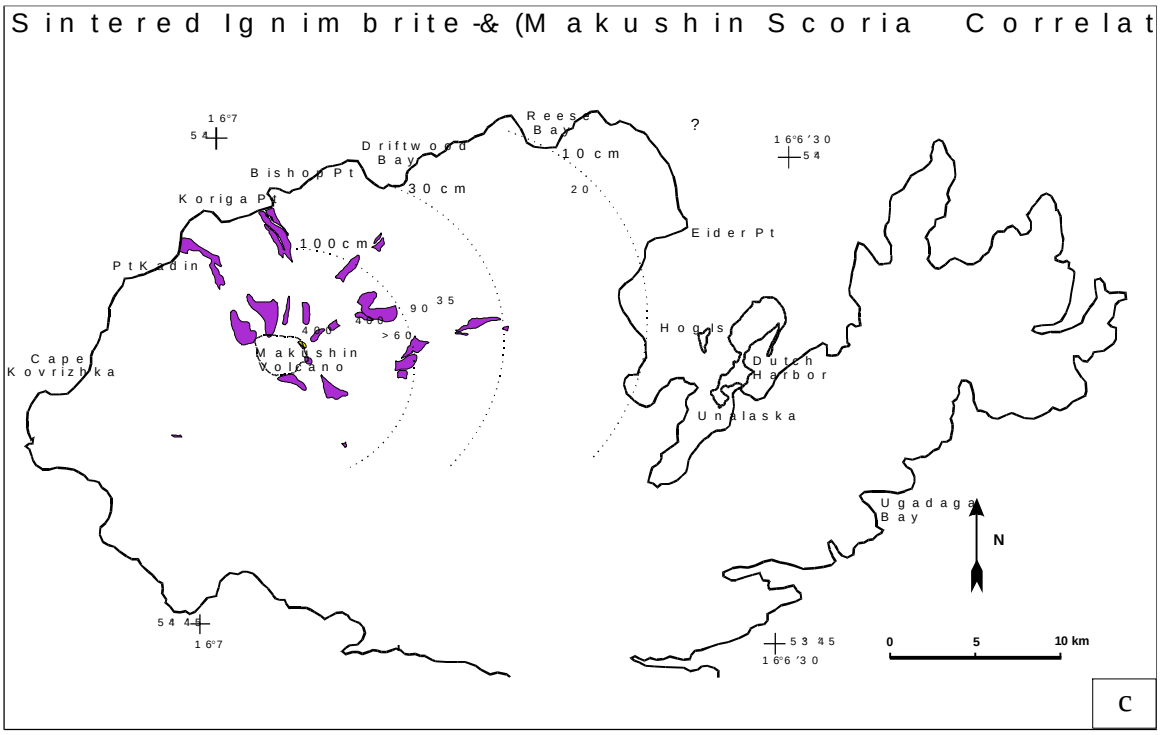

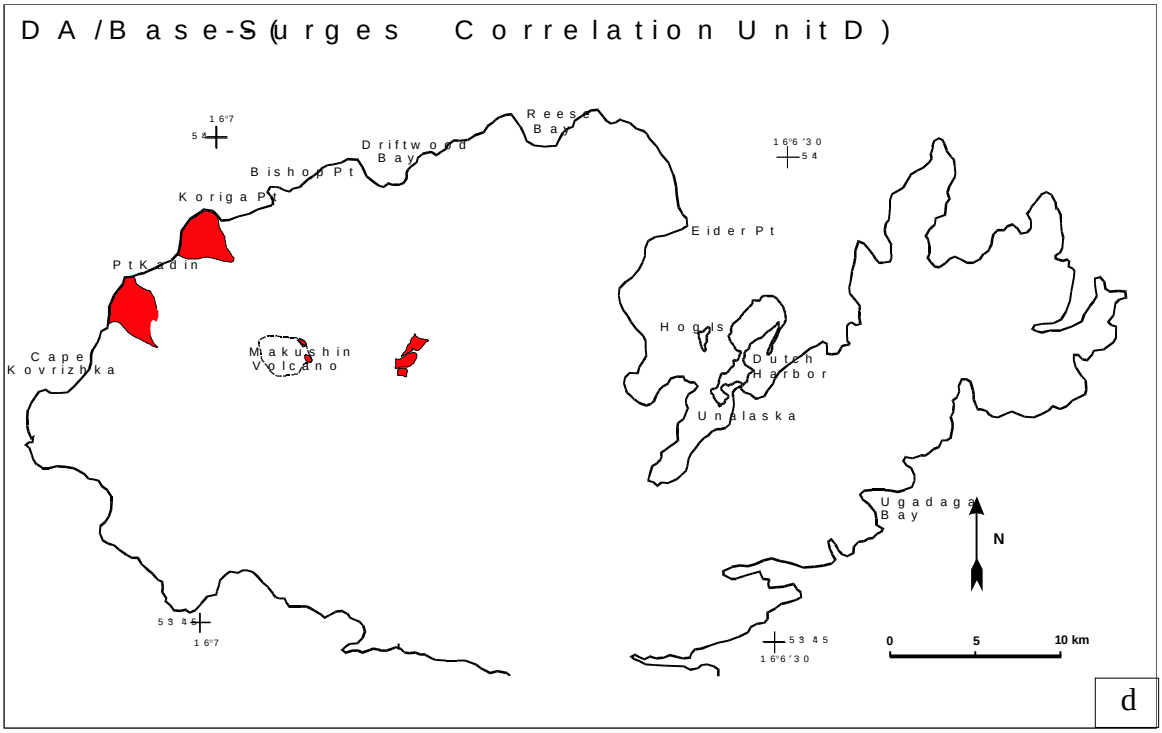

Fig. 5.2 cont. Maps of correlation units (c) sintered ignimbrite and Makushin Scoria, unit C and (d) debris avalanche and lithic base surge deposits. Contours isopach airfall components of unit C.

lithics. It is generally ten to several tens of centimeters thick. Clasts are scoria to pumice ranging from millimeters to a couple of centimeters in size. It is by far the thickest and most easily recognized distal unit.

5.3 Correlation C

Correlation C consists of a scoria flow/fall unit, about one meter thick on the lava ramp area where it appears to be mostly airfall. This unit is believed to be conformable with the overlying less consolidated pyroclastic flows. It can be traced to several meters of black, welded, cliff-forming ignimbrite in pyroclastic fans occupying upper Makushin Valley. Similar looking cliff forming units can be seen in Driftwood Valley. In Makushin Valley this unit unconformably overlies flood deposits which overlie dipping base surge deposits in Makushin Valley. It forms a resistant cap unit on the flanks of Makushin and can be traced to the caldera rim where it forms a very distinct 2 m thick semi-welded black agglutinate. Near the volcano, the base of this unit is underlain by mixed oxidized yellowish pumice and scoria associated with the earliest large Holocene eruption (CFE1). At the caldera rim it is underlain by several tens of meters of reddish-pink to tan surges and pebble breccias (Unit D). In the Dutch Harbor area unit C best correlates stratigraphically to the distal pyroclastic unit described as the layer 3 of the CFPF, a well sorted dark sandy scoria layer.

An angular unconformity between correlation unit C and underlying units at the caldera rim as well as in Makushin Valley indicates that unit C is not conformable with unit D. Correlation units B and C are conformable and considered individual flow units from the same eruptive event. Geochemical analyses of juvenile clasts from these flows supports this interpretation as well (Appendix II). Correlation units B and C are collectively referred to as the second early Holocene caldera forming event (CFE2). Age dates directly under units B and C at distal locations indicate an emplacement age of approximately 8050 ^{14}C yr B.P.

5.4 Correlation D

Steeply dipping base surge deposits in the lowest stratigraphic portions of Makushin Valley are defined as Correlation D. They are assumed to be correlative to surges and pebble breccias observed at the caldera rim. Based on age dates and similar looking lithology and textures the debris avalanche deposits, so prominent on the north side of the volcano, are also considered part of the correlation unit. These debris avalanche deposits show evidence of surges intercalated in them. This is similar to steeply dipping base surge deposits in the lowest portions of Makushin Valley. Soil directly overlaying debris avalanche deposits at Koriga Point has been dated at 8550 ^{14}C yr B.P. This is consistent with relative ages for the coarse base surges in Makushin Valley and surges and pebble breccias at the caldera rim. Distally, the thin pyroclastic flow unit (CFE1) under the ~8050 ^{14}C yr B.P. horizon is logically correlative. Collectively these deposits represent the first large early Holocene eruptive event (CFE1). The 8720 ^{14}C yr B.P. age below the CFE1 airfall component on the "Lava Ramp" provides a lower limiting age for this event. This is consistent with an 8550 ^{14}C yr B.P. age date on soil overlying the debris avalanche deposits near Koriga Point and with age dates in overlying CFE1 deposits near Dutch Harbor.

Chapter 6: Discussion of Radiocarbon Age Data

Twenty-five radiometric age determinations from organic samples were received from Beta Analytic Inc. of Miami, Florida. Measured ages were calculated using a ^{14}C half-life of 5568 years. Ratios of $^{13}C/^{12}C$ were directly measured on samples analyzed by AMS and estimated for samples analyzed with conventional dating techniques (see Appendix V for discussion of radiometric dating method and stable isotope corrections). Estimated stable carbon isotope ratios were based on values typical of the material type. The reported conventional ^{14}C age represent the measured age after measured or estimated $^{13}C/^{12}C$ ratio corrections were applied. Measured and estimated $^{13}C/^{12}C$ ratios were calculated relative to the PDB-1 international standard and the RCYBP ages were normalized to –25 ‰. All samples were pretreated with a hot acid/alkali/acid baths to remove unwanted carbonate material and secondary carbon components with the exception of soil samples which only underwent acid washes since there is the greater potential that the primary carbon is soluble in alkaline solutions. Conventional dating techniques were used for the majority of samples with ten exceptions. Six samples were given extended counting times due to small sample size and four samples were dated with the AMS technique. Ages ranged from 8800 ^{14}C yr B.P. to 150 ^{14}C yr B.P. (Table 6.1).

With conventional dating, measurement of stable carbon isotope ratios is not routine and fractionation ratios are usually estimated based on values typical of the identified material type. Direct measurement of stable carbon isotopes can lead to increased accuracy, especially in cases where unidentified plant material is used. Stable isotope ratios were not measured on our peat samples with one exception, sample 96MAK03-24, where AMS dating was necessary. On sample 96MAK03-24 stable isotope measurements revealed that $\delta^{13}C$ values for Makushin peat is –29.5 ‰ relative to the PDB-1 standard suggesting that –25 ‰ estimated for conventionally dated peat material is inappropriate for our samples. Conventional ages for our peat samples have

Table 6.1: Stable isotope corrected radiocarbon age dates associated with Holocene deposits at Makushin Volcano.

Sample Number	Laboratory Number	Measured ^{14}C Age (BP) ± 1 stdev	$d^{13}C_{PDB}$	$d^{13}C$ Corrected ^{14}C Ages	Calendar Age Intercepts** (BP)	Material	Comments
96MAK07-01	Beta-98516	150±60[c]	-29.5‰*	80 ±60[c]	0	peat	Maximum age on youngest observed tephra
96MAK03-24	Beta-98511	1640±60[a]	-29.5‰	1640±60[a]	1530	peat	Maximum age on multiple tephras, Lava Ramp
96MAK12-02	Beta-98519	1640±60[c]	-29.5‰*	1570±60[c]	1420	peat	Maximum age on tephra deposits, Glacier valley
96MAK09-09	Beta-98517	2250±80[c]	-29.5‰*	2180±80[c]	2150	peat	Minimum age on Glacier valley debris avalanche
96MAK28-11	Beta-105994	2940±60	-29.5‰*	2870±60	2960	peat	Maximum age on surges in lower Makushin Valley
96MAK11-02	Beta-98518	3030±70	-29.5‰*	2960±70	3080, 3090, 3110	peat	Upper limit on avalanche, lower limit on lahar, Glacier valley
96MAK03-44	Beta-105991	3450±70[c]	-29.5‰*	3380±70[c]	3630	peat	Maximum age on at least 24 recent tephras, Lava Ramp
96MAK06A-06	Beta-98513	3780±80	-29.5‰*	3710±80	3990, 4030, 4080	peat	Maximum age on upper surge and tephra deposits, Lava Ramp
Nye83	Beta-7657	4280±230			4840		Upper limiting age on Glacier valley debris avalanche and lahars
96MAK03-50	Beta-98512	4980±90	-29.5‰*	4910±90	5640	peat	Maximum age multiple tephras, Lava Ramp
96MAK28-14	Beta-98521	5140±160[c]	-29.5‰*	5070±160[c]	5760, 5820, 5880	peat	Maximum age on thick pyroclastic deposits, Lava Ramp
96MAK32-10	Beta-105995	5640±70	-29.5‰*	5570±70	6320, 6340, 6370, 6390	peat	Minimum age on thick pumice, Little Driftwood valley
96MAK32-11	Beta-105996	5950±80	-29.5‰*	5880±80	6720	peat	Minimum age on thick pumice, Little Driftwood valley
96MAK23-14	Beta-105993	7100±60	-25.0‰*	7100±60	7910	soil	Under CFE1 in Dutch Harbor (Probable rootlet contamination)
96MAK06A-13	Beta-98514	7690±60	-29.5‰*	7620±60	8370	peat	Minimum and maximum age on two surge deposits, Lava Ramp
96MAK21B-10	Beta-98520	7710±80	-29.5‰*	7640±80	8400	peat	Lower limit on caldera-forming deposits, Broad valley (Probable rootlet contamination & WWII disturbance)
96MAK41-08	Beta-98525	7810±60	-29.5‰*	7740±60	8440, 8470, 8480	peat	Maximum age on pumice airfall, Lava Ramp
96MAK35-06	Beta-98523	7860±60	-29.5‰*	7790±60	8510, 8530, 8540	peat	Minimum age on caldera-forming deposits, Lava Ramp
97MAK02-01-B2	Beta-117194	7930±60[a]	-25.0‰	7930±60[a]	8710, 8690, 8660	charcoal	Maximum Age on caldera-forming deposits, Hog Island
Reeder83	Beta-7655	7950±90			8940,8920,8800,8720,8680		Upper limiting age on caldera-forming deposits, Lava Ramp
Dumond99	Beta-132225	8050±80[c]	-25.3‰	8050±80[c]	8980	charcoal	Maximum Age on caldera-forming deposits, Hog Island
Knecht97	Beta-109822	7950±90[a]	-25.4‰	7950±90[a]	8940,8920,8800,8720,8680	charcoal	Maximum Age on caldera-forming deposits, Hog Island
97MAK02-01-B3	Beta-117195	8090±50[a]	-24.3‰	8090±50[a]	8990	charcoal	Maximum Age on caldera-forming deposits, Hog Island
97MAK02-01-B1	Beta-117193	8110±50[a]	-25.2‰	8110±50[a]	8990	charcoal	Maximum Age on caldera-forming deposits, Hog Island
96MAK41-05	Beta-98524	8160±80	-29.5‰*	8090±80	8990	peat	Minimum age on caldera-forming eruptions, Lava Ramp
96MAK06A-15	Beta-98515	8270±70	-29.5‰*	8200±70	9170, 9180, 9200	peat	Minimum age on caldera-forming deposits, Lava Ramp
97MAK02-01-A	Beta-106905	8320±220[c]	-25.0‰*	8320±220[c]	9370, 9290, 9270	charcoal	Maximum Age on caldera-forming deposits, Hog Island
96MAK39-01	Beta-105998	8550±80	-25.0‰*	8550±80	9490	soil	Minimum age on Koriga Point debris avalanche
96MAK35-03A	Beta-105997	8780±60	-29.5‰*	8710±60	9650, 9780	peat	Maximum age on caldera-forming deposits, Lava Ramp
96MAK35-03	Beta-98522	8800±70	-29.5‰*	8730±70	9650, 9770, 9810	peat	Maximum age on caldera-forming deposits, Lava Ramp
Caldera-Formation (CFPF)				**8050±30**	**8960**		**Avg. of Knecht97, Dumond99, 97-01-02-A, 97-01-02-B1, 97-01-02-B2, and 97-01-02-B3**
Upper Limit on Caldera Formation				**8140±60**	**8990**		**Avg. of 96-41-05 and 96-06A-15**
Lower Limit on CFE1				**8720±50**	**9650, 9770, 9790**		**Avg. of 96-35-03 and 96-35-03A**

[a] indicates AMS date [c] indicates sample was given extending counting time *estimated value **Stuiver and Reimer, 1993

been recalculated using $\delta^{13}C$ values of –29.5 ‰ (Table 6.1). Recalculated ages are on average 70 radiocarbon years younger than reported measured ages. These ages correlate better with nearly equivalent AMS age dates and more accurately reflect the true conventional ages for Makushin peat samples. Because isotope ratios are directly measured on all AMS dated samples these ages are more accurate and are most likely to reflect the true age of the deposits. Stable isotope ratios for the AMS dated peat sample (96MAK03-24) suggests that carbon fractionation by some Aleutian plants significantly differs from that of wood. Previously reported conventional age dates on Aleutian peats that have not been corrected for carbon fractionation with measured stable isotope ratios may contain systematic errors which can approach 250 years.

All ages are in accord with known stratigraphic order, providing a small measure of quality assurance. However, at least two dates, 96MAK23-14 and 96MAK21B-10, are thought to have been contaminated by young organic material in the form of live rootlets. AMS age dates on more reliable charcoal (97MAK02-01x) from the same or higher organic horizons give older ages. The organic material in the first case (96MAK23-14) was a poorly developed soil and therefore among the least reliable materials dated for this study. Both sampling sites were near Dutch Harbor and, while local disturbance was not apparent, were in areas obviously occupied or used by the military during WWII.

Bracketing ages for two large early Holocene eruptive events were obtained. In addition age constraints were put on younger debris avalanches, lahars, lava flows and airfall pumice deposits in Glacier, Lava, Bishop Point, and Driftwood valleys. Late Holocene eruptive frequencies were also obtained as a result of age dates. Figure 6.1 illustrates the volcanic depositional history of several regions proximal to Makushin Volcano. Age dates are juxtaposed to a chronological sequence of deposits for each region. Shaded regions represent possible age ranges for specific deposits.

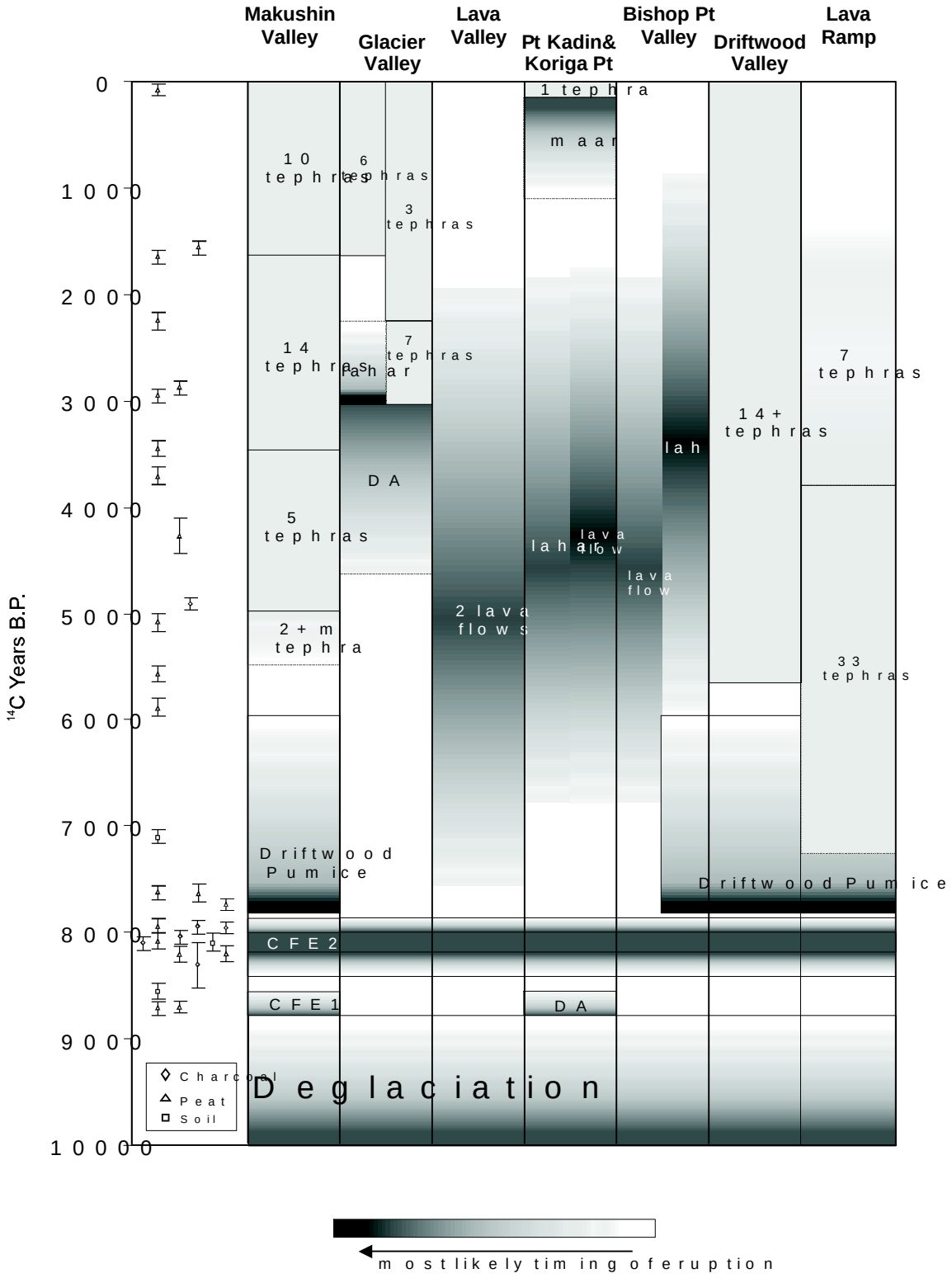

Fig. 6.1 Age constraints on eruptive events in selected valleys. Errors given for 1 sigma.

While correlations between proximal and distal caldera forming deposits are very strong, initial examination of age dates suggests a discrepancy between proximal and distal age dates. An average of upper limiting age dates on peat from the "Lava Ramp" indicate that correlation units B and C are 8140 ±60 ^{14}C yr B.P. The upper age limit is supported by samples 96MAK41-05 and 96MAK6A-15 (Table 6.2). Furthermore samples higher in the section (96MAK41-08, 96MAK35-06, and 96MAK6A-13) give slightly younger age dates (Table 6.2) than their lower counterparts as one would expect from stratigraphically younger material. Nearly equivalent AMS dates under distal CFE2 deposits give an average of 8030±40 ^{14}C yr B.P. Supporting lower limiting ages on charcoal fragments, are provided by samples 97MAK02-01-B1, 97MAK02-01-B2, 97MAK02-01-B3, Knecht97 and 97MAK02-01A. Although corrected age dates on proximal overlying peats are slightly older than age dates on the distal underlying charcoal fragments these bracketing ages are statistically the same at the 95% confidence level (Fig. 6.2). Additionally, calibrated age intercepts for upper and lower limiting ages are essentially the same and converge on 8990 cal yr B.P. (Table 6.1).

An average of dates on samples (96MAK35-03, 96MAK35-03A) under thin airfall pumice deposits on Lava Ramp correlated to the earliest caldera forming event give a lower limiting age of 8720±50 ^{14}C yr B.P. A date on a soil sample (96MAK39-01) above debris avalanche deposits at Koriga Point provides an upper limiting age of ~ 8550±80 ^{14}C yr B.P. on the earliest large Holocene eruption (Fig. 6.2).

We have reinterpreted the Reeder (1983) age date to be an upper limiting date on CFPF deposits on Lava Ramp. The Nye (1986) date has also been reinterpreted as an upper limiting age on debris avalanche and lahar deposits in Glacier valley. Sample 96MAK41-08 provides a close limiting date under the Driftwood Pumice of 7740±60 ^{14}C yr B.P. Younger age dates provide limiting dates on mid- to late-Holocene tephras (Fig. 6.1).

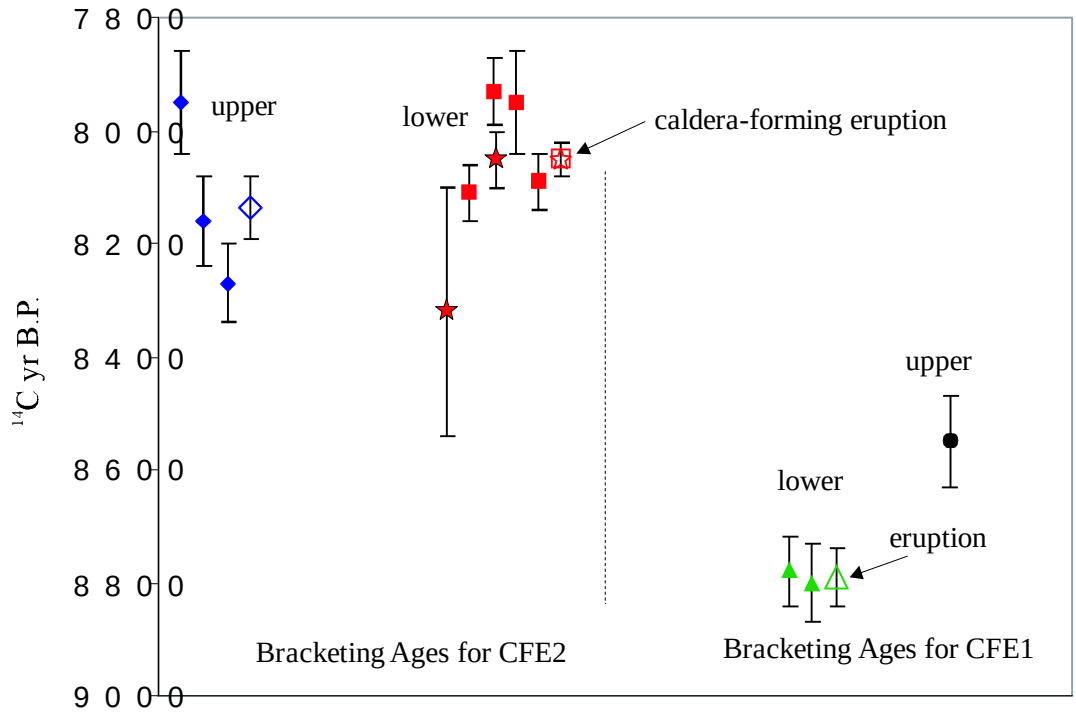

Fig. 6.2 Stable-isotope corrected bracketing ages for early Holocene eruptions of Makushin. Triangles and diamonds represent conventional age dates on peat, circles represent conventional age dates on soil, squares are AMS dates on charcoal, and stars are conventional dates on charcoal. Unfilled symbols represent averages of adjacent age dates. Upper and lower limiting age dates for CFE2 are statistically the same at the 95% confidence level.

Chapter 7: Discussion of Geochemical Data

7.1 Whole Rock Major and Trace Element Data

Whole rock compositions of major and trace elements for Makushin tephras are typical of convergent margin magmas. The tephras plot from the basaltic andesite to low silica dacite fields of LeBas *et al.* (1986) although most tephras analyzed are andesitic (Fig. 7.1). Tephras from Makushin fall into the tholeiitic geochemical field (Fig 7.2) of Miyashiro (1974). This is consistent with Makushin whole rock data reported by Nye *et al.* (1986) and McConnell *et al.* (1997) and is consistent with Aleutian arc rocks in general. Trace element concentrations from tephras (Fig. 7.3) suggest that they share the same or very similar parent magmas and/or similar magmatic evolution paths. Major and trace element whole rock data is presented in Appendix II.

Blocks, bombs, and scoria from valley-filling pyroclastics are mostly high silica andesite (SiO_2 ~60%) and are otherwise geochemically similar suggesting that multiple ash flows came from a single relatively homogenous magma source and most likely from a single eruptive event. At least some juvenile material (96MAK36-03) from surge deposits at the summit underlying flow unit C is basaltic. The Driftwood Pumice, a later deposit, is also andesitic and overlaps the valley-fill deposits compositionally One relatively young pumice deposit (96MAK14-01) found in Lava valley is also basaltic. This suggests that magma compositions have fluctuated over time as opposed to a slow progression from mafic to silicic magma.

7.2 Electron Microprobe Major Element Data

More than 50 glass shard samples were analyzed using electron microprobe analysis (EMA). Tephras were selected based on their potential as local and/or as possible regional tephras. Several tephras from suspected exotic sources were analyzed as well. Approximately 20 late Holocene mafic tephras from a single stratigraphic section were analyzed to characterize chemical variations in the magmatic system over time. One goal was to geochemically

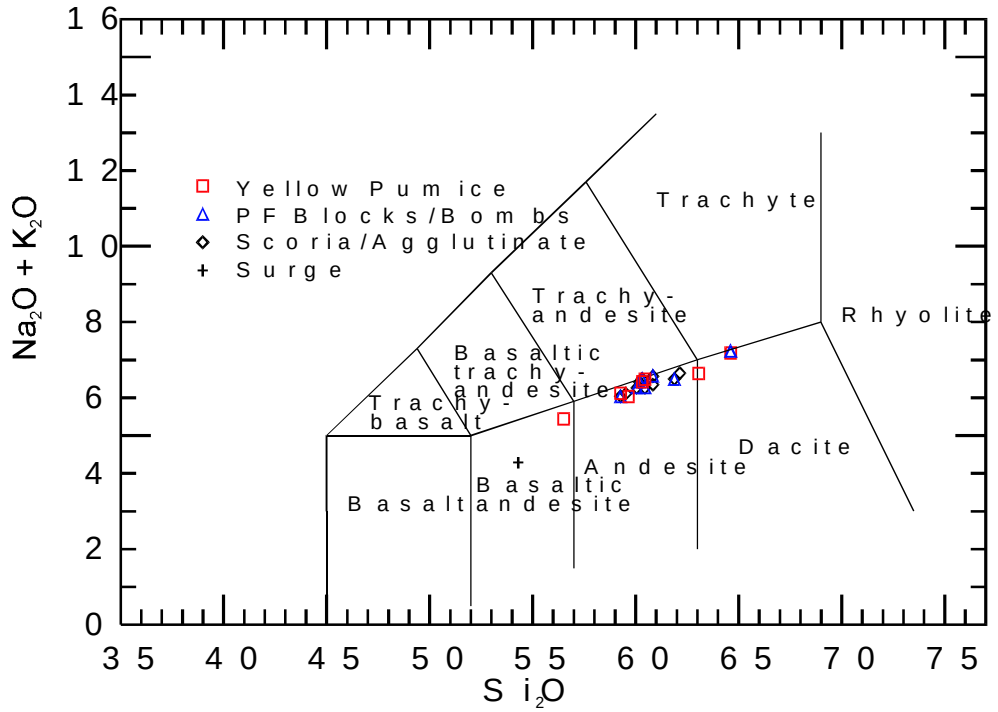

Fig. 7.1 Total alkalis vs. silica diagram showing volcanic rock fields and whole rock data for Holocene Makushin tephras.

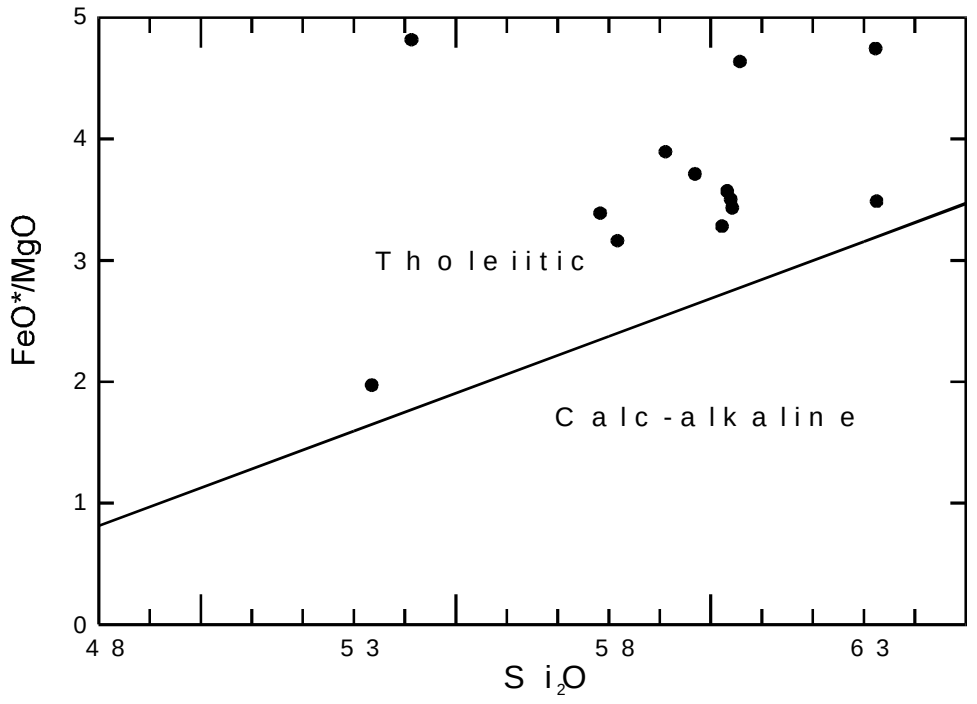

Fig. 7.2 FeO*/MgO diagram showing tholeiitic and calc-alkaline fields (after Miyashiro, 1974). Data is Makushin whole rock data for Holocene tephras. Total Fe expressed as FeO.

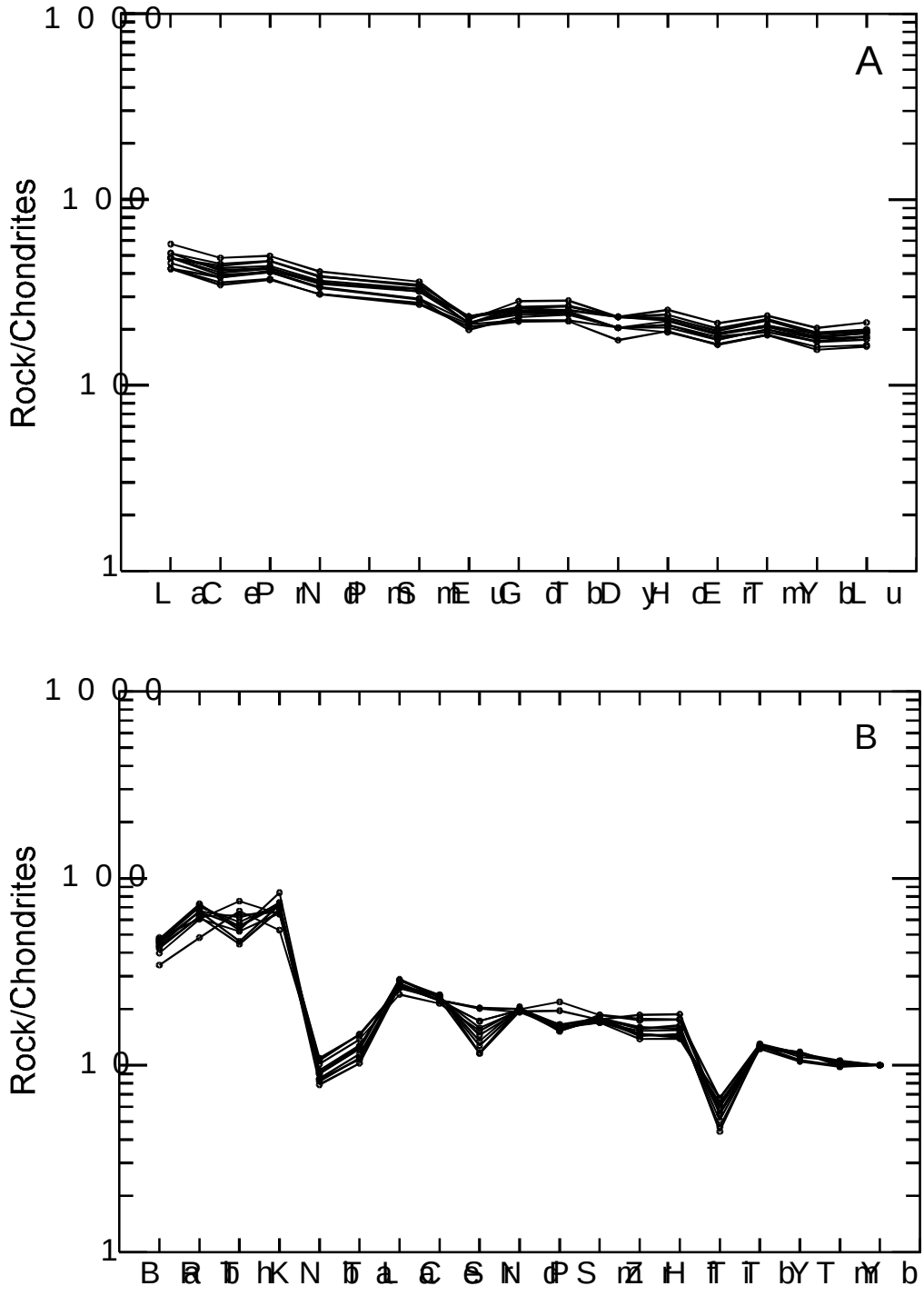

Fig. 7.3 Whole rock trace element spider diagrams for Makushin tephras. Chondrite normalization data are from Nakamura (1974), and Thompson (1982) for A and B respectively.

characterize these tephras and add them to the growing data base of Aleutian tephras. Glass compositions ranged from basaltic andesite to rhyolite in composition though the majority was dacitic (Fig. 7.4). In general tephra glass was up to 10% more silicic than whole rock compositions. Results of EMA analysis are presented in Appendix I.

7.3 Geochemical Correlation of Tephras

A major goal was to geochemically correlate the most significant tephras to be used as local and potentially regional chronostratigraphic markers. Correlation of tephra from site to site is usually done by comparison of major element geochemistry, stratigraphic relationships, and geochronology. The most useful means of tephra characterization has been to geochemically analyze discrete (glass) grains using the electron microprobe (Begét *et al.*, 1991b). Extensive regional tephras have been successfully used as chronostratigraphic markers in many interdisciplinary studies in Alaska (Riehle 1985, Beget *et al.* 1994, 1991a & 1991b, Begét and Keskinen 1991).

Statistical comparison of multivariate geochemistry is most often and most simply done by calculating similarity coefficients (Borchardt *et al.* 1972). Similarity coefficients compare the geochemical likeness of one sample to another based on sets of oxide analytical data. The similarity coefficient is an average ratio of mean normalized elemental concentrations in any two analyses (see Appendix IV for a more detailed explanation).

This method produces a coefficient between 0 and 1 with 1 being an exact match in all categories. In general, SC values = 0.94-.95 are considered to indicate equivalence of ash samples and SC values from < 0.90 are considered to be from two geochemically dissimilar samples SC values between 0.90 and .94 are considered to be from the same source volcano but are not considered to be from the same eruption (Begét *et al.* 1992). Generally only major oxides are used whose elemental oxide concentrations are > 0.5 wt. %, oxides with lower concentrations

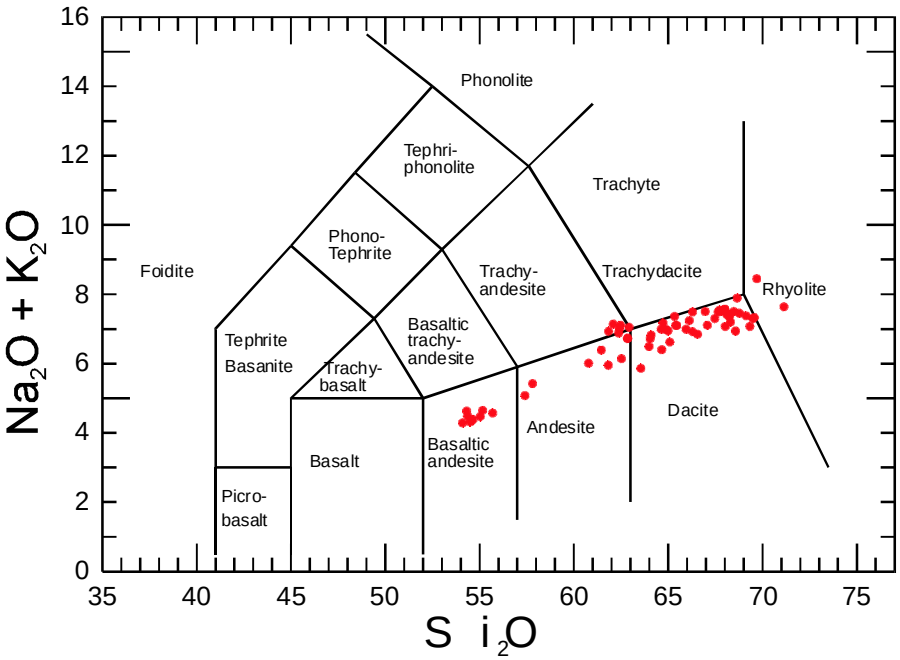

Fig. 7.4 Glass shard data from Makushin tephra plotted on a total alkalis vs. silica variation diagram. Classification and discrimination lines from LaBas and others (1986).

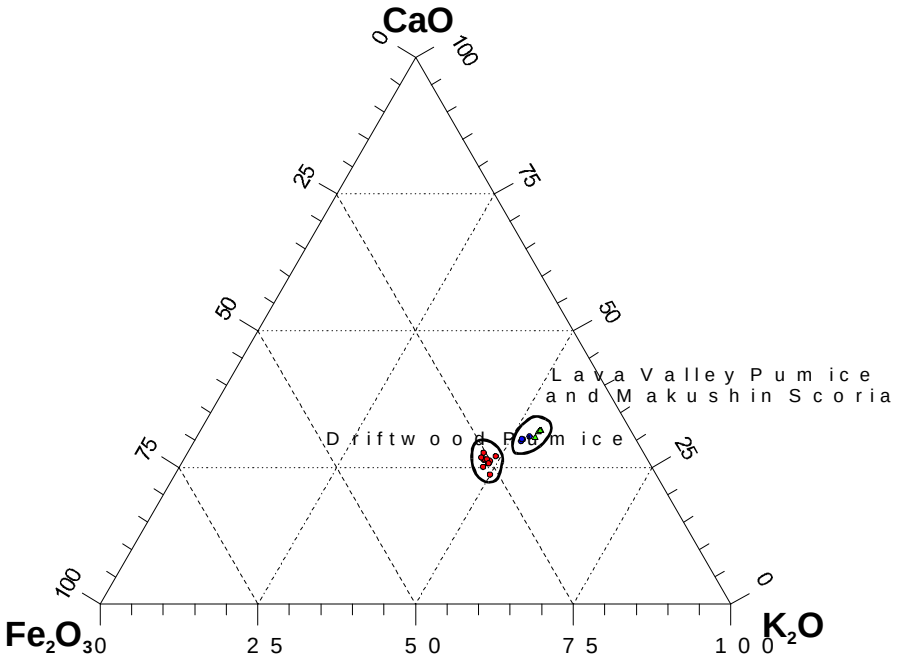

Fig .7.5 K_2O, Fe_2O_3, and CaO ternary diagram for glass shard data of distinct Makushin tephras. Discriminant fields are shown for Driftwood Pumice, Makushin Scoria, and Lava Valley Pumice (triangles).

are usually not included in the SC calculation because of low relative precision near the detection limits.

In this study two important stratigraphically and temporally correlated tephras also proved to be useful geochemical marker units as well (Table 7.1). Similarity coefficients helped to distinguish correlation unit A (Driftwood Pumice) from the airfall component of correlation unit B (Makushin Scoria). Discriminant fields for Makushin tephras are graphically described using a Fe_2O_3, CaO, K_2O ternary diagram (Fig. 7.5).

Table 7.1 Correlation matrix of Driftwood Pumice (correlation unit A) and Makushin Scoria (correlation unit C). Shaded values represent a positive match.

Driftwood Pumice	Makushin Scoria	96MAK 06B-05	96MAK 16-05	96MAK 35-01	96MAK 35-01	96MAK 35-07	96MAK 37-02	96MAK 41-09	96MAK 42-01	96MAK 45-01D	96MAK 45-04D	96MAK 45-05D	97MAK 07-01	96MAK 34-01	96MAK 34-01	96MAK 34-02	96MAK 41-02
96MAK06B-05		1.00															
96MAK16-05		0.95	1.00														
96MAK35-01		0.98	0.95	1.00													
96MAK35-01		0.97	0.94	0.96	1.00												
96MAK35-07		0.97	0.95	0.96	0.99	1.00											
96MAK37-02		0.96	0.94	0.97	0.94	0.95	1.00										
96MAK41-09		0.96	0.95	0.96	0.96	0.96	0.94	1.00									
96MAK42-01		0.98	0.95	0.97	0.97	0.97	0.95	0.95	1.00								
96MAK45-01D		0.97	0.96	0.97	0.98	0.98	0.96	0.97	0.96	1.00							
96MAK45-04D		0.99	0.96	0.98	0.97	0.97	0.97	0.97	0.97	0.98	1.00						
96MAK45-05D		0.98	0.94	0.98	0.96	0.96	0.97	0.94	0.96	0.96	0.97	1.00					
97MAK07-01		0.96	0.96	0.97	0.96	0.97	0.95	0.97	0.96	0.97	0.97	0.95	1.00				
	96MAK34-01	0.77	0.84	0.78	0.77	0.79	0.77	0.80	0.77	0.79	0.78	0.76	0.79	1.00			
	96MAK34-01	0.75	0.82	0.76	0.75	0.76	0.74	0.77	0.75	0.77	0.75	0.74	0.77	0.96	1.00		
	96MAK34-02	0.75	0.81	0.75	0.75	0.76	0.74	0.77	0.75	0.77	0.75	0.74	0.77	0.96	0.99	1.00	
	96MAK41-02	0.75	0.82	0.76	0.76	0.77	0.75	0.78	0.75	0.78	0.76	0.74	0.77	0.97	0.98	0.98	1.00

Chapter 8: Discussion of Caldera Forming Deposits

The vast bulk of proximal valley filling deposits of Makushin Volcano are of pyroclastic origin, and were produced during a series of large, early Holocene eruptions. The proximal deposits occur in two commonly observed facies, flat topped fans or valley ponded ignimbrites and thinner veneer deposits in the uplands (Walker *et al.* 1980, Walker 1983). The valley filling flow units themselves are classic scoria, block and ash, and pumice flow deposits (Cas and Wright 1987).

The distal caldera-forming pyroclastic flow (CFPF) deposits found around Dutch Harbor are separated from the source volcano by 6 to 7 km of water, and the lower portions of Makushin Valley are filled with alluvium making it impossible to directly trace distal pockets of preserved CFPF deposits to the CFPF valley fill near Makushin. Because of the great distance from the volcano and the separation from the source by open water, some field observers might mistakenly conclude that the CFPF deposits are of an airfall origin rather than of pyroclastic flow origin. Here I present evidence to support a pyroclastic flow origin for the distal CFPF deposits in an around Dutch Harbor. To provide context I borrow a pyroclastic flow model that has been used to explain other similar systems.

8.1 Distribution and Mapping

The distal CFPF unit is easily recognized as a relatively thick poorly sorted silty to sandy orange red to orange brown ash with pumice and lithics. It is exposed in the lower reaches of Makushin Valley and in cliff sections of Broad Bay, across the bay in Dutch Harbor and at least as far east as Ugadaga Bay. The CFPF is, however, present in significant thicknesses at relatively high elevations (530 meters on Amaknak Island in Unalaska Bay), appears to thin slightly with increasing elevation, and is absent at the highest elevations (>1000m). Similar distal deposits were not found in valleys to the north, west or south of the volcano although proximal facies

were. This does not exclude the possibility that the distal deposits exist or did exist in these areas. Each valley has a unique history and may have buried or not preserved these deposits. Also there is only the sea to preserve extreme distal deposits at these azimuths.

8.2 Absence of Correlative Proximal Airfall Facies

Probably the strongest argument that the CFPF is not of airfall origin is that there are no thick proximal airfall deposits. In every eruption known on earth, airfall deposits thicken systematically towards the source volcano. The absence of thick airfall deposits correlative with distal pyroclastic rocks is strong evidence that the distal deposits are not airfall tephra.

The vast majority of proximal deposits are of pyroclastic origin and the stratigraphy suggests a strong correlation between CFPF and proximal pyroclastic veneer and valley-ponded ignimbrites. In addition, radiocarbon ages taken from directly above the proximal veneer deposits and from under the CFPF on Hog Island strongly support this correlation.

In the Dutch Harbor area the CFPF deposits which are 20-80 cm thick at low elevation sites thins to a few centimeters with increases in elevation, and is absent in sections above 400 m elevation. In contrast, airfall tephras in the area found in low elevations can also be found at high elevations with no apparent change in thickness.

8.3 Sorting and Grain Size

Pyroclastic flows are often segregated into three distinct layers (Sparks *et al.* 1973). Distal layer 1 deposits are generally thin and well sorted and are directly overlain by the main flow body (layer 2). (Cas & Wright 1987). Layer 1 deposits that are fines-depleted and rich in dense lithic clasts and crystals, are called *ground layers.* Ground layers are often deposited by intermediate to high aspect ratio ignimbrites (Walker *et al.* 1981). Layer 1 deposits have also been attributed to blasts which immediately precede a flow (Wohletz *et al.* 1984), jetting of material from the flow front (Wilson & Walker 1982, Walker 1985), ingestion of air by the flow front causing

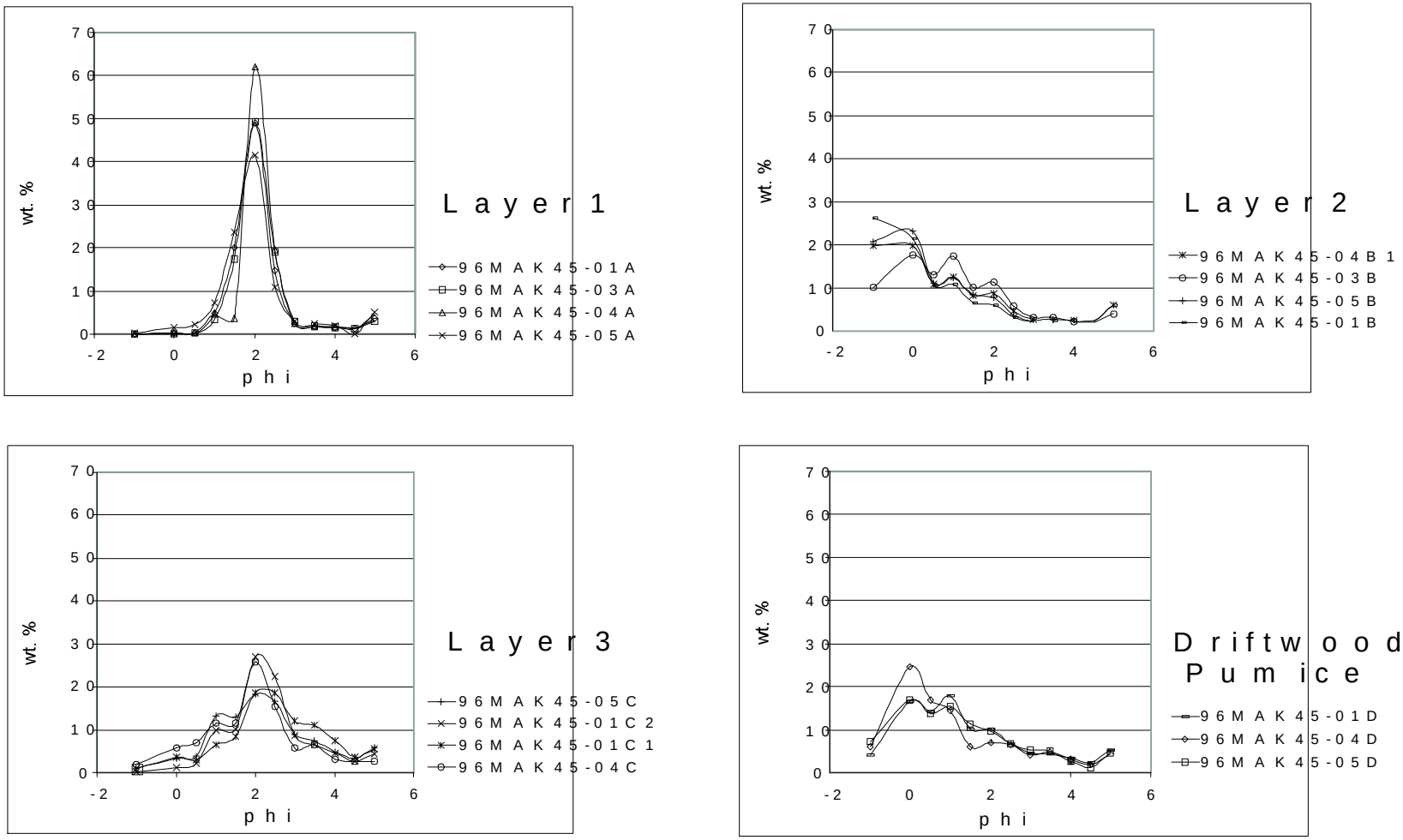

Fig. 8.1 Grainsize plots for distal pyroclastic deposits from the Dutch Harbor area.

sedimentation of heavies (Walker *et al.* 1981a) and deposition by overriding dilute ash clouds as they overrun the main flow (Hoblitt 1986). This type of deposit demonstrates that good sorting and mantle bedding is not exclusive to airfall deposits (Walker, 1983). Layer 2 deposits form the bulk of the deposit and are generally massive and poorly sorted. Layer 3 deposits are thin, fine-grained and well sorted and record elutriation of fine ash from layer 2. In general layer 3 deposits should be finer grained than layer 1 deposits (Sparks 1973). Layer 1 and 3 are not always observed or preserved in the field and if present are often not continuous to the full lateral extents of the deposit.

The distal CFPF deposits exhibit the classic internal layering of pyroclastic flows. A thick massive middle unit is often accompanied by thin, well-sorted underlying deposits as well as thin fine-grained overlaying deposits which have been designated layer 1, 2, and 3. Weight percent versus grainsize for layer 1, 2, 3, and for comparison distal pumice airfall deposits of the Driftwood Pumice are shown in Fig. 8.1. Layer 1 shows excellent sorting which is common in airfall as well as some layer 1 deposits. Layer 2 shows very poor sorting typical of pyroclastic flows, confirming field observations. Layer 3 is moderately well sorted with the bulk of its mass containing the same grainsize as layer 1. Layer 1 also exhibits a very sharp contact with Layer 2 which is common in layer 1 type deposits. This is presumably the result of shear caused by the overriding flow. In contrast layer 3 CFPF deposits forms an irregular and diffuse contact. This is also commonly observed as ash settles over the recently disturbed topography. This layer is often not preserved or recognized as it is easily eroded or altered in buried paleosols. Distal Driftwood Pumice shows a bimodal distribution typical of pumice containing a dense lithic component.

Median diameter vs. sorting coefficient plots of distal CFPF layer 1, 2,and 3 deposits (Fig. 8.2) are compared to pyroclastic flow, surge, and fall fields of Walker (1983). None of the deposits from this study fit well into the fields of Walker (1983) which are mostly derived from

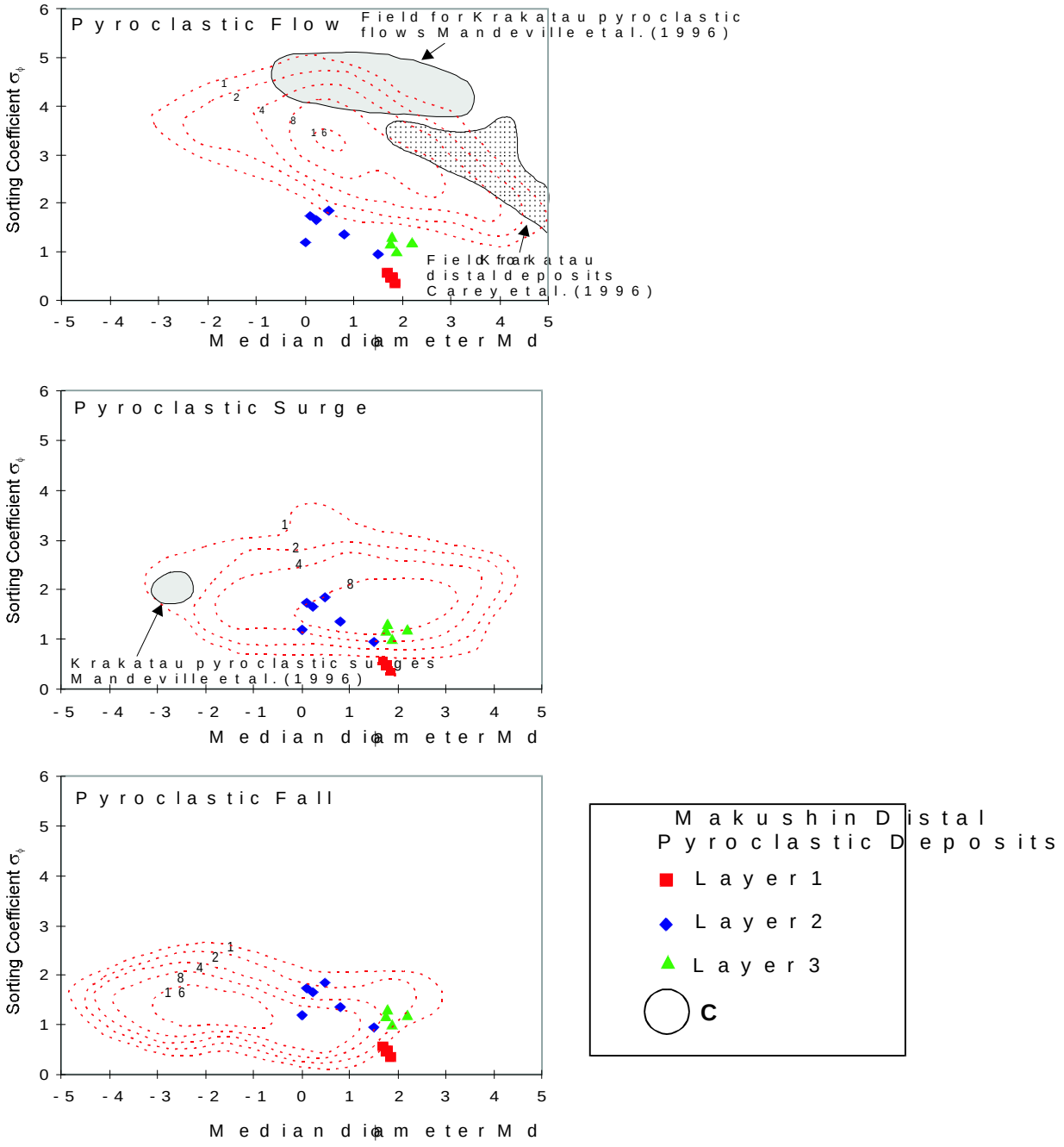

Fig. 8.2 Median diameter vs sorting coefficient plots of distal volcanic deposits. Layer 1, layer 2, and layer 3 Makushin distal pyroclastic deposits shown respectively as squares, diamonds, and triangles. Contoured data frequency fields for pyroclastic flow, surge, and fall deposits after Walker (1983). Contours are from Walker (1983) and are based on the percentage of samples at any point contained by a circle of size C. Pyroclastic flow and surge fields for deposits from the 1883 eruption of Krakatau from Mandeville et al. (1996) and Carey et al. (1996).

proximal deposits from large magnitude eruptions. The high degree of field overlap further suggests that grainsize parameters alone are not a good criteria by which to determine origin. Carey *et al.* (1996) also found that much of the distal pyroclastic flow and surge deposits from the 1883 eruption of Krakatau also plotted outside the fields of Walker (1983).

8.4 Internal Structure

The CFPF (layer 2) has numerous types of internal structures. Unlike airfall deposits stratigraphically above and below the CFPF, deposit thickness varies on outcrop scale. Faint cross-beds can be seen in a section (96MAK23) near Dutch Harbor (Fig. 4.25). Small dunes are also present in the deposit. Segregated pods of coarse material within the deposit are common. There is also a strong tendency for the deposit to fill depressions rather than to evenly mantle topography. These characteristics are highly suggestive of a turbulent flow regime.

8.5 Competence

Some clasts in the poorly sorted CFPF deposit are too large to be part of a distal airfall deposit. Two large round to cylindrical shaped slightly vesiculated, juvenile clasts were found in the CFPF deposit in a section near the Dutch Harbor airport. They had a maximum diameter of 3 and 2.5 cm and an average diameter of just over 2 cm, weighed 4 g, and had a density of ~2 g/cm^3. These clasts are unlikely airfall components, considering that they are much larger and denser than the average clast (Fig 8.1) and considering the 25 km distance from the source. Indeed a 3 cm lithic clast maximum diameter, at a distance of 25 km, exceeds the largest of lithics found at similar distances in the most voluminous of Plinian airfall deposits such as the Fogo A pumice (Walker and Croasdale, 1971). Ballistic models indicate that it is even more unlikely that these clasts could be emplaced ballistically during large explosions (L Wilson 1972). Although surges can also carry large particles for short distances they are less efficient than pyroclastic flows (Druitt 1998). In contrast, the ability to transport large fragments over large

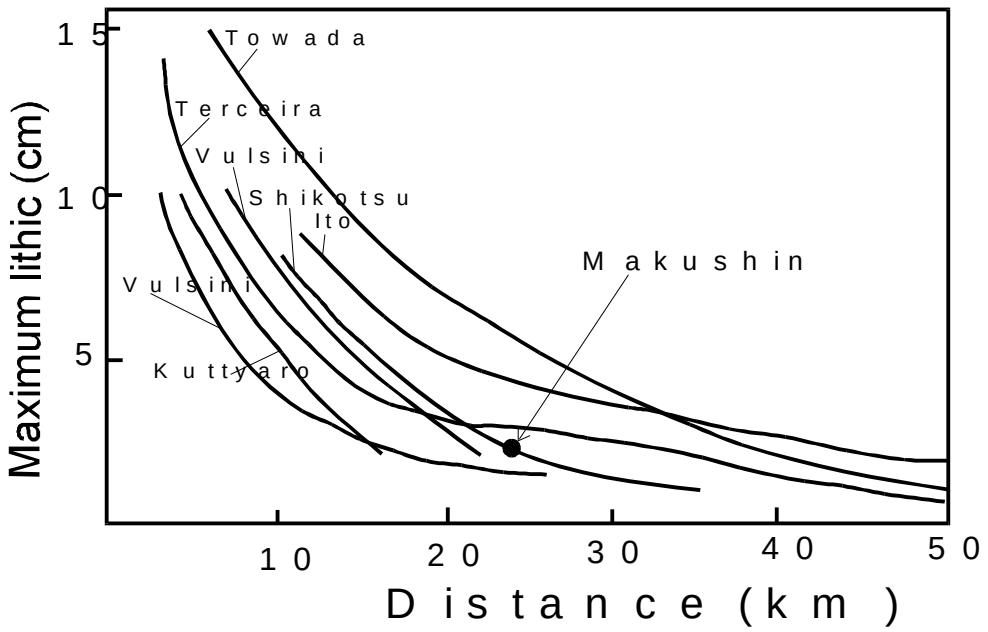

Fig. 8.3 Plot of maximum lithic vs. distance for various pyroclastic flows. Modified from Sparks (1975). Dot indicates maximum lithic clast for early Holocene pyroclastic flows from Makushin.

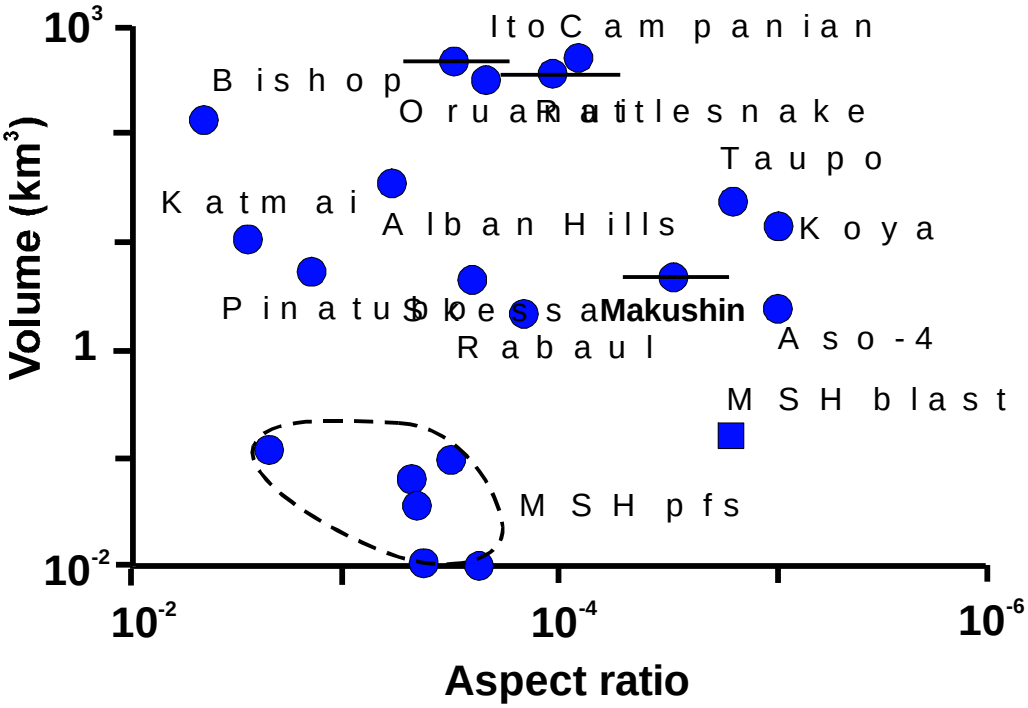

Fig. 8.4 Aspect ratio vs. volume for several ignimbrites and the Mount St. Helens blast. Modified fromWalker (1983) and Druitt (1998).

areas is almost characteristic of low aspect ratio pyroclastic flows. Lithics of greater size than reported here are often carried to much greater distances than 25 km (Fig. 8.3). The Taupo flow and Ito for instance distributed 10 cm lithics over distances greater than 40 km (Wilson 1985, Yokoyama 1974 in Druitt 1998).

8.6 Hot Emplacement

The proximal pyroclastic flows were clearly hot upon emplacement. Pink coloration, an indicator of thermal oxidation (of magnetite or other Fe or Mn rich oxides; Cas & Wright 1987), was noted in flow deposits near Makushin Valley and at the summit crater. In addition some flows are sintered to slightly welded and contain fossil fumarole pipes.

Carbonized remains of plant stems, and rootlets were found in a thin organic soil directly under the distal CFPF deposit at site 97MAK02 on Hog Island (Fig. 8.5). In places burned branches were found sticking up into the overlying deposit, suggesting that the distal deposits were also hot at the time of emplacement. Carbonized debris was also found in CFPF deposits at site 96MAK21 near Broad Bay. Hot emplacement may also explain the strong induration and extreme oxidation of this unit on Hog Island. Hog Island is a few kilometers nearer the source so the flow may have had more retained heat than when it arrived in the Dutch Harbor/Unalaska town area. In places on Hog Island the CFPF unit is so well indurated it has a nearly brick-like quality.

Ingestion and carbonization of organic material is commonly found mixed throughout pyroclastic flows, but is rare in airfall deposits and then only in very proximal regions (Cas & Wright 1987). It has been demonstrated that expanded flows can conserve heat during transport if they entrain little air and move in a subcritical regime (Bursik & Woods 1996). Historical accounts indicate that more than 1000 people on the southeast coast of Sumatra, 40 km from the volcano, were killed from exposure to hot ash flows from the Krakatau eruption of 1883 (Carey

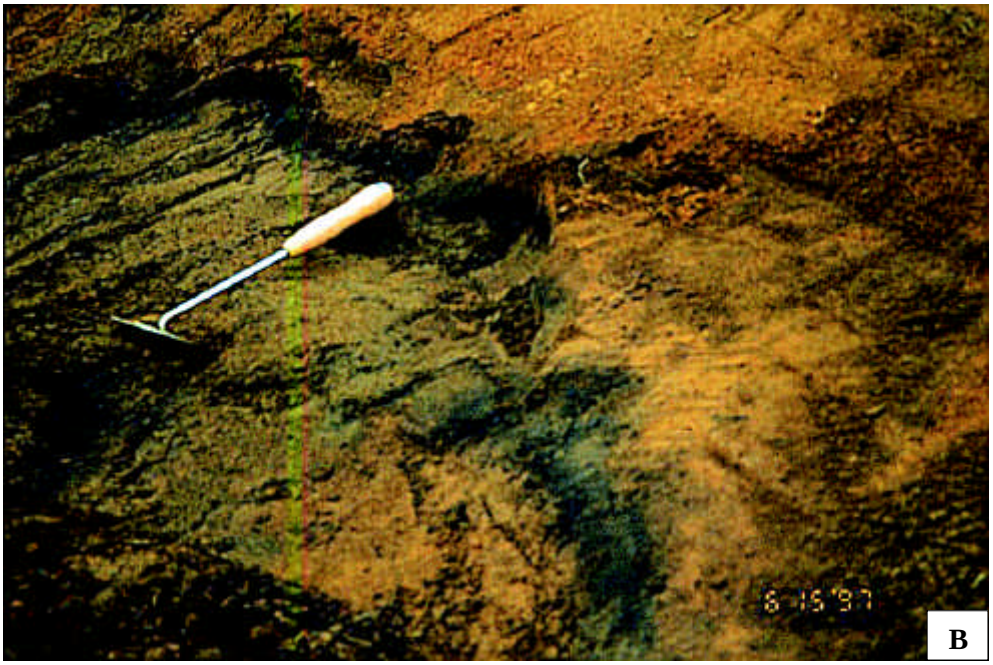

Fig 8.5 (A) Hog Island and location of sample site 97MAK02. The organic horizon (B) contains charred plant stems and small branches some of which stick up into the overlying distal (CFPF) volcanic deposits. Note quonset huts below sample site for scale.

et al. 1996). Even people protected inside huts were blistered and severely burned by hot ash pushing in through crevices. A very similar occurrence may have happened at Dutch Harbor as the 8050 ^{14}C yr B.P. organic/cultural horizon directly underlying the CFPF marks the end of an ancient native civilization (Knecht 1997, personal communication).

8.7 Emplacement Models for Pyroclastic Flows

The aspect ratio is a useful concept often used to describe pyroclastic flows. The aspect ratio is defined as the flow thickness versus the diameter of a circle of area equal to the deposit (Walker *et al.* 1981). High aspect ratio (HAR) ignimbrites are thick, confined, and largely comprised of valley-ponded facies. Low aspect ratio (LAR) ignimbrites are thin, widespread, and contain a significant proportion of ignimbrite veneer deposits (Walker *et al*. 1980, Walker 1983). HAR ignimbrites are generally produced by low mass flux rates while LAR ignimbrites result from high mass flux rates over shorter time periods (Druitt 1998). The pyroclastic flows from Makushin are clearly of the high aspect ratio type, (Fig. 8.4) and display all the associated characteristics.

High mobility and the ability, of LAR ignimbrites to surmount significant topographical barriers has been noted by many researchers of pyroclastic deposits. Flows from Fisher Caldera climbed obstacles more than 500 m high (Miller & Smith 1977). The Ito Ignimbrite surmounted barriers 600 m high (Yokoyama 1974 in Druitt 1998), the Campanian Ignimbrite 1000 m high (Barberi *et al.* 1978, Fisher *et al.* 1993) and the Taupo Ignimbrite 1500 m high (Wilson 1985). At Makushin, we find deposits of CFPF overtopped Hog Island (94 m) and deposited on low mountains in the Dutch Harbor area to an elevation of ~500 m. We identified very distal CFPF deposits at Ugadaga Bay, more than 35 km from the volcano, indicating it crossed a 300 m high pass (Fig 8.6).

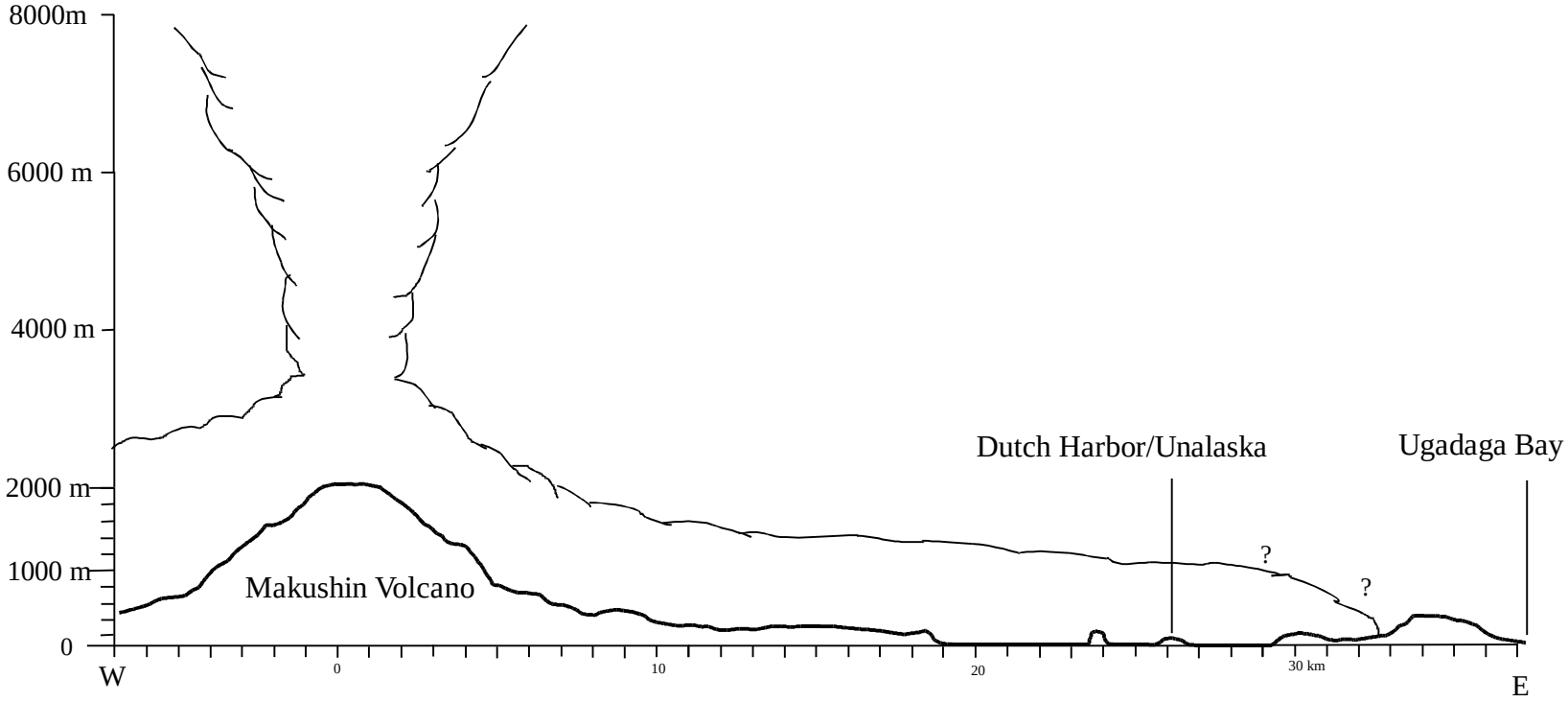

Fig. 8.6 Topographic profile accross Makushin Volcano to Ugadaga Bay where distal CFPF volcanic deposits were found. Column heights for VEI 5 and greater magnitude eruptions are typically greater than 25 km.

There is also strong evidence that pyroclastic flows such as the Campanian Tuff (Fisher *et al.* 1993) have traveled significant distances over water. The 1883 eruption of Krakatua produced flows which traveled more than 80 km over water before depositing thin poorly sorted deposits on land (Carey *et al.* 1996). This suggests that at least portions of these flow were less dense than water. The Makushin flows traveled ~7 km across Unalaska Bay, well within the realm of previously documented flow behavior.

The caldera forming pyroclastic deposits of Makushin are best explained by the following model, described in Druitt (1998), for intermediate to low aspect ratio ignimbrites. Limited periods of high discharge result in flow runout distances of up to many tens of kilometers. Sedimentation generates dense undercurrents which become trapped in topographic lows and pond in valleys. Upper, more dilute, portions of the flow are relatively unconfined and deposit veneer deposits in uplands. This part of the flow is able to traverse high obstacles because it is thick and expanded. The expanded less dense nature of these deposits also aid the crossing of open water. In this model, the distal limits are controlled by the lofting distance of the suspension current rather than the runout distance of the underflows. If little air is entrained heat is retained. In the case of Makushin, parts of the flow may have been partially channeled towards the east by deep glacial valleys, possibly increasing mobility. This and similar models have been applied to several intermediate-to high-aspect-ratio ignimbrites such as the Campanian Ignimbrite (Fisher *et al.* 1993) and Taupo Ignimbrite (Valentine 1987, Dade & Huppert 1996) the Ito Ignimbrite (Baer *et al.* 1997) and Rattlesnake Tuff (Streck & Grunder 1995).

This model accounts for the widespread occurrence of Makushin pyroclastic deposits, their presence at high elevations, their ability to surmount obstacles, carbonization of vegetation, and the ability to cross water.

Chapter 9: Volume Estimates

Reasonable volume estimates for intact, modern pyroclastic deposits can be simply determined by multiplying the surface area of a deposit by an average thickness. Of course the accuracy of this method is limited by the availability and quality of field data for prehistoric eruptions. Ignimbrite veneer deposits may comprise as much as 10% of the total volume in HAR ignimbrites and up to 75% of LAR ignimbrites (Druitt 1998). In addition it is estimated that at much as 50% of the original pyroclastic flow can enter into the coignimbrite ash or phoenix cloud which is more quickly and easily dispersed by higher altitude winds (Cas & Wright 1987, Druitt 1998). Large errors are to be expected in cases where flows of different eruptions are stacked upon one another thus obscuring the full extent of the underlying deposits. Further complicating volume estimates is the fact that multiple deposits can, of course, be created during one eruptive episode. In cases where a significant amount of erosion has occurred, or where a significant portion is deposited at sea, accurate estimates are simply not possible. Volumes can be inferred, however, by extrapolating from areas with complete and intact deposits. Table 9.1 summarizes volume estimates for the intact Makushin flow and debris avalanche deposits. Significant erosion has occurred for nearly all deposits however and these estimates represent absolute minimum volumes.

Table 9.1 Volume estimates of valley fill.

Location	~km^3
Glacier Valley	0.1
Lava Valley	0.02
Point Kadin	0.4
Koriga Point	0.3
Bishop Point Valley	0.3
Driftwood Valley	0.1
Makushin Valley	0.3
Veneer Deposits	~1.5?
Deposits at Sea	~1-2?
Total Volume	~4-5?

Several quantitative methods for determining fallout volumes have been developed. Walker (1980) used a crystal concentration method. This method takes advantage of the crystal to vitric ratio and assumes that crystals and pumice particles become increasingly segregated with distance from the vent due to differing densities. Pyle (1989) developed a method where plots of the natural log of thickness are plotted against the square root of isopach area and integrated to get volumes. Fierstein and Nathenson (1992) slightly modified and simplified this method.

These methods are unsuitable for small volcanic islands for several reasons. First they rely on isopach data. Even the log thickness versus the square root of area plots method requires a minimum of two closed isopach contours. For volcanoes typified by frequent small eruptions of similar size and chemical composition, correlation and mapping of a single deposit among a myriad of tephras can be nearly impossible. For small islands the majority of airfall may be deposited at sea making the creation of mid to distal range isopachs impossible as well. Contour thicknesses from proximal areas may be influenced by pyroclastic and ballistic airfall components and therefore volumes calculated using only proximal data can severely underestimate the true volume of a deposit.

A simple empirical method of airfall volume determination was developed for this study. This method makes the assumption that for a given distance from a source, maximum tephra thickness is directly related to volume. Data for which volumes and isopach data were available were taken from the published literature. Figure 9.1a shows the log of maximum thickness versus the log of the volume at a distance of 10 km from the vent. Note that there is a strong linear relationship as indicated by the R^2 value. A regression through the data yields an equation from which a volume for any thickness can be determined. Of course the plot is insensitive due to its log-log nature and the data itself is subject to large amounts of error. In the absence of other viable methods, however, this should provide a good estimate of tephra volume and eruption

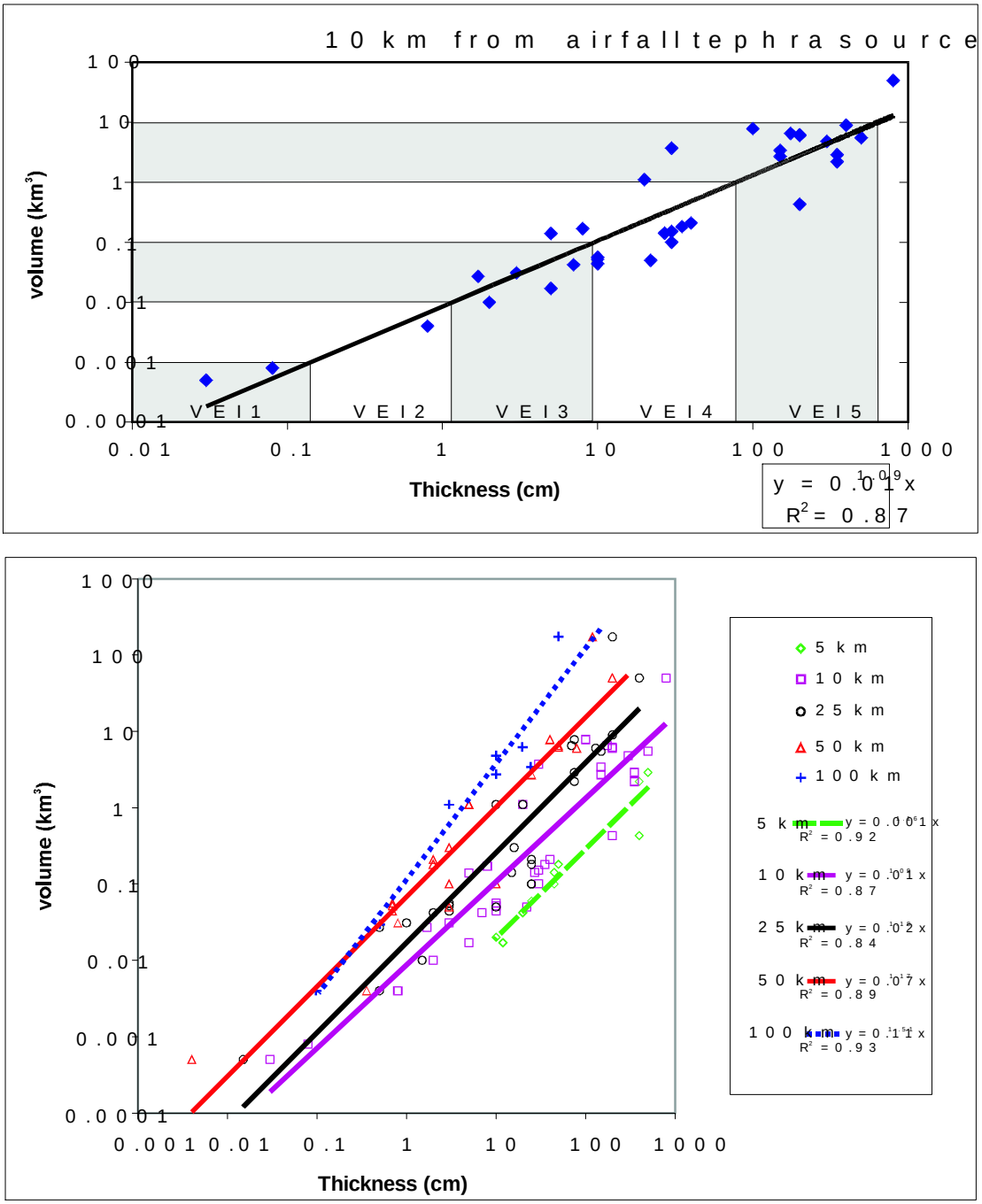

Fig. 9.1 Volume vs. thickness plots for airfall tephra layers at distances of 5, 10, 25, 50, and 100 km. Data from published literature.

References for volume and thickness data: Bloomfield et al. (1977) Booth et.al (1978) Cas and Wright (1988) Drexler et al. (1980) Fierstein, and Hildreth (1992) Fierstein, and Nathenson (1992) Fisher and Schmincke(1984) Gardner et al. (1998) Hayakawa (1985) Hildreth (1990) Neal et al.(1995) Paladio-Melosantos et al.(1996) Pyle(1989) Pyle (1990) Rose (1972)Rose et al. (1973) Rose et al. (1978) Sarna-Wojcicki et al. (1981) Self (1976) Self (1974) Self and Sparks (1978) Self et al. (1984) Sigurdsson (1982) Sussman (1985) Thorarinsson (1954) Thorarinsson and Sigvaldason (1972) Walker and Croasdale (1971) Walker (1981) Walker (1980) Wilcox (1959) Williams and Self (1983)

magnitude. It is best to apply this method to data taken downwind from the source volcano, increasing the chances that maximum thickness data are obtained.

An entire suite of plots was also developed for various fixed distances from the source (Fig.9.1b). It is encouraging that nearly all of the regression lines are parallel, as should be the case if thickness/volume decreases at the same rate away from the vent. The 100 km line is not parallel to the other data and probably reflects the limited data set and poorer quality of data at distal areas. Wind and other variables also may also increasingly affect dispersal of tephra with distance.

Chapter 10: Post Caldera Tephras

Because of the dominant westerly wind directions and gentle topography, the best preservation of Holocene tephras occurs on distributary fans and flat lying areas to the east of the volcano (~ 10 km from the caldera). In general, sequences in this area with ash deposits consist of approximately 2 meters of multiple airfall tephras and base surges interbedded with silt and peats. Tephras are typically mafic and gray to black in color, although several distinctly orange and yellow silicic tephras are also present. Some thicker beds exhibit wavy bedforms typical of high velocity surge deposits. Grain sizes typically range from fine sand to pebble sized lapilli. Tephras range from less than a centimeter to more several tens of centimeters in thickness. Especially good exposures can be found in gullies that dissect pyroclastic fans in upper Makushin Valley and tephra sequences overlying the Lava Ramp. Organic horizons tend to be very peat-rich east of Makushin although it is unclear whether this is due to flat local topography or local weather effects. Age dates from the lava ramp area indicate that smaller tephra eruptions, typical of the post caldera tephras, began soon after 7740 ^{14}C yr B.P.

10.1 Late Holocene Activity

Detailed stratigraphic studies are the most reliable means of reconstructing the eruptive history for a particular volcano. From these data recurrence intervals and estimates of eruption frequency, useful tools for predicting the approximate timing, likely size, and behavior of future eruptions, can be determined. It has long been recognized that eruption size is inversely related to frequency (Simkin & Seibert 1984). Small magnitude eruptive events should occur much more frequently than large magnitude events. Therefore it is valuable to determine both the timing and the frequency of past eruptions and to reconstruct the eruption magnitude a particular frequency estimate refers to.

A stratigraphic section from a fan in Makushin Valley (Fig. 10.1) has preserved an excellent record of small eruptive events over the last ~5000 years. Section 96MAK03 preserves 29 prehistoric tephras above a peat dated at 4910 ± 80 ^{14}C yr B.P. This is a minimum estimate on the number of eruptions because of varying wind directions, indistinguishable multiple fall layers, and erosion. It is unlikely that one section would preserve all erupted tephras. Also, the smallest magnitude eruptions are often not distinctly preserved in the geologic record. For example, a small tephra was discovered in the top layers of the recent snowpack on the upper flanks of Makushin. The young (~1995) tephra was not found at any of the sampling sites around the volcano. Column heights from pilot reports are consistent with an eruption of magnitude ~VEI 1. This supports the assertion that at least VEI 1 and smaller eruptions are not generally preserved in the geologic record. The corollary to this, of course, is that those tephras that are preserved in the geologic record represent VEI 2 and larger magnitude eruptions.

Volumes for each eruption have been determined using the method discussed in the previous chapter and are also diagrammatically shown in Fig. 10.1. These volume estimates have been used to assign a Volcanic Explosivity Index (VEI) number (Newhall and Self, 1982) to each of the prehistoric tephra eruptions. Fig. 10.2 summarizes the magnitudes and frequency of eruptions at Makushin during the Holocene. Because 4980 ^{14}C yr B.P. is approximately 5720 years of real time during the late Holocene, Makushin volcano has, on average, had a geologically recorded eruption every 200 years. Eruptions of magnitude VEIs 2, 3, and 4 occur at approximately every 400, 500, and 2800 years respectively. These frequency rates should be considered as minimums because it is unlikely that all eruptions will be preserved at a single location. Volume estimates tend to be underestimated as well since a single location is unlikely to record the maximum thickness of a deposit for a specific radial distance in all cases.

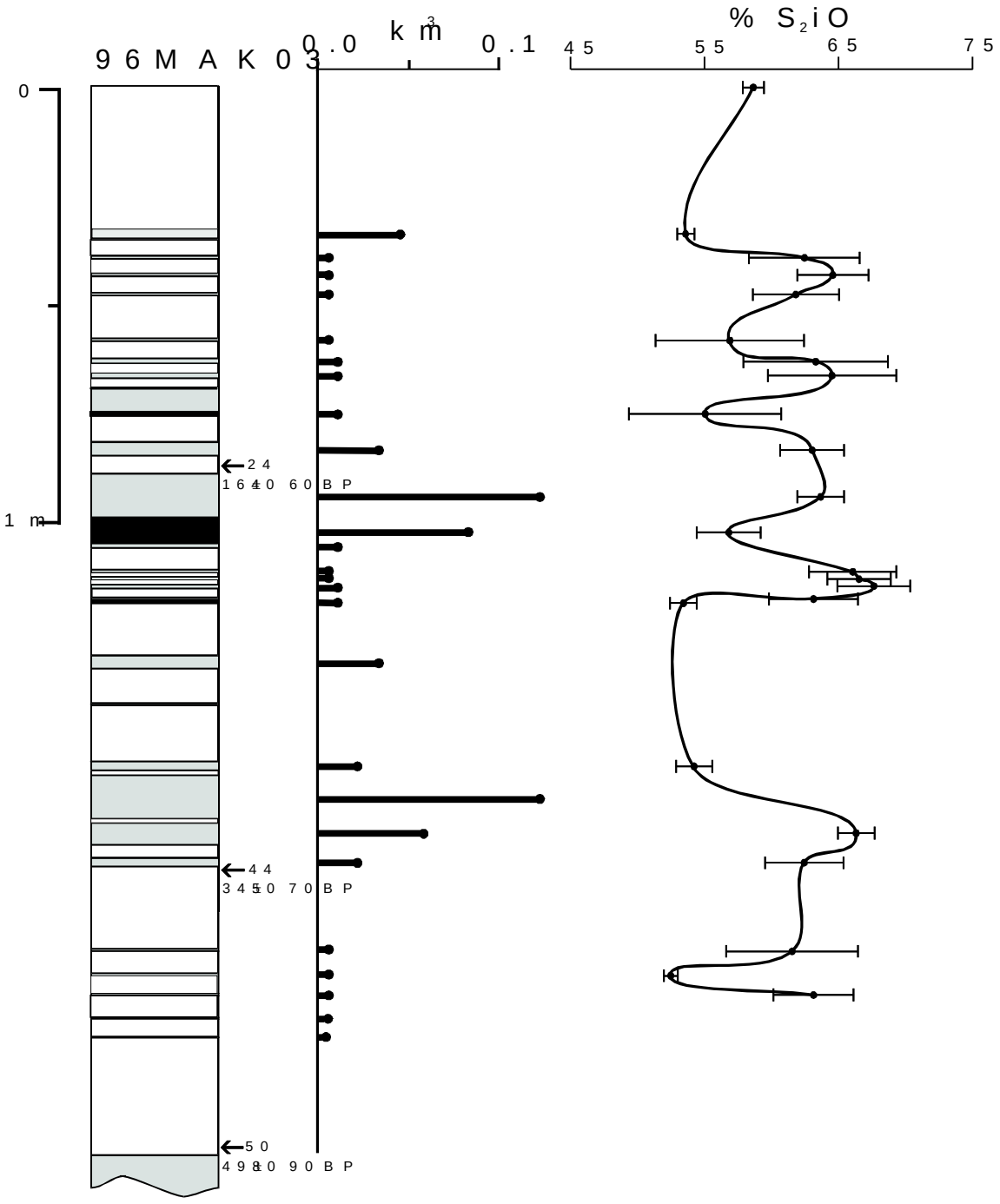

Fig. 10.1 Late Holocene stratigraphic section with corresponding geochemical analysis and volume estimates for tephra layers. Shaded areas represent tephras, unshaded areas represent organic horizons.

10.2 Historic Activity

Records of Makushin's activity date back to its discovery by Russian explorers in 1763. A summary of historic eruptive events is given in Table 10.1. Although very little information documents most of these eruptions we can guess that a VEI 1 or larger eruption was probably required to draw comment. It is also likely that many small eruptions went entirely unnoticed as severe Aleutian weather likely hampered travel and observations during the 18th and 19th centuries even more than today.

Table 10.1 Historic eruptions of Makushin Volcano. Modified from Arce (1983) and Miller *et al.* (1998).

Eruption Date	Volcanic Activity
1768-1769	violent ash eruption and a second volcano active on Unalaska Island
1790-1792	smoking
1795	submarine eruption off SE coast, w/ earthquakes
1802	violent ash eruption w/earthquakes
1818	smoking
1826	violent ash eruption w/ earthquakes
1827-1838	smoking
1844	smoking
1845	eruption from unspecified fissure
1865	smoking
1867	smoking
1871-1874	smoking
1880	
1883	ash eruption
1891	smoking
1892	strong thermal activity in caldera
1895	
1907	strong thermal activity along the north wall of the caldera, and a new crater formed between central cone on northern caldera wall
1912	smoking
1926	ash eruption w/ earthquakes
1938	ash eruptions
1944	strong thermal activity along the northern caldera wall and north flank
1951	phreatic ash eruption
1952	smoking
1980	phreatic eruption from parasitic crater
1995*	phreatic ash eruption

*Global Volcanism Network Bulletin V.20, No 1, Jan 1995

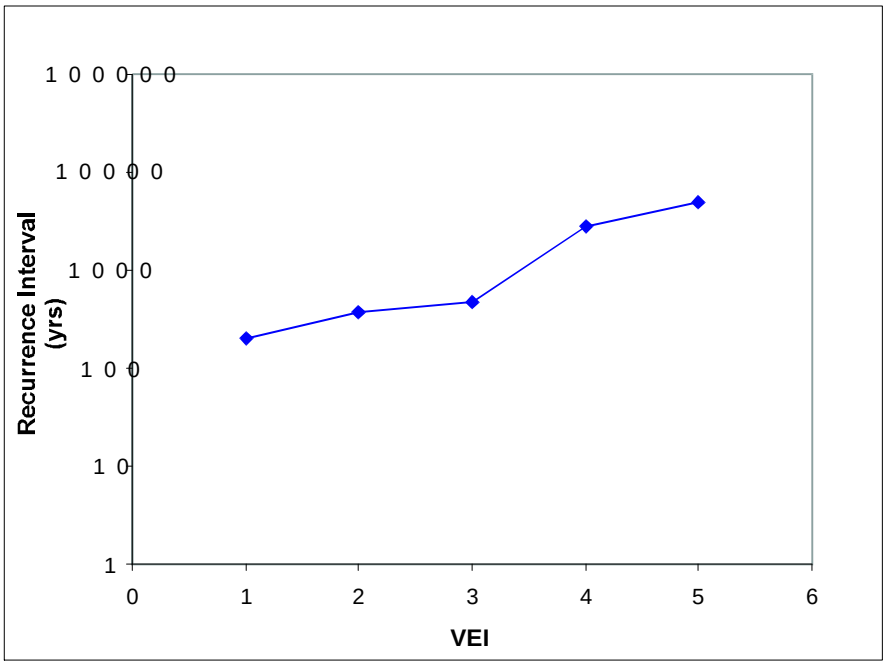

Fig. 10.2 Plot of recurrence interval vs. VEI for eruptions at Makushin volcano. An inverse relationship between the eruption size and eruption frequency exists throughout the Holocene.

From these accounts we can infer at least 26 historical eruptions of Makushin, most of VEI = 1, during the last 230 years. This gives as eruption frequency for VEI=1 events of approximately one occurrence every 8-10 years. Although the interpretation of some of these events as actual eruptions may be questionable the data none the less establishes a record of frequent activity.

Chapter 11: Hazards

The geologic record suggests there are several types of potential hazards from Makushin volcano (Fig.11.1). Anyone in very close proximity to the summit is potentially at risk from noxious gasses. Lahars and jökulhlaups (glacial outburst floods) are a potential threat to low lying areas in all of Makushin's tributaries. Debris avalanches in the past have reached the sea and will undoubtedly do so again. There is also the possibility that a debris avalanche could create a tsunami upon entering the sea. This would be a threat to small boats in the immediate vicinity. The largest Holocene eruptions at Makushin produced violent pyroclastic flows which traveled as far as 30 km crossing water and disrupting the area which now is occupied by the town of Unalaska/Dutch Harbor. Although unlikely in the near future another similar eruption is almost certain given enough time.

By far the most common and therefore the largest hazard to man comes from airborne volcanic ash and airfall tephra. Airborne ash is highly abrasive and is a danger to high flying aircraft. Ash particles have been known to cause engine failure when ingested glass particles melt coating vital sensors. The Aleutians are directly in the path of great circle air routes between the North America and Asia (Fig 11.2). Collision with ash plumes can be easily avoided if they are detected in time. Small and large aircraft attempting to use the Dutch Harbor airport are also vulnerable to low altitude ash clouds. A small magnitude eruption could conceivably make the airport inaccessible. Any large turbine engine such as those used by power generating facilities is potentially vulnerable to ingestion of ash for the same reason as jet engines. A large amount of ash would also create problems for the local canneries and ships which frequent Dutch Harbor by heavily loading structures. Ash can also cause air quality problems for people in the community.

The likelihood of a specific eruption directly affecting Dutch Harbor/Unalaska is most dependent on eruption magnitude and wind direction. Unfortunately Dutch Harbor/Unlaska lies

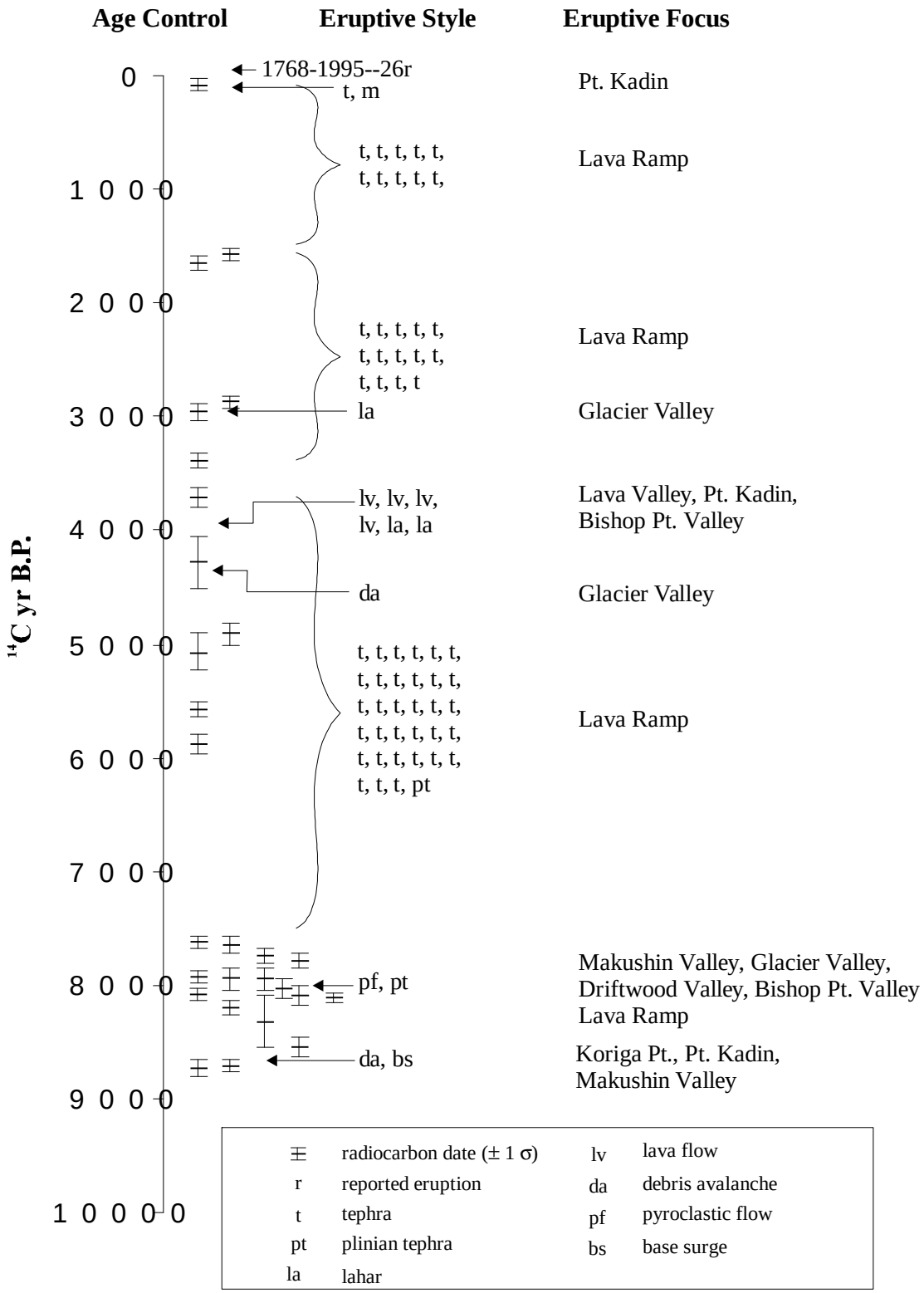

Fig. 11.1 Sequence of postglacial eruptive events recorded by deposits preserved around Makushin Volcano.

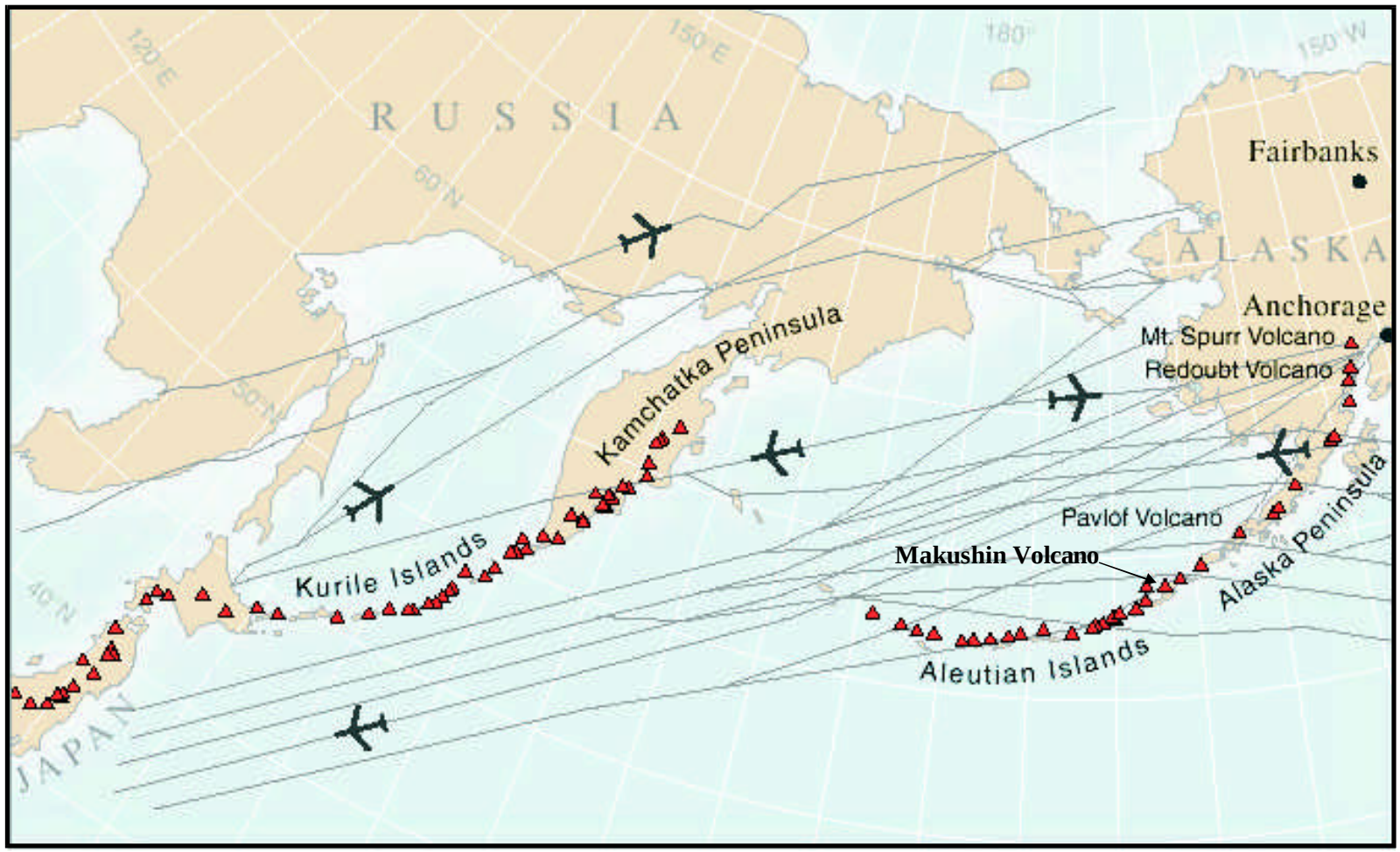

Fig. 11.2 Proximity of Aleutian and Kamchatkan volcanoes to Northern Pacific air traffic routes, after Neal et al.(1 997).

directly in the path of the dominant wind direction, increasing the likelihood that it will be affected by an eruption (Fig. 11.3). Wind diagrams and wind speed for various altitudes along the Aleutian chain from Cold Bay, east of Makushin, to Adak to the west illustrate that wind directions throughout the Aleutians have a strong easterly preference. Average wind speed increases from east to west. Wind speed also increases with altitude to approximately 10,000 meters and then decreases slightly. This implies that ash from larger eruptions may more quickly impact downwind communities. In any eruption where a significant amount of ash is produced, the Dutch Harbor community is very likely to be in its path. Ash from even a small low-altitude ash plume (VEI 2-3) would most likely reach Dutch Harbor in as few as 25 to 35 minutes leaving very little time for warning.

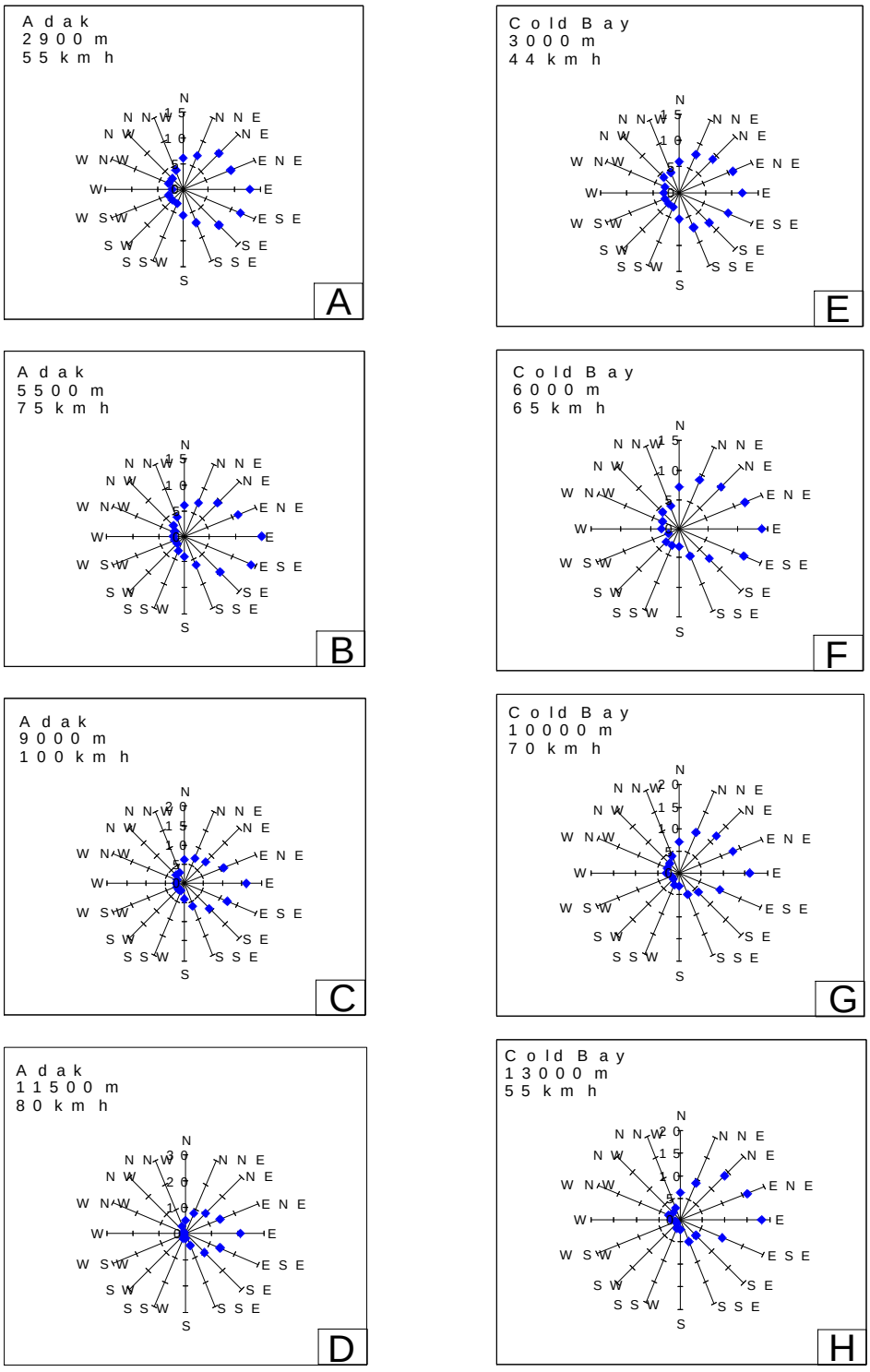

Figure 11.3 Annual percent of wind direction and average wind speed for specific Aleutian locations and altitudes. Source data from the National Climatic Data Center, National Oceanic and Atmospheric Administration. Adak data from 1952-1962 and Cold Bay data from 1945-1957.

Chapter 12: Summary and Conclusions

While the eruptive history of Makushin Volcano is overshadowed by early Holocene caldera-forming events, smaller scale background volcanism has continued through the present without significant periods of quiescence.

Early Holocene volcanic activity at Makushin Volcano is highlighted by two large eruptive events, separated by less than 1000 years. Deposits around the volcano suggest that the earliest event produced large debris avalanches and base surge type deposits. These events probably destroyed much of the summit edifice. A later large event produced mostly valley-filling pyroclastic flows and probably produced the summit caldera. Pyroclastic flows from the later event appear to have been highly mobile and less restricted to valleys than the earlier event. Radiocarbon age dates suggest that the earlier event occurred perhaps ca. ~8720 ^{14}C yr B.P. and no later than ~8550 ^{14}C yr B.P. Dates on material under and directly in the deposits indicate an age of ~ 8050 ^{14}C yr B.P. Although significant amounts of flow and airfall deposits from both events were deposited at sea or have since been removed or obscured by erosion and later events the total combined volume of the eruptions is estimated to be at least 5 km^3 and perhaps as high as 10 km^3. Separation of the two eruptive packages for volume estimates proved to be impractical for this project since the lower limits of valley fill were not exposed and much of early Holocene deposits were obscured by the later eruptive products.

Deposits from the earliest event were probably fairly mafic while flows from the second early Holocene event were largely high silica andesite to low silica dacite in composition (SiO_2 ~60 %). Post caldera tephras vary in glass composition between dacitic and basaltic (Fig. 9.1).

Thin, dark tephras suggest that base surges and phreatomagmatic eruptions were common through the mid-Holocene although small lahars, debris avalanches, and lava flows also occurred. The exception to this was a plinian type eruption ca. 7740 ^{14}C yr B.P. (~VEI 4) which produced a

distinct yellow pumice deposit that proved a significant marker unit throughout the study area and may have much wider regional distribution.

The late Holocene is characterized by frequent small tephras averaging VEI 2-3 at a rate of not less than 1 every 200 years. The historical record suggests that VEI 1-2 sized eruptions occur more frequently, and perhaps as often as every 10 years.

This study provides a historical framework as well as some new insights into the eruptive history of Makushin. However, it is by no means complete. There are several improvements that should be done to enhance this framework.

Although we did not find suitable material it is highly probable that an age date could be obtained on material underlying the older pyroclastic flow deposit at a distal location in the Dutch Harbor area. This would better constrain the timing of the earliest event as well as more tightly correlate it with low section valley-filling proximal and debris avalanche deposits to the northeast. Better upper age constraints and isopach mapping of the yellow pumice unit should be possible and would improve its' usefulness as a marker unit. More extensive mapping of the two distal caldera forming deposits would help to discern some of the physical constraints on these two eruptions. In addition it would shed more light on the eruptive potential of mid-sized caldera forming eruptions which are under represented in the published literature.

References

Anderson EC, Libby WF (1951) World-wide distribution of natural radiocarbon. Phys Rev 81:64-69

Arce GN (1983) Volcanic Hazards from Makushin Volcano, northern Unalaska Island, Alaska. M.S. thesis, University of Alaska, Fairbanks, pp. 1-142

Baer EM, Fisher RV, Fuller M, Valentine G (1997) Turbulent transport and deposition of the Ito pyroclastic flow: Determinations using anisotropy of magnetic susceptibility. J of Geophys Res 89:8485-8501

Barberi F, Innocenti F, Lirer L, Munro R, Pescatore T, Santacroce R (1978) The Campanian ignimbrite: A major prehistoric eruption in the Neapolitan area. Bull Volcanol 41:10-32

Begét JE, Stihler SD, Stone DB (1994) A 500-year-long record of tephra falls from Redoubt Volcano and other volcanoes in upper Cook Inlet, Alaska. J Volcan Geotherm Res 62:55-67

Begét JE, Mason O, Anderson P (1992) Age, extent and climatic significance of the c. 3400 BP Aniakchak tephra, western Alaska, USA. The Holocene 2:51-56

Begét JE, Keskinen M (1991) Stampede tephra: a middle Pleistocene marker bed in glacial and eolian deposits of central Alaska. Can J of Earth Sci 28:991-1002

Begét JE, Edwards M, Hopkins D, Keskinen M, Kukla G (1991a) Old Crow Tephra Found at the Palisades of the Yukon, Alaska. Quat Res 35:291-297

Begét JE, Reger RD, Pinney D, Gillispie T, Campbell K (1991b) Correlation of the Holocene Jarvis Creek, Tangle Lakes, Cantwell, and Hayes tephras in South-Central and Central Alaska. Quat Res 35:174-189

Black RF, (1986) Glacial Geology of the Aleutian Islands. in Hamilton TD, Reed KM, Thorson RM, eds, Glaciation in Alaska-the geologic record. Alaska Geol Soc, pp. 171-192

Bloomfield KG, Sanchez R, Wilson L (1977) Plinian Eruptions of Nevado de Toluca Volcano, Mexico. Geol Rundsch 66:120-146

Booth B, Croasdale R, Walker GPL (1978) A quantitative study of five thousand years of volcanism on Sao Miguel, Azores. Phil. Trans R. Soc Lond (A) 288:271-319

Borchardt GA, Aruscavage PJ, Millard HT Jr (1972) Correlation of the Bishop Ash, a Pleistocene marker bed, using instrumental neutron activation analysis. J Sediment Petrol 42:301-306

Brownlow AH (1986) Geochemistry. Prentice-Hall, Upper Saddle River, pp. 1-580

Bursik MI, Woods A (1996) The dynamics and thermodynamics of large ash flows. Bull Volcanol 58:175-193

Cas RAF, Wright JV (1988) Volcanic Successions: modern and ancient. Chapman & Hall, London, pp. 1-528

Craig H (1954) Carbon-13 in plants and the relationships between carbon-13 and carbon-14 variations in nature. J Geol 62:115-149

Craig H (1961) Mass-spectrometer analysis of radiocarbon standards. Radiocarbon 3:1-3

Dade WB Huppert HE (1996) Emplacement of the Taupo Ignimbrite by a dilute, turbulent flow. Nature, 381:509-512

Drewes H, Fraser GD, Snyder GL, Barnett HF Jr (1961) Geology of Unalaska Island and adjacent insular shelf, Aleutian Islands, Alaska. US Geol Surv Bull 1028-S:583-676

Drexler JW, Rose WI jr, Sparks RSJ, Ledbetter MT (1980) The Los Chocoyos Ash, Guatemala: A major stratigraphic marker in Middle America and in three ocean basins. Quat Res 13:327-345

Druitt TH, (1998) Pyroclastic density currents. in: The Physics of Explosive Volcanic Eruptions. (Gilbert JS and Sparks RSJ eds) Geol Soc London 145:147-184

Druitt TH, (1995) Settling behavior of concentrated, poorly sorted dispersions and some volcanological applications. J Volcanol Geotherm Res 65:27-39

Faure G (1986) Principles of isotope geology. John Wiley & Sons, New York, pp. 1-589.

Fierstein J, Hildreth W (1992) The plinian eruptions of 1912 at Novarupta, Katmai National Park, Alaska. Bull Volcanol 54:646-684

Fierstein J, Nathenson M (1992) Another look at the calculation of fallout tephra volumes. Bull Volcanol 54:156-167

Fisher RV, Orsi G, Ort M, Heiken G (1993) Mobility of a large-volume pyroclastic flow—emplacement of the Campanian Ignimbrite, Italy. Jour Volcanol Geotherm Res 17:375-392

Fisher RV, Schmincke H-U (1984) Pyroclastic Rocks. Springer-Verlag, Berlin, pp. 1-472

Gardner JE, Carey S, Sigurdsson H (1998) Plinian eruptions at Glacier Peak and Newberry volcanoes, United States: Implications for volcanic hazards in the Cascade Range. GSA Bull 110:173-187

Godwin H (1962) Half-life of radiocarbon. Nature 195:984

Hayakawa Y (1985) Pyroclastic geology of Towada Volcano. Bull Earthquake Res Inst 60:507-590

Hildreth W (1990) The 1932 plinian eruption of Quizapu, Chilean Andes (Abstr) International Volcanological Congress Sept 3-8 IAVCEI

Hildreth W, Fierstein J (1997) Recent eruptions of Mount Adams, Washington Cascades USA. Bull Volcanol 58:472-490

Hoblitt RP, Miller CD, Vallance JE (1981) Origin and stratigraphy of the deposits produced by the May 18 directed blast. In: Lipman PW Mullineaux DR (eds) The 1980 eruptions of Mount St. Helens, Washington. US Geol Surv Prof Paper 1250:379-400

Karlen I, Olsson UI, Kallberg P, Kilicci S (1966) Absolute determination of the activity of two C^{14} dating standards. Arkiv Geofysik 6:465-471

Le Bas MJ, Le Maitre RW, Streckeisen A, Zanettin B, (1986) A chemical classification of volcanic rocks based on the total alkali-silica diagram. J of Petrology 27:745-750

Le Maitre RW, Bateman P, Dudek A, Keller J, Lameyre Le Bas MJ, Sabine PA, Schmid R, Sorensen H, Streckeisen A, Woolley AR, and Zanettin B (1989) A classification of igneous rocks and glossary of terms. Oxford, Blackwell, pp. 1-193

McConnell VS, Begét JE, Roach AL, Bean KW, Nye CJ, (1997) Geologic map of the Makushin Volcanic Field, Unalaska Island, Alaska. Alaska Div Geol Geophys Surv, Report of Investigations 97-20, 2 sheets, scale 1:63,360

Mandeville CW, Carey S, Sigurdsson H, (1996) Sedimentology of the Krakatau 1883 submarine pyroclastic deposits. Bull Volcanol 57:512-529

Miller TP, McGimsey RG, Richter DH, Riehle JR, Nye CJ, Yount ME, Dumoulin JA (1998) Catalog of the Historically Active Volcanoes of Alaska. US Geol Surv Open-File Report 98-582

Miller TP, Smith RL (1987) Late Quaternary caldera-forming eruptions in the eastern Aleutian arc, Alaska. Geology 15:434-438

Miller TP, Smith RL (1977) Spectacular mobility of ash flows around Aniakchak and Fisher calderas, Alaska. Geology 5:173-176

Mirashiro A (1974) Volcanic rock series in island arcs and active continental margins. Am J Sci 274:321-355

Nakamura N (1974) Determination of REE, Ba, Fe, Mg, Na, and K in carbonaceous and ordinary chondrites. Geochim Cosmochim Acta 38:757-775

Neal CA, McGimsey RG, Gardner CA, Harbin ML, Nye CJ (1995) Tephra-fall deposits from the 1992 eruptions of Crater Peak, Mount Spurr volcano, Alaska: A preliminary Report on Distribution, Stratigraphy, and Composition US Geol Surv Bull Keith TEC ed, The 1992 Eruptions of Mt. Spurr Volcano 2139:65-79

Neal CA, Casadevall TJ, Miller TP, Hendley JWII, Stauffer PH (1997) Volcanic Ash-danger to aircraft in the North Pacific.US Geol Surv Fact Sheet 030-97, pp.1-2

Newhall CG, Self S (1982) The Volcanic Explosivity Index (VEI): An Estimate of Explosive Magnitude for Historical Volcanism. J Geophys Res 87: 1231-1238

Nye CJ (1986) Volcanic hazard constraints, In: Updike RG (ed) Engineering geology technical feasibility study, Makushin geothermal power project Unalaska, Alaska. Alaska Div Geol Geophys Surv, PDF 86-60e: E1-E15, 1 pl, scale 1:24,000

Nye CJ, Queen LD, Motyka RJ (1984) Geologic Map of the Makushin Geothermal Area, Unalaska Island, Alaska. Alaska Div Geol Geophys Surv, RI 84-3, 2 sheets, scale 1:24,000

Nye CJ, Swanson SE, Reeder JW (1986) Petrology and Geochemistry of Quaternary Volcanic Rocks from Makushin Volcano, central Aleutian Arc. Alaska Div Geol Geophys Surv, PDF 86-60, pp. 1-123

Paladio-Melosantos MAO, Solidum RU, Scott WE, Quiambao RB, Umbal JV, Rodolfo KS, Tubianosa BS, Delos Reyes PJ, Alonso RA, Ruelo HB (1996) Tephra falls of the 1991 eruptions of Mount Pinatubo. Fire and Mud: Eruptions and Lahars of Mt. Pinatubo, Phillipines. Newhall & Punongloayan eds, Philippine Institute of Volcanology and Seismology, Quezon City, pp. 513-535

Pinney DS (1991) Laboratory procedures for processing tephra samples. Alaska Div Geol Geophys Surv, PDF 91-30, pp. 1-12

Pyle DM (1989) The thickness, volume, and grainsize of tephra fall deposits. Bull Volcanol 51: 1-15

Pyle DM (1990) New estimates for the volume of the Minoan eruption. Thera and the Aegean World III, 2, Earth Sciences, 113-121: London, The Thera Foundation

Reeder JW (1983) Preliminary dating of the caldera-forming Holocene volcanic events for the eastern Aleutian Islands (abstr). Geol Soc Am abs w/ programs 15:688

Riehle JR (1985) A reconnaissance of the major tephra deposits in the upper Cook Inlet region, Alaska. J Volcanol Geotherm Res 26:37-74

Rose WI Jr (1972) Notes on the 1902 eruption of Santa Maria volcano, Guatemala. Bull Volcanol 36:29-45

Rose WI Jr, Bonis S, Stoiber RE, Keller M, Bickford T (1973) Studies of volcanic ash from two recent Central American eruptions. Bull Volcanol 37:338-364

Rose WI.Jr, Anderson AT, Woodruff LG, Bonis SB (1978) The October 1974 basaltic tephra from Fuego volcano: description and history of the magma body. J Volcanol Geotherm Res 4:3-53

Sarna-Wojcicki AM, Shipley S, Waitt RB Jr, Dzurisin D, Wood SH (1981) Areal distribution, thickness, mass, volume, and grain size of air-fall ash from the six major eruptions of 1980.

In: Lipman PW, Mullineaux DR (eds) The 1980 Eruptions of Mount St. Helens, Washington. US Geol Surv Prof. Pap 1250:577-600

Self S (1974) Explosive activity of Ngauruhoe, 27-30 March, 1974. NZ J Geol Geophys 18:89-195

Self S (1976) The recent volcanology of Terceira, Azores. J Geol Soc Lond 132:645-666

Self S, Sparks RSJ (1978) Characteristics of widespread pyroclastic deposits formed by the interaction of silicic magma and water. Bull Volcanol 41:196-212

Self S, Rampino MR, Newton MS, Wolff JA (1984) Volcanological study of the great Tambora eruptions of 1815. Geology 12:659-663

Sigurdsson H (1982) Tephra from the 1979 Soufriere explosive eruption. Science 216:1106-1108

Simkin T, Siebert L (1984) Explosive eruptions in space and time; durations,, intervals, and comparison of the world's active volcanic belt. In: Studies in Geophysics. Natl. Acad. Press, Washingon DC, pp. 110-121

Sparks RSJ (1975) Stratigraphy and geology of the ignimbrites of Vulsini volcano, Central Italy. Geol Rundsch 64:497-523

Sparks RSJ (1976) Grainsize variations in ignimbrites and implications for the transport of pyroclastic flows. Sedimentology 23:147-188

Sparks RSJ, Self S, Walker GPL (1973) Products of Ignimbrite Eruptions. Geology 1:115-118

Streck M Grunder AL (1995) Crystallization and welding variations in a widespread ignimbrite sheet; the Rattlesnake Tuff, eastern Oregon, USA. Bull Volcanol 52:325-333

Stuiver M, Reimer PJ (1993) Extended ^{14}C database and revised CALIB 3.0 ^{14}C age calibration program. Radiocarbon 35:215-230

Sussman D (1985) Apoyo Caldera, Nicaragua: A major Quaternary silicic eruptive center. J Volcanol Geotherm Res 24:249-282

Thompson RN (1982) British Tertiary volcanic province. Scott J of Geol 18:49-107

Thorarinsson S (1954) The tephra-fall from Hekla on March 29th 1947 The eruption of Hekla 1947-1948 II, 3 Societas Scientaruim Islandica, Reykjavik

Thorarinsson S, Sigvaldason GE (1972) The Hekla eruption of 1970. Bull Volcanol 36:269-288

Walker GPL (1980) The Taupo pumice: Product of the most powerful known (ultraplinian) eruption? J Volcanol Geotherm Res 8:69-94

Walker GPL (1981a) New Zealand case histories of pyroclastic studies. In: Self S, Sparks RSJ (eds) Tephra Studies. Reidal, Dordrecht, pp. 317-330

Walker GPL (1981b) The Waimihia and Hatepe plinian deposits from the rhyolitic Taupo Volcanic Center. NZ J Geol Geophys 24:305-324

Walker GPL (1983) Ignimbrite types and ignimbrite problems. J Volcanol Geotherm Res 17:65-88

Walker GPL, Croasdale R (1971) Two Plinian-type eruption in the Azores. J Geol Soc Lond 127:17-55

Walker GPL, Heming RF, Wilson CJN (1980) Low-aspect ratio ignimbrites. Nature 283: 286-287

Walker GPL, Self S, Froggatt PC (1981a) The ground layer of Taupo ignimbrite: a striking example of sedimentation from a pyroclastic flow. J Volcanol Geotherm Res 10:1-11

Walker GPL, Wilson CJN, Froggatt PC (1981b) An ignimbrite veneer deposit: the trail marker of a pyroclastic flow. J Volcanol Geotherm Res 9:409-421

Walker GPL, Wright JV, Clough BJ, Booth B (1981c) Pyroclastic geology of the rhyolitic volcano of La Primavera, Mexico. Geol Rundsch 70:1100-1118

Wilcox RE (1959) Some effects of recent volcanic ash falls with especial reference to Alaska. US Geol Surv Bull 1028-N 409-476

Williams SN, Self S (1983) The October 1902 plinian eruption of Santa Maria volcano, Guatemala. J Volcanol Geotherm Res 16:33-56

Wilson L (1972) Explosive volcanic eruptions-II the atmospheric trajectories of pyroclasts. Geophys J R Astr Soc 30:381-392.

Wilson CJN, Walker GPL (1981) Violence in pyroclastic flow eruptions. in: Self and Sparks (eds) Tephra Studies. Reidal, Dordrecht, pp. 441-448

Wilson CJN, Walker GPL (1982) Ignimbrite depositional facies: the anatomy of a pyroclastic flow. J Geol Soc London 139:581-592

Wilson CJN, Walker GPL (1985) The Taupo eruption, New Zealand I & II. Phil Trans R Soc Lond A314:199-310

Appendix I: Glass Shard Major Element Geochemistry

Major element glass geochemistry was determined using the electron microprobe. All electron microprobe analyses were performed on a Cameca SX-50 Electron Microprobe that resides with the Department of Geology and Geophysics at the University of Alaska Fairbanks. Analyses were run using the analytical routine of Begét *et al.* (1992).

Elemental concentrations for Na, Mg, Al, Si, Cl, K, Ca, Ti, and Fe were determined. The analytical routine used for these analyses used the calibration standards; BGLASS2 (basaltic glass), BGLASS3 (basaltic glass), SCAP (scapolite), and CCNM (obsidian).

The electron beam conditions were 15 kV, 10 nA, and a size of 10 µm. These parameters provide the necessary energy to analyze the heavier elements but not so much as to destroy the sample. Na was analyzed first to minimize possible errors resulting from elemental migration. The Old Crow tephra was used as a working standard to ensure a consistent calibration. The Old Crow tephra was chosen as a working standard due to its homogeneity and established composition. The electron microprobe was calibrated to within 0.1 wt % of the standard normalized values of the Old Crow tephra for each element analyzed. Calibration to these values provided a quantitative method of ensuring consistent and comparable results between sessions.

All concentrations are normalized and reported as oxides with the exception of Cl. All Fe is reported as Fe_2O_3.

Table A1.1 Glass shard major element geochemistry.

	Normalized Wt% Oxide										
Sample No	Na_2O (stdev)	MgO (stdev)	Al_2O_3 (stdev)	SiO_2 (stdev)	Cl (stdev)	K_2O (stdev)	CaO (stdev)	TiO_2 (stdev)	Fe_2O_3 (stdev)	Points
Driftwood Pumice										
96MAK06B-05	4.72 (0.16)	1.31 (0.04)	15.27 (0.15)	65.94 (1.25)	0.16 (0.02)	2.27 (0.07)	3.40 (0.07)	0.94 (0.14)	6.00 (0.16)	8
96MAK06B-05	4.74 (0.25)	0.91 (0.19)	14.73 (0.45)	68.25 (1.37)	0.18 (0.04)	2.68 (0.14)	2.69 (0.38)	0.74 (0.13)	5.09 (0.64)	11
96MAK16-05	5.01 (0.14)	1.18 (0.28)	14.99 (0.26)	66.29 (1.43)	0.17 (0.03)	2.48 (0.19)	3.30 (0.46)	0.81 (0.16)	5.78 (0.77)	24
96MAK35-01	4.81 (0.15)	0.94 (0.07)	15.12 (0.24)	67.80 (0.49)	0.19 (0.05)	2.69 (0.07)	2.72 (0.15)	0.83 (0.13)	4.91 (0.22)	16
96MAK35-01	4.71 (0.16)	0.86 (0.08)	14.90 (0.32)	68.24 (0.57)	0.17 (0.03)	2.64 (0.14)	2.69 (0.17)	0.75 (0.10)	5.04 (0.17)	22
96MAK35-07	4.84 (0.12)	0.94 (0.11)	14.95 (0.21)	67.84 (0.62)	0.18 (0.04)	2.69 (0.11)	2.75 (0.21)	0.83 (0.11)	4.98 (0.26)	12
96MAK37-02	4.82 (0.48)	0.86 (0.34)	15.04 (1.15)	68.00 (2.19)	0.17 (0.05)	2.74 (0.56)	2.46 (0.76)	0.71 (0.18)	5.19 (1.05)	19
96MAK41-09	4.32 (0.78)	0.85 (0.14)	14.14 (1.27)	69.32 (1.93)	0.16 (0.01)	2.75 (0.08)	2.82 (0.12)	0.69 (0.11)	4.94 (0.22)	4
96MAK41-09	4.60 (0.57)	0.94 (0.06)	15.09 (0.22)	68.02 (0.55)	0.16 (0.03)	2.47 (0.09)	2.81 (0.09)	0.80 (0.11)	5.11 (0.22)	29
96MAK42-01	4.84 (0.20)	0.92 (0.09)	15.09 (0.25)	67.64 (0.39)	0.20 (0.02)	2.65 (0.08)	2.76 (0.12)	0.75 (0.13)	5.14 (0.33)	19
96MAK45-01D	4.84 (0.13)	0.93 (0.10)	14.90 (0.22)	67.71 (0.70)	0.17 (0.04)	2.70 (0.11)	2.81 (0.22)	0.84 (0.15)	5.10 (0.39)	10
96MAK45-04D	4.71 (0.13)	0.92 (0.09)	14.76 (0.25)	68.11 (0.55)	0.17 (0.04)	2.70 (0.10)	2.72 (0.18)	0.76 (0.18)	5.15 (0.25)	22
96MAK45-05D	4.71 (0.16)	0.87 (0.15)	14.58 (0.60	68.47 (1.28)	0.18 (0.03)	2.79 (0.21)	2.62 (0.37)	0.75 (0.11)	5.03 (0.34)	18
97MAK07-01	4.93 (0.19)	0.94 (0.09)	14.81 (0.81)	68.00 (1.11)	0.16 (0.04)	2.64 (0.25)	2.88 (0.50)	0.76 (0.14)	4.88 (0.37)	23
Makushin Scoria										
96MAK34-01	4.89 (0.15)	1.78 (0.27)	15.43 (0.32)	62.92 (0.77)	0.14 (0.03)	2.16 (0.28)	4.18 (0.42)	1.12 (0.17)	7.37 (0.47)	5
96MAK34-01	5.09 (0.33)	1.91 (0.33)	15.73 (0.57)	62.08 (0.68)	0.13 (0.03)	2.05 (0.38)	4.40 (0.46)	1.08 (0.15)	7.52 (0.78)	25
96MAK34-02	4.89 (0.16)	1.91 (0.09)	15.60 (0.21)	62.37 (0.40)	0.13 (0.03)	1.99 (0.14)	4.45 (0.19)	1.11 (0.16)	7.56 (0.34)	30
96MAK41-02	5.02 (0.35)	1.92 (0.12)	15.51 (0.43)	62.41 (0.50)	0.14 (0.03)	1.98 (0.32)	4.43 (0.31)	1.08 (0.15)	7.52 (0.50)	25
Yellow Ash										
96MAK16-04	4.47 (0.40)	0.81 (0.07)	14.36 (0.50)	69.56 (0.92)	0.19 (0.04)	2.86 (0.12)	2.37 (0.09)	0.73 (0.16)	4.66 (0.19)	7
96MAK31-03	4.53 (0.16)	0.80 (0.05)	14.63 (0.37)	69.12 (0.58)	0.19 (0.02)	2.85 (0.08)	2.39 (0.14)	0.77 (0.15)	4.72 (0.22)	10
CFPF pumice										
97MAK01-03	4.92 (0.57)	1.57 (0.27)	16.63 (1.03)	61.45 (1.25)	0.19 (0.06)	1.47 (0.16)	4.71 (0.61)	1.11 (0.18)	7.94 (0.81)	7
97MAK12-02	4.45 (0.33)	1.79 (0.21)	16.02 (0.78)	61.82 (0.68)	0.16 (0.04)	1.50 (0.12)	4.71 (0.35)	1.08 (0.16)	8.46 (0.56)	18

Table A1.1 cont.

Normalized Wt% Oxide																					
Sample No	Na_2O	(stdev)	MgO	(stdev)	Al_2O_3	(stdev)	SiO_2	(stdev)	Cl	(stdev)	K_2O	(stdev)	CaO	(stdev)	TiO_2	(stdev)	Fe_2O_3	(stdev)	Points
Regional tephras?																					
96MAK08-01	4.61	(0.16)	0.55	(0.04)	14.89	(0.53)	71.13	(0.75)	0.28	(0.03)	3.03	(0.12)	2.00	(0.27)	0.50	(0.13)	3.01	(0.22)	13
97MAK14-01	4.91	(0.15)	0.93	(0.05)	14.72	(0.32)	68.57	(0.47)	0.16	(0.03)	2.03	(0.05)	3.05	(0.07)	0.70	(0.11)	4.95	(0.18)	22
Late Holocene tephras																					
96MAK01-10	4.63	(0.42)	1.72	(0.94)	15.27	(1.78)	62.85	(3.61)	0.13	(0.03)	2.11	(0.57)	4.23	(1.22)	1.36	(0.15)	7.72	(0.67)	5
96MAK03-01	3.44	(0.71)	4.25	(1.49)	15.33	(1.37)	54.31	(5.21)	0.13	(0.03)	1.19	(0.64)	7.78	(2.07)	1.72	(0.22)	11.85	(2.26)	3
96MAK03-01	3.55	(0.19)	4.26	(0.58)	14.72	(1.10)	55.16	(0.66)	0.10	(0.03)	1.10	(0.14)	8.45	(0.41)	1.49	(0.20)	11.18	(0.94)	24
96MAK03-04	4.66	(0.76)	1.78	(1.34)	15.32	(1.66)	62.84	(4.14)	0.12	(0.05)	2.06	(0.66)	4.99	(1.63)	1.07	(0.45)	7.16	(2.79)	15
96MAK03-06	4.65	(0.65)	0.99	(0.70)	15.49	(2.56)	65.33	(2.66)	0.11	(0.06)	2.71	(0.82)	4.19	(1.49)	0.89	(0.35)	5.63	(2.37)	14
96MAK03-08	4.70	(0.48)	1.44	(0.91)	15.92	(2.07)	62.47	(3.22)	0.11	(0.04)	2.41	(0.63)	4.90	(1.39)	1.13	(0.33)	6.92	(2.32)	18
96MAK03-12	3.62	(0.65)	3.20	(1.37)	15.24	(1.57)	57.40	(5.54)	0.11	(0.04)	1.46	(0.73)	7.87	(2.83)	1.41	(0.36)	9.69	(2.39)	20
96MAK03-14	4.54	(0.54)	2.18	(2.28)	15.51	(1.50)	63.98	(5.39)	0.08	(0.06)	1.95	(1.03)	4.71	(1.83)	0.95	(0.39)	6.09	(2.41)	19
96MAK03-16	4.75	(0.94)	1.43	(1.36)	15.02	(1.47)	65.40	(4.80)	0.14	(0.05)	2.35	(0.62)	3.89	(1.46)	1.07	(0.38)	5.93	(3.29)	12
96MAK03-20	3.38	(0.72)	4.81	(1.75)	15.66	(1.09)	55.03	(5.70)	0.09	(0.04)	1.09	(0.74)	8.73	(2.72)	1.22	(0.25)	9.99	(1.95)	26
96MAK03-23	4.42	(0.12)	0.73	(0.09)	14.52	(0.43)	69.48	(0.62)	0.18	(0.02)	2.88	(0.12)	2.19	(0.18)	0.84	(0.13)	4.76	(0.16)	9
96MAK03-23	4.85	(0.34)	1.13	(0.65)	15.41	(1.75)	64.63	(2.39)	0.10	(0.04)	2.14	(0.61)	4.64	(1.02)	1.01	(0.28)	6.09	(1.65)	22
96MAK03-25	4.59	(0.38)	1.30	(0.73)	14.27	(1.24)	64.88	(1.73)	0.11	(0.03)	2.39	(0.33)	4.16	(0.56)	1.11	(0.24)	7.18	(1.35)	26
96MAK03-26	3.84	(0.38)	3.18	(0.67)	15.76	(0.62)	57.81	(2.39)	0.09	(0.03)	1.58	(0.37)	6.72	(1.16)	1.42	(0.16)	9.60	(1.14)	23
96MAK03-28	4.58	(0.54)	1.16	(0.97)	14.17	(2.19)	67.07	(3.26)	0.10	(0.04)	2.53	(0.57)	3.57	(1.11)	0.87	(0.28)	5.95	(1.86)	24
96MAK03-30	4.95	(0.58)	0.62	(0.50)	15.35	(1.98)	67.47	(2.36)	0.09	(0.05)	2.35	(0.62)	3.77	(1.01)	0.72	(0.26)	4.67	(1.58)	20
96MAK03-31	4.54	(0.48)	0.98	(1.04)	14.34	(2.05)	68.30	(2.72)	0.10	(0.03)	2.66	(0.59)	3.25	(1.21)	0.76	(0.19)	5.07	(1.47)	22
96MAK03-33	4.97	(0.67)	1.68	(0.76)	15.47	(0.87)	64.09	(3.33)	0.13	(0.03)	1.85	(0.68)	4.42	(1.16)	0.97	(0.29)	6.41	(1.83)	23
96MAK03-34	3.33	(0.42)	3.08	(1.19)	16.99	(2.80)	54.65	(0.99)	0.07	(0.03)	1.05	(0.21)	9.12	(0.70)	1.54	(0.39)	10.18	(2.27)	24
96MAK03-38	3.11	(0.49)	4.25	(1.16)	13.81	(1.52)	55.69	(1.35)	0.09	(0.03)	1.46	(0.24)	7.80	(0.75)	1.80	(0.34)	11.99	(1.67)	19
96MAK03-41	4.82	(0.33)	0.99	(0.54)	14.06	(1.43)	66.95	(1.36)	0.14	(0.03)	2.68	(0.41)	3.21	(0.59)	1.01	(0.21)	6.15	(1.11)	23
96MAK03-43	4.52	(0.45)	1.94	(1.16)	15.83	(0.91)	63.54	(2.93)	0.11	(0.03)	1.34	(0.32)	5.17	(1.28)	0.98	(0.16)	6.56	(1.05)	26
96MAK03-45	4.10	(0.63)	2.28	(1.50)	14.39	(1.62)	62.52	(4.92)	0.15	(0.04)	2.04	(0.32)	4.77	(1.39)	1.25	(0.36)	8.51	(2.98)	20
96MAK03-46	2.92	(0.25)	4.93	(0.25)	13.88	(0.43)	54.09	(0.51)	0.07	(0.02)	1.37	(0.25)	8.64	(0.24)	1.78	(0.24)	12.34	(0.57)	22

Table A1.1 cont.

Normalized Wt% Oxide																					
Sample No	Na_2O	(stdev)	MgO	(stdev)	Al_2O_3	(stdev)	SiO_2	(stdev)	Cl	(stdev)	K_2O	(stdev)	CaO	(stdev)	TiO_2	(stdev)	Fe_2O_3	(stdev)	Points
96MAK03-48	4.00	(0.51)	1.32	(0.92)	15.23	(2.24)	64.65	(2.98)	0.12	(0.05)	2.40	(0.46)	4.45	(1.39)	1.11	(0.38)	6.70	(2.42)	16
96MAK07-02	3.43	(0.26)	4.01	(0.38)	15.75	(1.93)	54.36	(0.72)	0.11	(0.03)	1.05	(0.20)	8.42	(0.92)	1.62	(0.38)	11.26	(1.56)	9
96MAK21-01	3.30	(0.36)	4.43	1.38)	15.72	(2.17)	54.50	(0.49)	0.11	(0.03)	1.02	(0.17)	8.30	(0.59)	1.59	(0.26)	11.04	(1.51)	6
96MAK28-04	4.75	(0.45)	0.79	(0.41)	14.87	(1.31)	68.77	(1.32)	0.17	(0.04)	2.70	(0.38)	2.60	(0.55)	0.75	(0.12)	4.59	(0.68)	9
96MAK33-02	4.80	(0.18)	1.24	(0.16)	15.11	(0.19)	66.11	(0.80)	0.16	(0.03)	2.44	(0.09)	3.34	(0.31)	0.89	(0.13)	5.91	(0.41)	29
96MAK36-02	5.34	(0.26)	2.00	(0.17)	15.61	(0.39)	61.83	(0.41)	0.13	(0.04)	1.59	(0.14)	4.89	(0.28)	1.05	(0.19)	7.57	(0.48)	27
97MAK14-02	3.89	(0.41)	2.60	(0.75)	15.75	(0.93)	60.77	(0.78)	0.09	(0.02)	2.12	(0.20)	5.22	(0.37)	1.09	(0.16)	8.47	(0.99)	22
97MAK14-03	4.84	(0.31)	0.57	(0.12)	14.36	(1.06)	68.65	(1.23)	0.15	(0.04)	3.05	(0.33)	2.37	(0.57)	0.94	(0.17)	5.06	(0.49)	22
pumice																			
96MAK14-01	4.83	(0.32)	1.64	(0.84)	15.83	(1.79)	64.04	(0.85)	0.12	(0.03)	1.89	(0.28)	4.48	(0.73)	0.96	(0.29)	6.21	(1.61)	6
96MAK14-01	4.81	(0.34)	1.42	(0.11)	15.70	(0.44)	64.99	(0.52)	0.16	(0.03)	2.14	(0.10)	3.60	(0.25)	0.95	(0.15)	6.21	(0.24)	22
96MAK15-01	4.93	(0.16)	1.33	(0.20)	15.41	(0.44)	65.45	(1.05)	0.17	(0.04)	2.17	(0.15)	3.52	(0.32)	0.91	(0.15)	6.12	(0.40)	25
96MAK29-02	4.92	(0.18)	1.50	(0.09)	15.25	(0.28)	64.73	(0.40)	0.16	(0.04)	2.25	(0.11)	3.76	(0.17)	0.98	(0.12)	6.45	(0.16)	17
96MAK31-01	4.58	(0.81)	1.57	(0.43)	15.26	(0.55)	65.08	(1.13)	0.17	(0.03)	2.04	(0.17)	3.76	(0.26)	1.08	(0.14)	6.47	(0.72)	11

Appendix II: Whole Rock Major and Trace Element Geochemistry

Approximately 40 g splits of dry crushed sample were submitted to the Geoanalytical Laboratory of the Geology Department at Washington State University in Pullman, Washington for whole rock analysis. Concentrations of major and some trace elements were obtained using the XRF analytical technique while the ICPMS analytical technique was used for most trace elements. All major elements are reported as weight percent oxides and all Fe reported as FeO. All trace elements reported as parts per million (ppm).

Table A2.1 Whole rock major element geochemistry.

	Normalized Wt% Oxide										
Sample No	SiO2	Al2O3	TiO2	FeO*	MnO	CaO	MgO	K2O	Na2O	P2O5	Total
Correlation Unit A—(Driftwood Pumice)											
96MAK15-01	62.17	17.30	1.032	6.71	0.177	4.18	1.45	1.99	4.68	0.313	100.00
96MAK35-01	59.48	20.61	1.125	7.19	0.163	3.61	1.30	1.86	4.27	0.414	100.00
96MAK41-09	64.66	16.61	0.952	4.89	0.161	3.77	1.40	2.20	4.99	0.362	100.00
97MAK07-01	60.84	18.38	1.104	7.27	0.169	4.13	1.41	1.85	4.54	0.308	100.00
Correlation Units B&C (Valley-Filling Pyroclastics)											
96MAK24-01	64.56	15.92	0.888	5.72	0.164	4.03	1.20	2.23	4.99	0.296	100.00
96MAK33-02	61.84	16.64	1.006	6.71	0.176	4.84	1.96	1.88	4.64	0.298	100.00
96MAK34-01	60.07	17.31	1.141	7.60	0.192	5.15	1.95	1.75	4.53	0.300	100.00
96MAK34-02	60.85	16.45	1.100	7.27	0.184	5.28	1.96	1.82	4.77	0.301	100.00
96MAK35-02	59.22	17.32	1.070	7.31	0.177	6.25	2.31	1.61	4.47	0.270	100.00
96MAK36-01	60.46	16.57	1.064	7.62	0.174	5.56	2.02	1.74	4.52	0.280	100.00
96MAK36-02	62.99	16.99	0.964	6.44	0.183	4.10	1.34	2.02	4.65	0.324	100.00
97MAK07-02	59.60	17.15	1.070	7.45	0.175	6.09	2.13	1.62	4.44	0.269	100.00
Other Tephras											
96MAK14-01	56.58	21.18	1.284	8.36	0.168	4.84	1.74	1.42	4.00	0.423	100.00
96MAK36-03	54.34	17.95	1.026	8.90	0.180	8.65	4.51	0.96	3.30	0.193	100.00

All Fe expressed as FeO

Table A2.2 Whole rock trace element geochemistry (XRF).

	Unit A-Driftwood Pumice				Unit B & C –Valley Filling Pyroclastics								Other	
Element	96 MAK 15-01	96 MAK 35-01	96 MAK 41-09	97 MAK 07-01	96 MAK 24-01	96 MAK 33-02	96 MAK 34-01	96 MAK 34-02	96 MAK 35-02	96 MAK 36-01	96 MAK 36-02	97 MAK 07-02	96 MAK 36-03	96 MAK 14-01
Ni	1	3	2	2	2	3	1	0	0	0	0	0	8	0
Cr	8	6	0	3	1	9	7	4	9	6	5	5	40	8
Sc	17	15	19	17	14	18	25	21	25	22	18	22	30	22
V	87	75	72	76	67	115	109	112	139	127	72	130	246	119
Ba	598	552	662	553	645	568	637	579	509	514	596	522	342	462
Rb	46	41	52	41	51	43	37	41	36	39	46	35	19	31
Sr	285	258	276	297	286	318	357	339	371	354	295	369	435	323
Zr	207	240	218	227	197	179	179	173	152	162	203	156	105	212
Y	41	39	45	40	43	37	40	39	34	36	42	35	24	36
Nb	6	7	7	8	6	6	5	5	5	7	8	6	3	7
Ga	22	24	20	23	21	21	21	19	23	22	21	20	21	27
Cu	33	28	33	34	21	27	28	25	46	42	35	38	81	31
Zn	86	77	116	82	81	87	96	94	82	87	84	87	84	79
Pb	15	16	18	21	15	12	9	11	10	11	16	12	5	19
La	32	14	8	27	20	32	15	19	23	12	14	17	15	26
Ce	42	39	45	63	51	53	36	27	35	36	47	41	33	29
Th	6	3	6	0	3	5	4	6	4	2	2	3	5	2

all analyses expressed in ppm

Table A2.3 Whole rock trace element geochemistry (ICP).

	Correlation Unit A—Driftwood Pumice				Correlation Units B & C –Valley-Filling Pyroclastics								Other	
Element	96 MAK 15-01	96 MAK 35-01	96 MAK 41-09	97 MAK 07-01	96 MAK 24-01	96 MAK 33-02	96 MAK 34-01	96 MAK 34-02	96 MAK 35-02	96 MAK 36-01	96 MAK 36-02	97 MAK 07-02	96 MAK 14-01	96 MAK 36-03
La	17.44	15.80	19.29	16.13	17.29	15.77	16.21	15.38	13.96	14.73	17.94	13.82	13.99	9.50
Ce	38.87	36.67	41.67	37.79	36.25	34.26	35.40	33.36	31.02	31.53	41.48	30.09	33.29	20.08
Pr	5.25	4.91	5.57	5.21	4.79	4.56	4.76	4.56	4.19	4.21	5.18	4.13	4.64	2.79
Nd	24.35	23.08	25.82	24.21	22.21	21.10	22.78	21.32	19.46	19.72	24.05	19.59	22.37	13.33
Sm	6.93	6.73	7.33	7.07	6.51	5.88	6.48	5.95	5.52	5.67	7.03	5.62	6.70	3.86
Eu	1.66	1.66	1.74	1.80	1.68	1.53	1.81	1.68	1.59	1.58	1.78	1.64	1.79	1.30
Gd	7.22	6.92	7.82	7.30	6.76	6.41	7.20	6.61	6.09	6.16	7.25	6.17	6.98	4.18
Tb	1.25	1.20	1.34	1.26	1.16	1.13	1.19	1.14	1.04	1.07	1.25	1.05	1.17	0.71
Dy	7.90	7.52	8.43	8.08	7.40	6.89	7.61	7.16	6.50	6.87	7.88	6.52	7.40	4.48
Ho	1.68	1.56	1.78	1.61	1.55	1.43	1.57	1.48	1.37	1.42	1.65	1.35	1.48	0.92
Er	4.55	4.23	4.86	4.42	4.21	3.96	4.30	4.10	3.72	3.85	4.48	3.75	3.97	2.53
Tm	0.68	0.63	0.71	0.67	0.62	0.60	0.63	0.58	0.56	0.58	0.67	0.56	0.60	0.37
Yb	4.23	4.16	4.48	4.12	3.96	3.77	4.02	3.79	3.54	3.61	4.24	3.42	3.92	2.33
Lu	0.68	0.67	0.74	0.66	0.65	0.60	0.65	0.62	0.56	0.58	0.69	0.55	0.62	0.38
Ba	579.44	518.97	647.64	545.03	586.82	554.32	606.62	538.71	478.79	515.51	589.58	483.46	421.59	329.84
Th	4.73	5.57	5.05	5.10	4.29	4.06	3.99	3.68	3.20	3.34	4.62	3.21	4.57	1.84
Nb	6.31	7.20	6.45	6.96	5.64	5.48	5.41	5.07	4.43	4.68	6.07	4.47	6.31	2.80
Y	43.82	39.65	47.33	41.45	42.32	39.79	42.46	40.31	36.88	37.53	43.63	35.70	37.90	25.01
Hf	6.10	7.09	6.65	6.61	5.62	5.27	5.37	4.92	4.47	4.73	6.05	4.37	6.23	2.84
Ta	0.49	0.55	0.51	0.55	0.44	0.43	0.42	0.37	0.33	0.37	0.48	0.34	0.49	0.21
U	2.79	3.25	2.85	3.00	2.59	2.39	2.29	2.14	1.92	1.98	2.75	2.05	2.64	1.03
Pb	17.86	19.58	19.05	19.83	15.49	16.59	14.83	13.82	12.40	14.17	18.27	12.38	18.14	8.36
Rb	45.07	40.01	49.95	41.22	46.12	42.95	38.95	39.84	35.41	36.91	43.68	35.83	30.28	19.29
Cs	4.21	3.82	4.84	3.89	4.32	3.89	3.69	3.52	3.11	3.29	4.20	3.17	2.82	1.64
Sr	289.40	257.69	280.31	297.60	307.63	320.38	371.45	350.52	382.10	358.86	296.46	371.07	320.80	446.78

concentrations expressed in ppm

Appendix III: Grainsize Data

Grainsize analysis was performed on dry samples using nested standard 8 inch mesh sieves. Mesh size ranged from –1 to 4.5 phi in ½ phi increments. Sieves were cleaned between analyses. Sample weights are reported in Table A3.1.

Table A3.1 Distal tephra grainsize data.

		sample weight (g)												
Sample No	Layer	-1ϕ	0ϕ	1/2ϕ	1ϕ	1 1/2ϕ	2ϕ	2 1/2ϕ	3ϕ	3 1/2ϕ	4 ϕ	4 1/2ϕ	pan	total (g)
96MAK45-05A	1	0.3	2.4	3.3	11.2	36.6	64.1	16.9	4.4	3.8	3.1	0	7.9	154
96MAK45-01A	1	0.1	0.3	0.4	6	24.3	59.5	18	2.8	2.1	1.8	1.5	4.5	121.3
96MAK45-04A	1	0.1	0.2	0.3	6.4	5.1	86	27.2	3.2	2.2	2	2	4.2	138.9
96MAK45-03A	1	0	0	0.1	1.2	6	17	6.6	1	0.7	0.6	0.4	1	34.6
96MAK22-02	1?	0	0.1	0.2	0.6	2.2	7.3	2.3	0.5	0.5	0.4	0.3	0.4	14.8
96MAK45-04B2	2	6.5	22.8	11.9	5.3	2.6	2.9	2.1	1.3	1.1	0.5	0.4	1	58.4
96MAK45-05B	2	38.6	43.1	20.5	22.6	15.5	14.2	6.6	3.9	3.6	3.7	3.4	9.7	185.4
96MAK45-01B	2	38.1	37.9	20.8	24.1	15.8	16.5	8.8	5.1	5.1	4.6	4.1	11.5	192.4
96MAK45-04B1	2	74.2	60.4	29.8	30.2	18.5	17	8.9	6	6.7	6.2	6	17.2	281.1
96MAK45-03B	2	8.1	14	10.3	13.7	8.1	9	4.5	2.4	2.5	1.7	1.6	3.3	79.2
96MAK22-01	2?	13	17.3	15.2	25.6	30.4	52.5	25.4	7.4	6.5	5.1	3.3	5.8	207.5
96MAK45-05C	3	0.8	2.8	3.1	10.7	10.5	14.9	13.6	7.3	6.1	4	2.7	4.8	81.3
96MAK45-01C	3	0.2	0.8	1.5	7.2	7.4	19.7	16.4	6.4	4.8	3.3	2	3.2	72.9
96MAK45-04C1	3	0.1	0.4	0.3	0.7	0.9	2	2	1.3	1.2	0.8	0.4	0.6	10.7
96MAK45-04C2	3	0.3	0.9	1.1	1.8	1.8	4	2.4	0.9	1	0.5	0.4	0.4	15.5
96MAK45-04D	4	1.8	7.3	5	4.3	1.8	2.1	1.9	1.2	1.4	0.9	0.6	1.3	29.6
96MAK45-05D	4	4.4	10.3	8.4	9.5	7	5.9	4.2	3.2	3.1	1.7	0.8	2.8	61.3
96MAK45-01D	4	2.2	9	7.7	9.6	5.5	5.4	3.6	2.5	2.3	1.8	1.3	2.8	53.7

Appendix IV: Calculation of Similarity Coefficients

Similarity coefficients are used to compare the geochemical likeness of one sample to another based on multivariable data sets. The similarity coefficient is an average ratio of mean normalized elemental concentrations in any two analyses and can be expressed by the equation

$$d(_{A,\,B}) = \frac{\sum_{i=1}^{n} R_i}{n}$$

where d(A,B) equals d(B,A) and is the similarity coefficient for comparison between sample A and sample B. Variable i is the elemental number, n is the number of elements, R_i is X_iA/X_iB where A is the smaller value, X_iA is the concentration of element i in sample A, and X_iB is the concentration of element i in sample B (Borchardt *et al.* 1972).

Appendix V: Radiocarbon Dating Method

A variety of nuclear reactions based on interactions of cosmic-ray neutrons with stable isotopes of nitrogen, oxygen, and carbon are responsible for producing ^{14}C in the upper atmosphere. The most important of these reactions is between slow cosmic-ray neutrons and ^{14}N:

$$ {}^{1}_{0}n + {}^{14}_{7}\mathrm{N} \rightarrow {}^{14}_{6}\mathrm{C} + {}^{1}_{1}\mathrm{H} $$

where *n* is the neutron and H is the proton emitted by the product nucleus (Faure 1986). Radiocarbon is then incorporated into CO or CO_2 and mixed in the atmosphere and hydrosphere. Equilibrium concentrations are maintained by continuous production in the atmosphere and continuous decay. Molecules of $^{14}CO_2$ enter plants through photosynthesis and by absorption through roots, equilibrium concentrations are maintained by continuous absorption. Animals also absorb ^{14}C from plants, the atmosphere, and hydrosphere. When a living organism dies, absorption stops, and the activity of ^{14}C declines due to radioactive decay. ^{14}C decays by the emission of a negative beta particle forming stable ^{14}N:

$$ {}^{14}_{6}\mathrm{C} \rightarrow {}^{14}_{7}\mathrm{N} + b^{-} + \bar{n} + Q $$

The radioactivity of a sample of age *t* years is given by the equation:

$$ A = A_o e^{-lt} $$

where *A* is the measured activity of the sample in disintegrations per minute per gram (dpg/g), A_o is the activity of the sample prior to death, and ? is the decay constant. The best estimates of ^{14}C activity that is in equilibrium with the atmosphere is 13.56±0.07 dpm/g (Karlen *et al.* 1966). Solving for t yields the equation:

$$ t = \frac{1}{l}\ln\left(\frac{?_o}{A}\right) \text{ or } t = \frac{1}{l}\ln\left(\frac{N_o}{N}\right) $$

when isotope concentrations *N* are directly measured using mass spectrometry.

F.W. Libby is credited with the development of the carbon-14 dating method, for which he was awarded a Nobel Prize for chemistry in 1960. He first estimated, in 1946, that ^{14}C production rates were high enough to be detected. He later demonstrated that the activity of ^{14}C in the biosphere is nearly constant and mostly independent of latitude (Anderson & Libby 1951). The Libby ^{14}C half-life of 5568+-30 years is still used in conventional age dating to maintain consistency with older age dates even though later studies more accurately determined the actual half-life to be 5730+-40 years (Godwin, 1962).

The accuracy of radiocarbon dating is dependent on several assumptions. It is assumed that the initial activity of ^{14}C in plants and animals is a known constant which has been independent of time, geographic location, or specific plant or animal species and that contamination by modern ^{14}C has not occurred. These assumptions are now known to not be strictly true. The amount of the neutron flux is dependant on the cosmic-ray proton flux which mostly come from the Sun. Thus the changing activity of the Sun, over time, has affected the production and therefore the activity of ^{14}C in the atmosphere. In addition the cosmic-ray proton flux is modulated by the Earth's magnetic field (Faure 1986). Analysis of trees dated by dendrochronology has shown that carbon content in the atmosphere has systematically varied in the past. Fortunately tree ring and coral data allows radiocarbon ages to be calibrated to calendar years back as far as 20 ka.

Introduction of "dead" stable carbon into the atmosphere by the burning of fossil fuels decreased the activity of ^{14}C in the atmosphere during 19^{th} and 29^{th} centuries by. However, nuclear devices are responsible for creating the much greater effect of a net increase in the amount of ^{14}C on the Earth's surface during the later half of the 20^{th} century. Conventional ages (yr B.P.) are consequently reported as years before 1950 A.D.

Modern conventional dating procedures generally involve purification and conversion of at least 1 g of sample carbon into CO_2 by combustion. The CO_2 is then converted to benzene and the activity measured with a liquid scintillation counter. Carbon is converted to graphite prior to analysis by mass spectrometry with the AMS technique. Because carbon ions are directly measured using AMS, samples containing a few milligrams of carbon can be dated. Direct measurement of stable carbon ratios in the sample is also routine with AMS dating.

To maintain consistency with other labs most conventional radiocarbon labs use the oxalic acid calibration standard (NBS No. 4990) which has an age corrected activity equal to 95% of the activity of the oxalic standard for wood grown between 1840 and 1850 A.D. Unfortunately fractionation of carbon isotopes occurs during laboratory combustion of oxalic acid to CO_2.and the degree of fractionation is dependant on experimental conditions. Experiments by Craig (1954 and 1961) showed that CO_2 produced from the reaction have $\delta^{13}C$ values of approximately –19 ‰ relative to the PDB-1 standard. Most laboratories now correct the activity of each batch of CO_2 derived from the combustion of oxalic acid using the following equation:

$$A_{ox} = A'_{ox}\left[1 - \frac{2(19 + d^{13}C')}{1000}\right] \text{dpm/g}$$

where A_{ox} is the activity of the oxalic acid corrected for fractionation to $\delta^{13}C$ = 19 ‰ relative to the PDB-1 international standard, A'_{ox} is the observed activity of a particular batch of CO_2 gas prepared from the oxalic acid standard and $\delta^{13}C'$ is the measured value of this parameter of the CO_2 gas, relative to the PDB-1 standard (Faure 1986). Corrections assume that fractionation depends on mass differences and that ^{14}C is enriched or depleted twice as much as ^{13}C relative to ^{12}C. Applying these corrections, the initial activity of nineteenth century wood yields the equation:

$$A_o = 0.95A'_{ox}\left[1 - \frac{2(19 + d^{13}C')}{1000}\right] \text{dpm/g}$$

Another source of variation of radiocarbon in natural samples is that physical and chemical reactions in nature also can cause fractionation. As a result isotopic abundances of carbon in plants differ from that in the atmosphere. Plants are generally enriched in ^{12}C relative to ^{13}C with $\delta^{13}C$ values ranging from approximately –6 to –34 ‰ (Brownlow 1996) and average –25 ‰ relative to the PDB-1 international standard.

$$d^{13}C = \left[\frac{\left(\frac{^{13}C}{^{12}C}\right)_{spl} - \left(\frac{^{13}C}{^{12}C}\right)_{std}}{\left(\frac{^{13}C}{^{12}C}\right)_{std}}\right] \times 10^3 \text{ ‰}$$

Differences in fractionation can result in accuracy errors as high as 250 years if no $^{12}C/^{13}C$ correction is made. These errors can be eliminated by measuring the isotopic abundance of stable isotopes ^{12}C and ^{13}C in the sample. For samples whose carbon isotope compositions differ significantly from that of average wood $\delta^{13}C$ ‰ (i.e. unidentified plant material with a mixture of C4, C5, and CAMS pathway plants) the follow correction can be applied:

$$A_{corr.} = A_{meas.}\left[1 - \frac{2(25 + d^{13}C_{PDB})}{1000}\right] \text{dpm/g}$$